© 2020

JINGNAN ZHAO

ALL RIGHTS RESERVED

TRAFFIC LOADING IMPACT ON ASPHALT PAVEMENT PERFORMANCE: VEHICLE-TIRE-PAVEMENT INTERACTION MODELING AND MACHINE LEARNING APPROACH

By

JINGNAN ZHAO

A dissertation submitted to the

School of Graduate Studies

Rutgers, The State University of New Jersey

In partial fulfillment of the requirements

For the degree of

Doctor of Philosophy

Graduate Program in Civil and Environmental Engineering

Written under the direction of

Hao Wang

And approved by

_____

_____

_____

_____

New Brunswick, New Jersey

October, 2020

ABSTRACT OF THE DISSERTATION

Traffic Loading Impact on Asphalt Pavement Performance: Vehicle-Tire-Pavement Interaction Modeling and Machine Learning Approach

by JINGNAN ZHAO

Dissertation Director:

Dr. Hao Wang

Pavement responses are affected by the magnitude and frequency of dynamic loads generated by vehicles, which are significantly dependent on axle configuration, pavement roughness conditions, and vehicle speed. Random amplitudes of dynamic loads are generated by rough road surface due to development of pavement distresses after initial construction. Therefore, vehicle-tire-pavement interaction model is needed for analyzing dynamic pavement responses and pavement damage to moving loads and taking pavement roughness into consideration.

The first objective of the research is to analyze dynamic responses of flexible pavement structure using an integrated vehicle-tire-pavement interaction approach. A full-truck model was adopted to estimate the dynamic tire forces considering pavement surface conditions, vehicle speeds, truck configuration, and axle type and loads. A modified method was proposed to derive frequency response functions under harmonic loads using the equivalent modulus of asphalt layer at the specific temperature and loading frequency. After that, the convolution integral method was used to simulate pavement responses under non-stationary loads with random amplitudes. The impulse response method was used to calculate pavement responses induced by dynamic loads considering vehicle-tire-pavement

interaction. A methodology was proposed to incorporate the impact of dynamic loads on fatigue cracking development in the framework of M-E pavement design and analysis. In addition, dynamic responses of flexible pavements induced by wide-base tires considering pavement roughness condition were analyzed through the ratio of critical pavement responses between wide-base tire and dual-tire assembly, respectively, for the potential of fatigue cracking, near-surface cracking, and subgrade rutting.

Long-term monitoring of in-service pavements is used to develop pavement performance models in pavement management system. The weigh-in-motion (WIM) data help to comprehensively understand vehicular loadings on pavement performance. Previous studies mainly used traditional statistical methods to quantify pavement damage due to vehicular loading. Because of the complexity of problem, the relationship between pavement performance and influential variables may not be apparent in traditional regression models.

The second objective is to use machine learning approaches, including support vector regression and random survival forest models, to quantify the impact of traffic loading on pavement performance based on field data. Multi-variable nonlinear regression method and support vector regression method were applied and compared in terms of prediction accuracy and error. Random survival forest method was used to investigate the influence of traffic loading on pavement survival life. The variable importance technology was used to select the appropriate variables in the model and reduce prediction error. The proposed pavement performance models were further used to analyze pavement deterioration caused by overweight trucks with different truck traffic and axle load distributions.

DEDICATION

I dedicate this dissertation to my parents

ACKNOWLEDGEMENT

I would first like to express my gratitude to my advisor, Dr. Hao Wang, whose expertise was invaluable in formulating the research topic and methodology throughout my Ph.D. study at Rutgers, The State University of New Jersey. His insightful feedback is instrumental in defining the path of my research. It is such an honor to have him as my Ph.D. advisor and work with him.

It is my great honor and privilege to have Dr. Nenad Gucunski, Dr. Husam Najm, and Dr. Pan Lu as the members of my graduate committee. Their patient support, encouragements, and valuable suggestions during my Ph.D. study go far beyond the completion of my dissertation and defense.

Great appreciation is also made to Dr. Zilong Wang, Dr. Maoyun Li, Dr. Jiaqi Chen, Dr. Abbas Fadhil Jasim, Dr. Yangmin Ding, and Pengyu Xie for their help, assistance, and guidance throughout my research. I would like to thank all the member in Dr. Hao Wang's group for their assistance and support as well as encouragement and friendship. I also want to express my appreciation to the CEE departmental staff: Gina Cullari and Linda Szary.

And my biggest thanks to my parents, Xuedong Zhao and Yongmei Jiang, for all the patience, comprehension, love, support, and encouragement they have shown me through my research, without whom I would not have been able to complete the Ph.D. study.

TABLE OF CONTENT

ABSTRACT OF THE DISSERTATION ..... **ii**

ACKNOWLEDGEMENT ..... **v**

TABLE OF CONTENT ..... **vi**

LIST OF FIGURES ..... **xi**

LIST OF TABLES ..... **xvi**

CHAPTER 1 INTRODUCTION **1**

1.1 Background **1**

1.2 Problem Statement **3**

1.3 Objective and Methodology **6**

CHAPTER 2 LITERATURE REVIEW **10**

2.1 Estimation of Dynamic Loads Under Moving Vehicle **10**

2.2 Calculation of Pavement Response Under Dynamic Loads **15**

2.2.1 Pavement Response Under Point or Line Loads *15*

2.2.2 Pavement Response Under Area Loads *18*

2.3 Evaluation of Pavement Damage Under Dynamic Loads **21**

2.3.1 Effect of Dynamic Loads on Pavement Damage *21*

2.3.2 Effect of Wide-Base Tire on Pavement Response and Damage *24*

2.4 Machine Learning Approach for Pavement Performance Prediction **25**

2.4.1 Support Vector Machine *25*

2.4.2 Random Forest *26*

2.4.3 Gradient Boost Model *28*

CHAPTER 3 DYNAMIC LOADS OF VEHICLE DUE TO ROUGH PAVEMENT SURFACE **30**

3.1 Estimation of Dynamic Tire Force **30**

3.1.1 Truck Modeling *30*

3.1.2 Pavement Profile Data *33*

3.1.3 Dynamic Tire Force *35*

3.2 Effect of Axle Load on Dynamic Loads **38**

3.2.1 Vehicle Dynamics Simulation *38*

3.2.2 Dynamic Loads Due to Pavement Roughness *39*

3.3 Effect of Wide-Base Tire on Dynamic Loads **42**

3.3.1 Truck Modeling with Wide-Base Tire *42*

3.3.2 Dynamic Tire Force Comparison *44*

3.4 Summary **47**

CHAPTER 4 ANALYSIS OF PAVEMENT RESPONSE UNDER DYNAMIC LOADS WITH STOCHASTIC AMPLITUDE **49**

4.1 Principle of Impulse Response Method **49**

4.1.1 Theoretical Background *49*

4.1.2 Non-uniform Tire Contact Stresses *52*

4.1.3 Validation of Frequency Response Function 53

4.2 Pavement Test Section from LTPP 58

4.2.1 Field Truck Testing 58

4.2.2 Pavement Structure and Material Properties 60

4.3 Analysis of Dynamic Pavement Responses 63

4.3.1 Road Surface Profile and Dynamic Load 63

4.3.2 Determination of Equivalent Elastic Modulus of Asphalt Layer 67

4.3.3 Results of Calculated Pavement Responses 68

4.4 Analysis of Asphalt Pavement Fatigue Cracking under Dynamic Loads 71

4.4.1 Pavement Response Calculation under Dynamic Loads 71

4.4.2 Effects of Temperature and Vehicle Speed 74

4.4.3 Fatigue Life Analysis Considering Dynamic Loads 76

4.4.4 Consideration of Dynamic Loads in M-E Pavement Design and Analysis 79

4.5 Impact Analysis of Wide-Base Tire on Pavement Responses 83

4.5.1 Tire-Pavement Contact Stresses 83

4.5.2 Calculation of Pavement Responses 84

4.5.3 Pavement Response Ratios between Different Tire Configurations 88

4.6 Summary 91

CHAPTER 5 COMPARISON ANALYSIS OF TRAFFIC LOADING IMPACT USING NONLINEAR REGRESSION AND SUPPORT VECTOR REGRESSION MODELS 92

5.1 Data Collection and Processing 92

5.1.1 Truck Traffic Data from WIM 92

5.1.2 Pavement Structure and Field Performance 95

5.1.3 Climate Condition 97

5.2 Traditional Nonlinear Regression Model 98

5.3 Machine Learning Method 102

5.3.1 Principle of Support Vector Regression 102

5.3.2 Results and Discussion 104

5.4 Impact of Overweight Truck on Pavement Deterioration 108

5.5 Summary 114

CHAPTER 6 IMPACT ANALYSIS OF TRAFFIC LOADING ON ASPHALT PAVEMENT LIFE USING RANDOM SURVIVAL FOREST MODEL 115

6.1 Data Collection and Analysis 115

6.1.1 Data Collection from LTPP Database 115

6.1.2 Analysis of Axle Load Spectra 117

6.2 Random Survival Forest Model 119

6.2.1 Algorithm of Random Survival Forest 119

6.2.2 Ensemble of Cumulative Hazard Function 120

6.2.3 Prediction Error and Cross-Validation 122

6.3 Random Survival Forest Model Results 123

6.4 Impact of Overweight Traffic on Pavement Life 127

6.4.1 Effect of Overweight Traffic on Survival Probability 127

6.4.2 Effect of Overweight Traffic on Pavement Life Reduction 129

6.5 Summary 131

CHAPTER 7 CONCLUSIONS AND RECOMMENDATIONS 133

7.1 Findings 133

7.2 Conclusions 136

7.3 Limitations of Study 137

7.4 Recommendations for Future Work 138

REFERENCES 139

LIST OF FIGURES

Figure 1.1 Flowchart of pavement performance analysis considering vehicle-tire-pavement interaction 8

Figure 3.1 14-DOF full vehicle model (Setiawan et al., 2009) 31

Figure 3.2 Illustration of Class-5 Truck (Texas DOT, 2013) 32

Figure 3.3 Surface profiles used in the analysis: (a) profile 1; (b) profile 2; and (c) profile 3 at the selected LTPP section 35

Figure 3.4 Vertical tire forces under front and rear tires at 80 km/h on (a) profile 1 (IRI= 1.03 mm/km); (b) profile 2 (IRI= 2.05 mm/km); and (c) profile 3 (IRI= 3.09 mm/km) 37

Figure 3.5 Comparison of dynamic loads at different speeds (IRI=3.09m/km) 38

Figure 3.6 Illustration of axle configurations for (a) Class-7 and (b) Class-9 trucks (after Texas DOT (2013) 39

Figure 3.7 Dynamic tire forces: (a) Class-5 truck (Fz_R2); (b) Class-7 truck (Fz_R2); and (c) Class-9 truck (Fz_R3) at 48 km/h 41

Figure 3.8 DLCs on different pavement surface conditions: (a) Class-5 truck (Fz_R2); (b) Class-7 truck (Fz_R2); and (c) Class-9 truck (Fz_R3) at 48 km/h 42

Figure 3.9 Dynamic loads on different pavement surface conditions at 48 km/h: (a) dual-tire assembly (Class-5 truck); (b) wide-base tire (Class-5 truck); (c) dual-tire assembly (Class-9 truck) (d) wide-base tire (Class-9 truck) 45

Figure 3.10 Power spectral density of dynamic tire forces for dual-tire assembly and wide-base tire on different pavement roughness conditions at 48 km/h (Class-9 truck): (a) IRI = 1.01 m/km; (b) IRI = 2.05 m/km; (c) IRI = 3.09 km/h 46

Figure 3.11 Calculated DLCs of dynamic tire forces: (a) dual-tire assembly (Class-5 truck) (b) wide-base tire (Class-5 truck); (c) dual-tire assembly (Class-9 truck); (d) wide-base tire (Class-9 truck)..... 47
Figure 4.1 Flowchart of the impulse response method..... 49
Figure 4.2 Vertical tire contact stresses under each tire rib..... 53
Figure 4.3 (a) 3D FE model for steady-state dynamic analysis; (b) Non-uniform distribution of loads applied on the 3-D FE model in steady-state dynamic analysis..... 56
Figure 4.4 Frequency response functions of transverse strains obtained using the proposed FE model and compared to measured and simulated results in Hardy and Cebon (1992) 57
Figure 4.5 Creep compliance of the asphalt mixture at (a) wearing course; and (b) binder course 62
Figure 4.6 The converted relaxation modulus of the asphalt mixture at (a) wearing course; and (b) binder course (temperature = 5°C) 63
Figure 4.7 Pavement surface profiles on LTPP Ohio SPS-1 section (390108) 64
Figure 4.8 Dynamic loads under tandem axle in (a) time domain; and (b) frequency domain (PSD)..... 66
Figure 4.9 (a) Calculated vertical stress at the bottom of AC layer; (b) loading time calculation based on the results of the approaching-leaving model..... 67
Figure 4.10 Frequency response functions of transverse strains (E11) and longitudinal strains (E22) at the bottom of asphalt layer due to harmonic excitations 69
Figure 4.11 Frequency response functions of longitudinal strains (E22) at the bottom of asphalt layer in the wavenumber domain..... 70

Figure 4.12 Longitudinal strains at the bottom of asphalt layer at the selected loading frequencies in spatial domain (after the inverse Fourier transform) 71
Figure 4.13 Horizontal strains at the bottom of asphalt concrete layer: (a) single axle, (b) tandem axle, and (c) tridem axle in Class-5, Class-7, and Class-9 trucks 73
Figure 4.14 Relative ratio of fatigue life due to dynamic loads of single, tandem, and tridem axles on rough pavement with IRI of (a) 1.01 m/km; (b) 2.05 m/km; and (c) 3.09 m/km 78
Figure 4.15 Example of axle load distribution used in the analysis 81
Figure 4.16 Fatigue damage ratios calculated at different IRI values 81
Figure 4.17 Consideration of dynamic loads in M-E pavement analysis 83
Figure 4.18 Non-uniform distribution of contact stress (tire inflation pressure: 690 kPa): (a) dual-tire assembly; (b) wide-base tire 84
Figure 4.19 Comparison of pavement responses at critical locations under unit load of dual-tire assembly and wide-base tire (Class-9 truck; 48 km/h): (a) tensile strain; (b) compressive strain; (c) near-surface shear strain 86
Figure 4.20 Pavement responses at critical locations along road profile between the dual-tire assembly and wide-base tire (Class-9 truck at 48 km/h): (a) tensile strain; (b) compressive strain; (c) near-surface shear strain 88
Figure 5.1 Frequency distribution of average annual daily ESALs on (a) state highways, (b) Interstate highways and (c) US highways in NJ 93
Figure 5.2 Gaussian distribution of axle load spectra of (a) single, (b) tandem, and (c) tridem axle on I-80 in 2000 95

Figure 5.3 Frequency distribution of (a) surface layer thickness of flexible pavement and (b) surface layer thickness of composite/rigid Pavement 96

Figure 5.4 Example of deterioration trend of pavement performance (I-80B)..... 97

Figure 5.5 Actual observed and fitted SDI based on multiple nonlinear regression models for flexible pavement structure on (a) state highways; (b) Interstate highways; (c) US highways; and composite/rigid pavement structure on (d) state highways; (e) Interstate highways; (f) US highways..... 101

Figure 5.6 Actual observed and fitted SDI based on SVR models for flexible pavement structure on (a) state highways; (b) Interstate highways; (c) US highways; and composite/rigid pavement structure on (d) state highways; (e) Interstate highways; (f) US highways 107

Figure 5.7 Axle load spectra at the selected sites: (a) NJ-138; (b) I-195; (c) US-30; (d) NJ-33; (e) I-80; (f) US-202 (solid line—: non-overweight; dotte dline---: overweight). 111

Figure 5.8 Pavement performance under total and nonverweight truck traffic for flexible pavements (a) state highway; (b) Interstate highway; (c) US highway; and composite pavements (d) state higway; (e) Interstate highway; (f) US highway..... 113

Figure 6.1Example of fitted Gaussian distribution of axle load spectra: (a) single axle; and (b) tandem axle (SHRP_ID: 040501, 1998)..... 118

Figure 6.2 Variable Importance for (a) alligator cracking; (b) longitudinal cracking at wheel-path; and (c) rut depth 125

Figure 6.3 Prediction error of survival models: (a) alligator cracking; (b) longitudinal cracking at wheel-path; and (c) rut depth..... 126

Figure 6.4 Axle load spectra: (a) non-overweight traffic; (b) total traffic..... 128

Figure 6.5 Example of survival curve for total and non-overweight traffic: (a) alligator cracking; (b) longitudinal cracking at wheel-path; (c) rut depth at the selected pavement section 129
Figure 6.6 Distribution of survival life: (a) alligator cracking; (b) longitudinal cracking; (c) rut depth; and (d) Boxplots of survival life differences under total traffic and non-overweight traffic 131

LIST OF TABLES

Table 3.1 Truck configuration and parameters in TruckSim software 32

Table 3.2 IRI of pavement section (320201) in Nevada measured at different years 33

Table 3.3 Tire configuration and parameters applied in the vehicle simulation..... 44

Table 4.1 Material parameters of the instrumented pavement section at TRL test track (Hardy and Cebon, 1992)..... 54

Table 4.2 Measured tensile strains under front and rear axles of tandem axle at LTPP Ohio SPS-1 section (390108) at 47 km/h (unit: micro) 60

Table 4.3 Measured tensile strains under front and rear axles of tandem axle at LTPP Ohio SPS-1 section (390108) at 62 km/h (unit: micro) 60

Table 4.4 Prony series parameters for the asphalt mixtures at AC layer at reference temperature of 5°C..... 62

Table 4.5 Tensile strains caused by different axle types and loads (micro) 74

Table 4.6 Tensile strains caused by dynamic axle loads at different vehicle speeds and temperatures (micro)..... 75

Table 4.7 Calculated amplification ratio of tensile strains at different vehicle speeds and temperatures..... 76

Table 4.8 Response ratio of maximum pavement response (Class-5 truck)..... 89

Table 4.9 Response ratio of maximum pavement responses (Class-9 truck) 89

Table 4.10 The range of pavement response ratio along pavement section 90

Table 5.1 Coefficients and R-square values of regression model based on average daily ESALs..... 99

Table 5.2 Coefficients of regression models based on axle load spectra..... 102

Table 5.3 Error metric of regression model based on axle load spectra 102

Table 5.4 Cross-validation results of SVR with different variables 106

Table 5.5 Total and non-overweight (N-O) traffic at the selected routes 110

Table 5.6 Percentage of overweight axles and pavement life ratio for selected routes .. 114

Table 6.1 LTPP InfoPave database tables and extracted data elements 117

Table 6.2 Summary of Gaussian distribution model parameters for axle load spectra .. 119

CHAPTER 1 INTRODUCTION

1.1 Background

Pavement responses are affected by the magnitude and frequency of dynamic loads generated by vehicles, which are significantly dependent on axle configuration, pavement surface conditions, and vehicle speed. Random amplitudes of dynamic loads are generated by rough road surface due to development of pavement distresses after initial construction. In addition, tire-pavement contact stresses in the contact patch are not the same as tire inflation pressure and varies depending tire loads and vehicle operation condition. Pavement deterioration is induced by mechanistic responses in pavement structure under vehicle loads. It is expected that dynamic loads on rough road surface would accelerate pavement deterioration and degrade surface smoothness. Therefore, vehicle-tire-pavement interaction model is needed for analyzing dynamic pavement responses and deterioration subjected to moving loads and taking pavement roughness into consideration.

Mechanical-empirical (M-E) method is implemented to design pavement structures, which was developed under National Cooperative Research Program Projects 1-37A (ARA Inc., 2004). In Mechanical-Empirical Pavement Design Guide (MEPDG), principles of engineering mechanics are applied to calculate pavement response under traffic loading. The empirical transfer functions are then used to predict long-term pavement performance through local calibrations.

The new generation of wide-base tires 445/50R22.5 and 455/55R22.5 came to the market in the early 2000s and show sustainable benefits in trucking operations and environment impacts due to less rolling resistance at tire-pavement interface. The wide-base tires enhance fuel efficiency and hauling capacity, reduce tire costs and repair, and

improve ride comfortability and vehicle stability (Al-Qadi and Elseifi, 2007). Besides, wide-base tires show better safety potential due to less hydroplaning potential at rainy conditions (Ding and Wang, 2020). Despite the advantages of new wide-base tires mentioned above, it was critical to estimate the influence on critical pavement response and long-term performance after switching from conventional dual tires to new wide-base tires.

On the other hand, Long-term monitoring of in-service pavements is used to develop pavement performance models in pavement management system. Previous studies mainly used traditional statistical regression methods to quantify pavement damage due to vehicular loading. Because of the complexity of problem, the relationship between pavement performance and influential variables may not be apparent in traditional regression models.

Machine learning has the ability of automatically learning and improving from data mining without being explicitly programmed, which make it applicable for the field measurement datasets with high-dimensionality and high-complexity. Application of machine learning approach for pavement performance prediction has become popular in recent years. Machine leaning method can provide more accurate prediction models of pavement performance when complex traffic variables are taken into consideration. The developed models can be applied to predict future pavement condition and assist in optimally allocating maintenance and rehabilitation costs in pavement management system.

1.2 Problem Statement

In previous studies, dynamic pavement responses subjected to moving loads were investigated using the concentrated or distributed moving loads with harmonic shapes, or time-dependent moving loads, which neglected the random nature of moving loads due to pavement surface roughness (Al-Qadi et al., 2008b; Beskou and Theodorakopoulos, 2011; Wang and Al-Qadi, 2011). It has been documented that tire-pavement contact stresses are three-dimensional (3-D) and their magnitudes and distributions vary depending on loads and tire inflation pressure (Al-Qadi and Wang, 2011; Wang et al., 2012; Hu et al., 2015). Previous works have proposed to use advanced finite element models to capture pavement responses under moving loads considering realistic tire-pavement contact stresses, viscoelastic property of asphalt layer, and nonlinear modulus of unbound materials in M-E pavement analysis (Wang and Li, 2015; Wang et al., 2015a; Chen et al., 2016). However, the pavement response induced by dynamic loads with stochastic magnitude on rough pavement surface were not considered in the pavement analysis, which might result in underestimation of pavement damage. Therefore, impact of dynamic loads due to pavement roughness condition need to be analyzed to accurately predict pavement performance in the framework of M-E pavement design and analysis.

The impulse response method was originally introduced by Newland (1985) to investigate the responses of a linear system subjected a time-dependent input combined with the Fourier transform. It was used in conjunction with convolutional integral method to calculate flexible pavement responses flexible pavement response under dynamic loads with stochastic amplitudes (Hardy and Cebon, 1992; 1993). These previous works used simplified model in the steady response analysis, such as uniform loading the circular or

rectangular area and quarter-car model. It is not clear how these simplifications affect the calculated dynamic pavement responses. Few researches have used field measurements to validate the prediction of dynamic pavement responses subjected to random dynamic loads under moving truck. In addition, the effect of pavement surface roughness on critical responses of asphalt pavement such as the tensile or shear strain in the asphalt layer and the compressive strain on top of subgrade has not been thoroughly investigated.

The wide-base 455/55R22.5 would cause greater potential of bottom-up fatigue cracking and subgrade rutting than the dual-tire assembly on most tested sections, but less potential of near-surface cracking in the accelerated pavement testing. The asphalt pavement was simulated under moving load with constant force and non-uniform contact stress, and the results indicated that the near-surface pavement response were more impacted by the localized distribution of contact stress (Xue and Weaver, 2011; Al-Qadi and Wang, 2012). However, few researches have considered vehicle-tire-pavement interaction for analyzing flexible pavement responses under wide-base tires. Due to the different tire stiffness and load transmissibility values, it is expected that the impact of wide-base tire on pavement response would be affected by dynamic loads excited by uneven pavement surface profiles.

Previous studies have employed machine learning approaches to predict the pavement performance considering a variety of influential factors and concluded that the machine learning models significantly outperformed linear and nonlinear regression models (Ziari et al., 2016; Gong et al., 2018; Marcelino et al., 2019). Two or more algorithms could be combined for better prediction performance to investigate the influence of independent variables on pavement performance (Fathi et al., 2019;

Karballaeezadeh et al., 2019). Furthermore, machine learning approaches could be extended and applied for survival analysis (Breiman, 2001). Unlike traditional survival analysis, an assumption of distribution of the lifetimes or a linear-exponential form for the treatment effects was not needed in advanced survival analysis models (Ishwaran and Kogalur, 2007).

It is well accepted that vehicular loading has significant influence on development of load-related asphalt pavement distresses, such as alligator cracking, longitudinal cracking at wheel-path, and rutting. Weigh-in-motion (WIM) devices are used to capture and store gross vehicle weight, axle loads, and truck configurations information when trucks are passing over the stations. The WIM data helps to comprehensively understand real vehicular loadings on pavement sections, but it is a challenge to incorporate traffic data into pavement performance models. Therefore, it is needed to use machine learning approaches to investigate the impact of traffic loads on pavement performance when complicated axle load spectra are considered in the models.

To preserve infrastructure, federal and state transportation agencies regulate the limit of truck loads on highways (Federal Highway Administration, 2015; US Department of Transportation, 2018). The impact of overweight traffic on pavement damage and service life reduction need be considered to preserve infrastructure condition. Prediction model of pavement performance developed using machine learning method is expected to provide an advanced approach to investigate the impacts of overweight on pavement damage.

1.3 Objective and Methodology

This study aims to quantify traffic loading impact on flexible pavement performance using vehicle-tire-pavement interaction modeling and machine learning approaches. The first objective is to analyze dynamic responses of flexible pavement and develop an approach to consider roughness-induced dynamic loads in M-E analysis. The following research tasks were conducted:

1) A full-truck model was adopted to estimate the dynamic tire forces considering pavement surface conditions. The influence of pavement roughness conditions, vehicle speeds, truck configurations, and axle type and loads on dynamic tire forces were considered.
2) A modified method was proposed to derive frequency response functions under harmonic loads using the equivalent modulus of asphalt layer at the specific temperature and loading frequency. After that, the convolution integral method was used to simulate pavement responses under non-stationary loads with random amplitudes. The field instrumentation measurements in Long-Term Pavement Performance (LTPP) database were utilized to validate the impulse response method.
3) The relative ratio of fatigue life was defined to estimate fatigue damage induced by dynamic axle loads on different pavement roughness conditions. A methodology was proposed to incorporate the impact of dynamic loads on fatigue cracking development in the framework of M-E pavement design and analysis.
4) Dynamic responses of flexible pavements induced by wide-base tires considering pavement roughness condition were analyzed using the integrated vehicle-tire-

pavement interaction approach. The impact of wide-base tire was evaluated through the ratio of critical pavement responses between wide-base tire and dual-tire assembly, respectively, for the potential of fatigue cracking, near-surface cracking, and subgrade rutting.

Figure 1.1 shows the flowchart of pavement performance analysis considering vehicle-tire-pavement interaction. The dynamic tire forces under moving vehicles were estimated using a full-vehicle model. The effects of pavement roughness, vehicle speeds, axles load, and tire types on dynamic tire forces were investigated. The impulse response method was used to calculate pavement responses under dynamic loads. The dynamic pavement responses subject to various axle loads on three pavement surface profiles at different vehicle speeds were estimated. The effect of wide-base tire on pavement responses was analyzed by comparing pavement responses under wide-base tire and dual-tire assembly. The relative ratio of fatigue life was defined to estimate fatigue damage induced by dynamic axle loads on different pavement roughness conditions. Finally, a methodology was proposed to incorporate the impact of dynamic loads on fatigue cracking development in the framework of M-E pavement design and analysis.

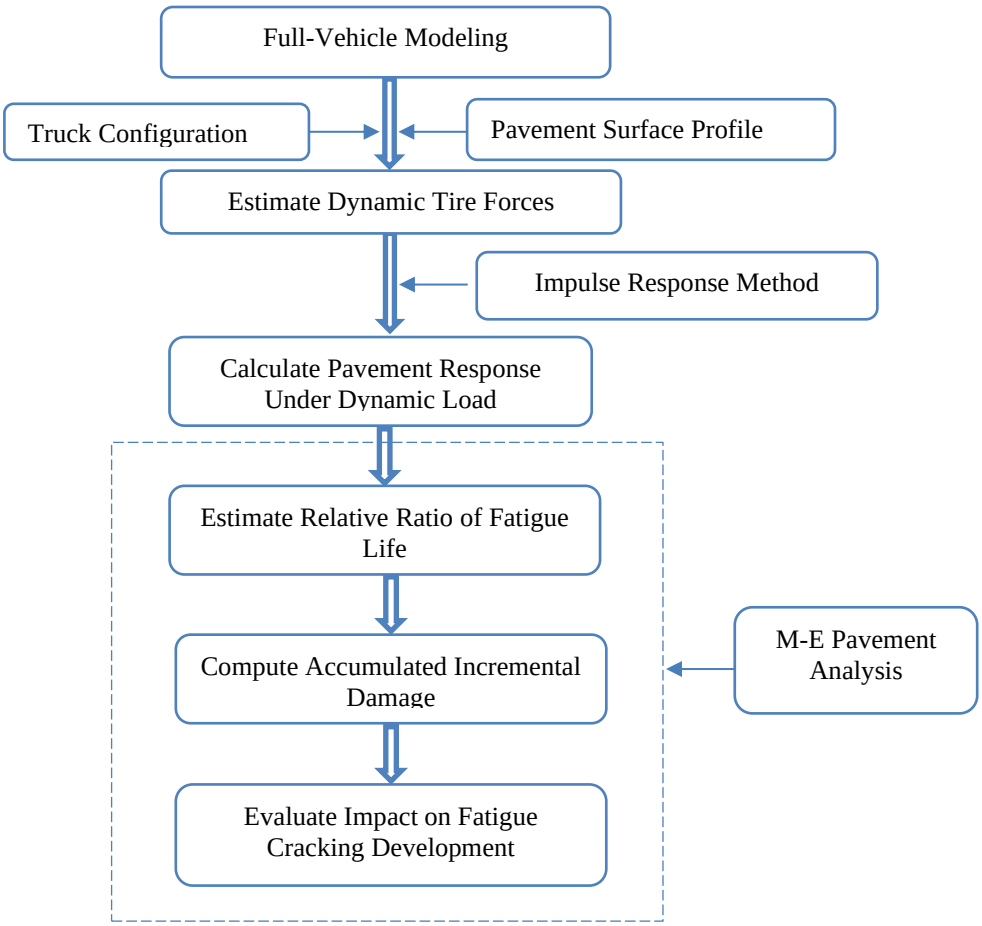

Figure 1.1 Flowchart of pavement performance analysis considering vehicle-tire-pavement interaction

The second objective is to use machine learning approaches, including support vector regression (SVR) and random survival forest models, to investigate the impact of traffic loads on pavement performances. The following research tasks were conducted:

1) Traditional regression model and machine learning method were employed to quantify the impact of traffic loading on pavement performance based on field data collected from pavement management system of NJDOT. Multi-variable nonlinear regression method and SVR method were applied and compared in terms of prediction accuracy and error.

2) The proposed SVR models of pavement performance were further used to analyze pavement deterioration caused by overweight trucks with different truck traffic and axle load distributions.
3) Random survival forest method was used to establish the prediction models of load-related pavement distresses under the influence of traffic loading, pavement structure, and climate condition extracted from LTPP database. The variable importance technology was used to select the appropriate variables in the model and reduce prediction error.
4) The derived random survival forest models were applied to estimate survival probability of asphalt pavement life and evaluate the impact of overweight traffic on the reduction of pavement life.

CHAPTER 2 LITERATURE REVIEW

2.1 Estimation of Dynamic Loads Under Moving Vehicle

Experimental programs and truck modeling are the two basic approaches that have been used to estimate dynamic loads. DLC, defined as the ratio of the standard deviation of dynamic loads to the static load (Cebon, 1999), is commonly adopted to assess the variation level of dynamic loads. Kulakowski and Kenis (1995) characterized the dynamic wheel loads induced by a two-axle truck instrumented with strain gauges, accelerometers, and linear variable differential transformer to investigate the correlations among DLCs and test variables. It was found that the DLCs generated by wide-base tire was 10-12% lower than that generated by dual tire, and air suspension induced lower dynamic loads if the induced DLC was below 0.15.

Mikhail and Mamlouk (1997) calculated the structural response of flexible pavements under different dynamic loads and pavement roughness conditions. The Florida Comprehensive Pavement Analysis System conducted by the Texas Transportation Institute for the Florida Department of Transportation, which included a tire-force prediction model that predicted the dynamic tire loads for different types of vehicles traveling on a straight asphalt road at constant speeds, was adopted. The FE models were used to analyze the vehicle-pavement interaction. The walking-beam suspension caused more dynamic-load variation than the other two suspension types. Higher speeds produced more dynamic-force variability, and an increase in pavement roughness produced more dynamic-load variability. The stiffness of the pavement section affected the response of pavement, with weak pavement sections producing higher displacements and strains in the

pavement structure. For example, the pavement displacement increased by approximately 10 times at 20 km/h as compared to 130 km/h.

Liu et al. (1998) employed actual road profiles and a half-axle load model to estimate the dynamic forces and rate of dynamic forces exerted on a pavement surface using a spectral density method and a finite difference method, respectively. A very good correlation existed between the physical variables and ride quality index or serviceability index, indicating that the deterioration of pavement structures was closely related to the rate of dynamic forces.

Sun (2001) presented a theoretical model for determining IRI and present serviceability index in term of the power spectral density (PSD) of pavement roughness. The frequency response functions of quarter-car model and CHOLE-type profilometer were obtained by means of stochastic process theory. Correlation of IRI and PSD became possible based on their PSD-based expression. Sun (2003) simulated the IRI for evaluating the pavement surface roughness using the PSD of pavement surface fluctuation. Quarter-car models were adopted to simulate the vehicle response. Surface roughness in time domain was generated based on 36 known PSDs of roughness. The statistical analysis of the system output showed that IRI was linearly correlated with the standard deviation of relative vertical velocity between the axle and sprung mass. A linear regression equation was obtained based on which further analysis was conducted to represent IRI in terms of PSD of pavement roughness.

Steyn et al. (2013) investigated the dynamic attribution of pavement unevenness. Based on ISO 8608 grading, the inverse Fourier transform was applied to generate the 300-meter pavement surface profile with the distance sampling interval of 0.1 m. The surface

profiles were used in TruckSim to calculate the dynamic loads. Car, bus, and truck were simulated at the speeds of 20, 40, 60, 80, 100, and 120 km/h. The root mean square value of total weighted acceleration was computed to evaluate the drivers' riding comfort and goods' integrity. It was found that, compared to speed, surface roughness was more critical. The magnitudes of acceleration and DLCs varied depending on different spring types of vehicles, and generally the pavement deterioration meant the increase of human riding discomfort, acceleration, and dynamic overload.

Almeida and Picado-Santos (2015) presented a methodological framework of the traffic factor (TF) estimation taking vehicle-pavement interaction into account. A five-axle single-trailer truck and a two-axle single-unit truck driving at the speeds of 40, 80, 60, and 100 km/h were assumed to simulate the dynamic loads. Empty, fully loaded, overloaded by 10% 20% and 30%, and underloaded by 10% 20% and 30% trucks were utilized. The 120-mm and 280-mm thick flexible pavements with the specific international roughness index (IRI) (0, 1, 2, 3, 4, and 5 m/km) were considered. A 3-D boundary element method was applied to calculate the structure responses at the critical locations, while the mechanistic-empirical pavement design guideline was used to compute the pavement responses. TF was found in linear relation with IRI and in exponential relationship with GVW. The results indicated that increasing the IRI by 1m/km would lead to up to 27% increase of TFs.

Navarrina et al. (2015) derived a comprehensive model for fatigue analysis of flexible pavements taking the impacts of dynamic axle loads into consideration. The development of the accumulated pavement fatigue damage in terms of the time passed since the construction was quantified by the accumulated fatigue damage indicator, and the

dynamic counterpart of the accumulated fatigue damage indicator function was derived. To quantify the IRI and effective dynamic load amplification factor, a quarter-vehicle model was proposed to develop the Laplace transforms of road profiles. Based on the IRI and prediction functions of the amplification factor of effective dynamic loads, the fully operational function, which predicted the time evolution of the road profile, was derived. It was indicated that the dynamic axle loads caused a dramatic decrease in the predicted pavement life.

Bilodeau et al. (2017) used a new multibody dynamic truck model to calculate the vertical force on pavement with various surface profiles, after which the DLCs estimated for 5400 subsections in Quebec were related to the corresponding IRI. The pavement response was evaluated by WinJulea to compute the allowable number of load repetitions prior to fatigue failure and structural rutting failure. The static life consumption rates and relative life consumption were calculated for static loading scenarios, and the dynamic load ratio and relative life consumption were computed for dynamic loading scenarios. The linear curve of relative life consumption for static loading and the nonlinear curve of relative consumption for dynamic loading were plotted and compared. It was found that the pavement life determined by fatigue failure was reduced by the average of 29.2% and the life based on rutting failure decreased by the average of 20% if dynamic loading was considered in the analysis.

Ueckermann and Oeser (2015) developed approaches for a 3-D assessment of pavement evenness data, including pavement evenness in longitudinal and transverse directions, based on 3-D vehicle models using MATLAB. According to the criteria of effective evenness index, a passenger car was created to assess driving comfort, and the

transfer functions of dynamic wheel loads for front wheels and driver's vertical acceleration were presented. A truck-semitrailer was used to assess the pavement and cargo loading, and the transfer functions of dynamic wheel loads for pure vertical excitation and the vertical acceleration on the cargo area of the semitrailer above the central axle were obtained. The 3-D models were verified using the measured data and results of the ADAMS model. The wheel tracks, acceleration of cargo load, dynamic wheel loads, and acceleration the driver perceived in the 3-D models were compared with those in the one-dimensional/two-dimensional models in existence. It was found that the planar model was subjected to a much lower vibrational impact, and the acceleration and forces in the 3-D models were well in line with the values in the existing one-dimensional/two-dimensional models, which could be used for values of limit in terms of target.

Goenaga et al. (2019) evaluated the effects of pavement roughness and vehicle speed on the dynamic loads generated at the interface of tire and pavement along with their effects on the performance of pavement structures. A quarter-truck model was used to simulate the dynamic axle loads generated at interface due to roughness. A correlation model between IRI and dynamic load index was developed. The traffic correction factor was proposed to account for the effects of dynamic load induced by roughness and vehicle speed. The proposed traffic correction factor could be used to modify the estimation of traffic damage on the road sections with high roughness levels, therefore improving the future prediction of pavement performance.

2.2 Calculation of Pavement Response Under Dynamic Loads

2.2.1 Pavement Response Under Point or Line Loads

2.2.1.1 Beam or Plate Laid on Foundation

Lombaert et al. (2000) developed a numerical modelling of free field traffic-induced vibrations during the passage of a vehicle on an uneven road. A transfer function between source and receiver for the dynamic interaction between road and soil was used to calculate the free field response. The calculation was based on a dynamic substructure approach, by using an analytical beam model for road and a boundary element method for soil. The methodology was validated utilizing the analytical results and finally presented by a numerical example of which the free field vibrations during the passage of a vehicle on the traffic plateau were estimated.

Lombaert et al. (2004) presented the procedure of a stochastic solution for the calculation of non-stationary free field responses induced by a moving load with a random amplitude. A non-stationary autocorrelation function and a time-dependent spectral density were used to characterize the free field response at a fixed point. The non-stationary solution was obtained from the solution in the case of a moving load with a deterministic amplitude. The solution for non-stationary free field response induced by a moving load with a random amplitude was derived in terms of a double forward Fourier transform of the non-stationary auto correlation function.

Sun (2005) investigated the dynamic displacement of a plate under moving harmonic point and line loads. The solution was represented by the convolution of the dynamic Green’s function of plate. An approximate relationship between the critical load velocity and critical frequency was established analytically. It was indicated that the

maximum displacement response occurred at the center of the moving load and traveled at the same speed with the load. Sun (2006) used the triple Fourier transform to derive the formulation of a plate with infinite dimensions (without boundary conditions) on an elastic foundation under a moving concentrated and line load of constant speed and amplitude. A closed-form solution of displacement field was obtained for moving loads with subsonic, transonic, and supersonic speeds.

Yao et al. (2009) characterized the geometric roughness of the pavement through considering the pavement roughness as a sine function and simplifying the quarter-vehicle to the vibration system with two degree of freedom. The expressions of dynamic loads of the system were obtained and utilized to investigate the steady-state responses of the infinite rough pavement on a Kelvin-type foundation to calculate the dynamic responses of rough pavement structure under traffic loads. The theoretical solutions of vertical displacement responses of the pavement structure were formulated based on the double Fourier transform, and the solutions could be transformed to the corresponding classical solution of static problem. By adopting the fast Fourier transform (FFT), the numerical results were obtained to investigate the influence of velocity of moving load and parameters of rough pavement and foundation on the dynamic displacement responses.

Lv et al. (2010) proposed a dynamic model of asphalt pavement under a moving concentrated load. The viscoelastic characteristics of asphalt and base layers were considered, the pavement was regarded as an infinite beam on a viscoelastic base. By applying the Green's functions, Fourier transforms, and Laplace transforms, the analytical solution in transient was derived. Since the viscosity of the asphalt pavement was considered in the model, the analytical solution could be employed to analyze more of

factors that impacted the dynamic response, for example road material properties, temperature, and vehicle speed.

Lu and Yao (2013) developed a new model for calculating the pavement vibration due to the dynamic vehicle-road interaction. This model included vehicles, an uneven pavement surface layer, a base layer, and a subgrade, and utilized the moving axle loads and geometric unevenness as the inputs. Using the Fourier transform, the dynamic equilibrium equations of the coupling system were then solved in the frequency-wavenumber domain. The responses in time domain were evaluated by applying the inverse fast Fourier transform. The influence of pavement properties, moving vehicle speed, wavelength and magnitude of pavement unevenness on the dynamic displacement response were investigated systematically.

2.2.1.2 Multi-Layer System

De Barros and Luco (1994) introduced a procedure to obtain the steady-state displacements and stresses within a multi-layered viscoelastic half-space generated by a buried or surface point load moving with a constant speed parallel to the surface of the half-space. The approach was based on an integral representation of the complete response in terms of wavenumbers. The results in the time domain were obtained by the Fourier synthesis of the frequency response which in turn was obtained by numerical integration over one horizontal wavenumber. The numerical results of displacement and stress fields on the surface and within the half-space were presented for surface and buried loads moving with various subsonic and supersonic speeds.

Liu (2001) established a multi-layer, four-dimensional spatial and temporal, physical model for the dynamic responses of a road structure in an analytic framework by

integrating vehicle dynamics, road profiles characteristics, frictional characteristics of vehicle-road contacts, and pavement viscoelastic properties. The surface roughness effect on the dynamic response of road structures was investigated.

Zhao et al. (2015) investigated a frequency domain approach to calculate the transient response by applying the discrete Fourier transform. The analytical and calculated responses were compared for the standard Maxwell model with three parameters and the solutions in time and frequency domains for asphalt concrete were compared to verify the accuracy and effectiveness of the frequency domain approach. The impact of aliasing of the frequency domain approach could effectively decrease by adopting a small sampling interval for the time domain excitation function.

2.2.2 Pavement Response Under Area Loads

2.2.2.1 Beam or Plate Laid on Foundation

Hardy and Cebon (1992; 1993) used the impulse response method, which was originally introduced by Newland (1985), to investigate the responses of a linear system subjected a time-dependent input combined with the Fourier transform to assess the flexible pavement responses subjected to moving loads estimated by quarter-car vehicle model. Hardy and Cebon (1994) used a validated dynamic road-response model and simplified the dynamic calculation procedure (quasi-dynamic computation) to investigate the dynamic responses of flexible pavements to the fluctuating and moving wheel loads. Hardy (1995) extended the convolution integral method to consider time-dependent loads on an infinite system.

Kim and Roesset (1998) applied the triple Fourier transform in time, space (in transverse direction), and moving space (in longitudinal direction) to consider the moving

loads with random amplitudes, and used the double Fourier transform in space and moving space for steady-state responses to moving harmonic loads. The pavement model consisted of an infinite plate placed on an elastic foundation.

Cai et al. (2009) presented an investigation of the steady-state response of pavement systems subjected to a moving traffic load. The traffic loads were simulated by four rectangular load pressures, and the rigid and flexible pavement systems were regarded as an infinite plate resting on a poroelastic half-space soil medium. The frequency-wavenumber domain solution of the pavement system was obtained by the compatibility condition between the plate and poroelastic half-space. By applying the inverse fast Fourier transform, the time-domain solution was obtained.

Sun (2013) introduced a unified theory for dynamics of vehicle–pavement interaction under moving and stochastic loads, including three major aspects of the subject: pavement surface, tire–pavement contact forces, and response of continuum media under moving and stochastic vehicular loads. Under the subject of pavement surface, the spectrum of thermal joints was analyzed using the Fourier analysis of a periodic function. The one-dimensional and two-dimensional random field models of the pavement surface were discussed given three different assumptions. At a constant speed of travel, random field of pavement surface served as a stationary stochastic process exciting vehicle vibration, which, in turn, generated contact force at the interface of tire and pavement. The contact forces were analyzed in the time and frequency domains using random vibration theory. Under the subject of response of continuum media under moving and stochastic vehicular loads, both time-domain and frequency-domain analyses were presented for the analytic treatment of moving load problem.

Lu et al. (2014) developed a 3-D model for the steady-state response of a pavement-subgrade-soft ground system subjected to moving traffic loads. A semi-analytical model of wave propagation which was subjected to four rectangular moving loads was introduced based on a calculation method of the dynamic stiffness matrix of the ground. The pavement and subgrade were regarded as two elastic layers resting on a poroelastic half-space soil medium. The frequency-wavenumber domain solution of the road system was obtained by the compatibility condition at the interface of structural layers. The numerical results showed that the influence of load speed and excitation frequency on the dynamic response of the road system was significant.

2.2.2.2 Multi-Layer System

Chatti and Yun (1996) proposed a complex response method of transient analysis to consider circular area moving arbitrary loads on an elastic and damped multi-layered system, incorporating the influences of wave propagation and frequency-dependent material properties of asphalt concrete. The moving loads were simulated as a series of pulses with their periods equaled to the time taken for a wheel to pass a fixed point in pavement.

Khavassefat et al. (2014) introduced a computational framework to calculate flexible pavement responses induced by moving vehicles. FE models were used to establish the frequency response function of the pavement, and the dynamic loads were calculated via a quarter-car model. The convolution method was applied to predict the horizontal stresses in the frequency-wavenumber domain. The effect of pavement detonation on the pavement response was investigated based on the field measurements of road surface profiles in Sweden.

2.3 Evaluation of Pavement Damage Under Dynamic Loads

2.3.1 Effect of Dynamic Loads on Pavement Damage

Chatti and Lee (2002) studied the relationship between distress index and ride quality index (RQI) using three independent data sets selected from the pavement network in Michigan. It was indicated that the composite and flexible pavements had lower critical RQI-values than the rigid pavements, after which the correlation between dynamic truck response and RQI was analyzed. According to the dynamic load generated by TruckSim program, the second axle of a typical 5-axle tractor-semi-trailer was used to represent the aggregate loads from all trucks. The DLC and 95th percentile dynamic load vs. RQI curves were plotted for various roughness levels (RQI=30, 40, 50, 60, 70, and higher than 80). The relative dynamic load-induced damage in the pavements was estimated by a 4th power law, and the roughness threshold values were determined through computing the theoretical percent reduction in pavement life. The lower bound values were found to be 61, 50, and 47 for rigid, composite, and flexible pavements, respectively. The upper bound values were found to be 77, 70, and 66 for rigid, composite, and flexible pavements, respectively.

Kanai et al. (2010) analyzed the impacts of dynamic loads under heavy vehicles caused by pavement roughness on asphalt pavement damage. The pavement surface profile was obtained through the displacement of the oscillator expressed by Langevin equation, and Profile Viewing and Analysis (ProVAL) was used to compute IRI based on the surface profile. Eight surface profiles ranging from 0.5 to 4.0 m/km at an internal of 0.5 m/km were generated. Multiple regression analysis was applied to present IRI in terms of temperature and cohesive resistance. According to the surface profile, TruckSim, a vehicle running

imitation software, was used to estimate the dynamic wheel loads of a 20-ton dump vehicle at the speeds of 40, 60, 80, and 100 km/h. The compressive strain at the top of the subgrade and the strain at the bottom of the asphalt layer under circular uniformly distributed loads of dual-tire assembly were calculated by a analysis program for multi-layer elasticity. The allowable number of repetitions of wheel passage reached to the critical points when the cracking ratio equaled to 20% and when the rut depth due to permanent deformation equaled to 15 mm. It was found that, at some points, the low allowable number of repetitions of wheel passage either of asphalt layer or subgrade decreased extremely, and as IRI increased the asphalt layer or subgrade pavement damage increased with a higher rate at higher speed.

Park (2010) assessed the pavement damage index of the 12.5 mm+PG58-22 and 12.5mm+PG64-22 asphalt mixtures. Vehicle speed, suspension type, and pavement surface profiles were considered as factors that affected the dynamic load generated by moving vehicles. For the 3-axle vehicle with 10 tries and the GVW of 204.6 kN, the flat leaf suspension was used at the front axle, and the walking beam and air spring suspensions were applied at the rear tandem axle to simulate the dynamic loads in TruckSim. The IRI of 0, 0.9, 1.2, 1.7, 2.3, and 3.0 m/km and vehicle speeds of 40, 60, 100, 120, and 160 km/h were applied to predict the dynamic loads. It was found that rougher pavement surface and higher speed increased dynamic load significantly. The pavement damage index model, which could be used to predict pavement life based on the target and as-built profile, was developed by relating to the coefficient of the variance of dynamic loads. Creep compliance tests were conducted to estimate fracture parameter of the asphalt mixtures. It was indicated

that higher dynamic load variability, lower temperature, and walking beam suspension would cause more pavement fatigue life reduction.

Navarrina et al. (2015) used quarter-car model and introduced dynamic load amplification factor to obtain vertical dynamic loads. The pavement structure was considered as a linear elastic system, and stresses and strains were proportional to external loads. The accumulative pavement damage was computed under the time evolution of IRI. It indicated that the service life of asphalt pavement was reduced by 40% after considering dynamic loads.

Bilodeau et al. (2017) developed a linear relationship between DLC and IRI to estimate dynamic loads. Multi-layer elastic theory was used to calculate mechanistic pavement responses. The relative life consumption was computed using the allowable load repetitions prior to failure distress for static and dynamic loading cases. It was found that the pavement life reduced by 29% due to fatigue cracking and by 20% due to rutting when dynamic loads were considered.

Rys (2019) derived the dynamic axle load spectrum from the static axle load spectrum obtained from Weigh-in-Motion (WIM) data. Given the dynamic axle load spectrum, pavement performance was estimated for different pavement structures. The analysis results indicated that thinner pavement structures were more impacted by dynamic loads.

Goenaga et al. (2019) defined traffic correction factor to consider the relative damage induced by rough pavement surface and fitted the traffic correction as a function of speed and IRI. It was found that the remaining life reduced by up to 40% if dynamic loads were taken into consideration. Therefore, it is important to consider dynamic loads

in performance analysis and life prediction of asphalt pavement. In the previous researches, quarter-car model was used to estimate dynamic tire forces on rough pavement surface condition. The complicated interaction between vehicle and pavement was not considered, and the impacts of axle type and tire configuration were ignored.

2.3.2 Effect of Wide-Base Tire on Pavement Response and Damage

To assess the impacts of the new generation of wide-base tires, FE models have been applied to calculate the pavement responses in flexible pavements. FE models are efficient at simulating characterization of viscoelastic materials, behavior of nonlinear granular material, 3-D contact stresses, moving loads, and layer interaction. Al-Qadi and Wang (2012) investigated the influence of wide-base tires on full-depth and thin asphalt pavements based on accelerated pavement testing and advanced FE modeling. Dual, the first-generation 425, and the new-generation 455 wide-base tires were considered. The analysis revealed that the wide-base 425 induced the greatest pavement damage. The wide-base 455 caused greater bottom-up fatigue cracking and increased potential for subgrade rutting than the dual-tire assembly on most tested sections. The effect of wide-base tires on fatigue cracking and subgrade rutting potential became less obvious on a stronger pavement structure. The FE modeling results indicated that the wide-base 455 tires caused less or similar rutting potential in thin asphalt pavement and less near-surface cracking potential in thick asphalt pavement.

Greene et al. (2010) reported that the 445/50R22.5 wide-base tire was found to produce more rutting on a dense-graded pavement surface and was shown to produce more bottom-up cracking than the dual-tire assembly in a controlled accelerated pavement testing program. Wang et al. (2014) calculated damage ratios between wide-base tire and

dual-tire assembly using the pavement response and performance data from previous studies. It was suggested that wide-base tire increased the pavement damage on thin asphalt pavements but the influence on Interstate highways was limited.

Hernandez et al. (2016) used the validated FE modeling of the new generation of wide-base tires and a conventional dual-tire assembly to evaluate the effects of wide-base tires on pavement responses. The pavement responses under wide-base tire were higher than those under conventional dual-tire assembly, and the difference decreased as the pavement thickness increased. The average percent differences of longitudinal tensile strains at the bottom of the asphalt concrete layer were 23.2% and 14.7% for thin and thick pavements, respectively. The difference could be used as input into transfer functions to indicate potential damage and estimate pavement life when wide-base tires were utilized.

2.4 Machine Learning Approach for Pavement Performance Prediction

2.4.1 Support Vector Machine

Schlotjes et al. (2015) used SVM method to predict the probability of structural failure of pavements using the datasets extracted from New Zealand LTPP study of state highways. Rutting, fatigue cracking, and shear failure were examined and identified the possible cases. It was indicated shear failure was more impacted by the combination of traffic, pavement composition, and strength.

Ziari et al. (2016) analyzed the capability of support vector machine method for predicting the pavement condition by comparing five kernel types of SVM algorithm. The IRI was considered as the pavement performance index, and nine variables were selected in the proposed model. The average traffic, truck traffic, and standard equivalent single-axle loads were included in the input.

Karballaeezadeh et al. (2019) developed a prediction model of remaining pavement service life using SVR optimized by particle filter. The temperature of asphalt surface and pavement thickness were considered in the proposed model. The model was validated by the results of heavy failing weight deflectometer and ground penetrating radar tests. It indicated that the prediction accuracy of proposed model was higher than those of support vector machine, ANN, and multi-layered perceptron models.

Wang et al. (2020b) developed a hybrid grey relation analysis and SVR technique to predict rut depth of asphalt pavements. Grey relation analysis was applied to select the main influential factors, and SVR was employed to conduct prediction of pavement performance. The predictive models overcame the drawbacks of the traditional models, such as limited explanatary variables, short prediction periods, and overfitting. It was concluded that the prediction model established by the proposed approach had better operability and higher accuracy which was promising to be used in long-term performance prediction.

Zeiada et al. (2020) used five machine learning techniques, including regression tree, ensembles, SVM, Gaussian process regression, and artificial neural network (ANN), to model the pavement performance in warm regions using seven parameters including relative humidity, average wind velocity, initial roughness, pavement structural capacity, traffic volume, average albedo, and average emissivity.

2.4.2 Random Forest

Gong et al. (2018) predicted the IRI of flexible pavements based on the distress measurements, climate, traffic, maintenance, and structural data using random forest regression. The performance of random forest regression model was compared to that of

the linear regression model, and the results indicated that the random forest regression model significantly outperformed.

Gong et al. (2019a) developed random forest models and determined relative importance of explanatory variables to investigate impacts of asphalt mixture properties on pavement performance using LTPP data. Totally 17 variables related to the physical properties of the HMA and pavement were considered as input of the model, and alligator cracking, longitudinal cracking at wheel-path, transverse cracking, rutting, and IRI were set as the performance indicators.

Marcelino et al. (2019) proposed a systematic approach to the development of machine learning models for the prediction of pavement performance in pavement management system. Various machine learning methods were supported, and the generalization performance was emphasized. A case study was illustrated to predict IRI for 5 and 10-years using random forest method based on structural, traffic, and climatic data.

Fathi et al. (2019) developed a hybrid machine learning method by combining random forest and ANN to predict the alligator cracking index based on measured quality control parameters. The model was applied to investigate the influence of independent variables on alligator cracking index.

Jia et al. (2019) employed random forest method to correlate the national performance measures to state performance indices and found the IRI generally increased with the increase of standard deviation of rut depth. The accuracy of the classification model with pavement smoothness and distress indices has higher accuracy than that with pavement quality index.

2.4.3 Gradient Boost Model

Inkoom et al. (2019) predicted the highway pavement condition based on the previous pavement condition ratings and selected time variant and invariant covariates using different machine learning methods, including multivariable linear regression, partition, bootstrap forest, gradient boosted trees, K-nearest neighbors, and naïve Bayes techniques. It was indicated that these machine learning methodologies were promising in predicting the crack of pavement with the coefficient of determination of 0.6-0.9.

Gong et al. (2019b) enhanced the fatigue cracking predictive performance of transfer functions in MEPDG. The transfer functions of alligator cracking and longitudinal cracking were considered. The calculated damage indices by MEPDG, pavement thickness, material related parameters, climate condition, and truck traffic were set as inputs in the models. For both cracking, the predictive performance of proposed gradient boost models as found significantly outperformed that of the national transfer functions.

Barua et al. (2020) utilized gradient boost models to investigate the impact of variables on deterioration trend of runway and taxiway pavement at airport. Pavement age, material, maintenance and rehabilitation, climate factor, and air traffic loading were considered as input variables. The developed models were shown to outperform other methods, including linear regression, nonlinear regression, random forest, and ANN, for better explanation of both taxiway and runway data.

Zhang et al. (2020) used gradient tree boosting model to predict asphalt overlay performance and identity influential factors based on the field measurement from LTPP database. Alligator cracking, longitudinal cracking, transverse cracking, rutting, and IRI were selected to indicate asphalt overlay performance. It was suggested that transverse

cracking and pre-overlay rutting were important to the development of overlay performance.

Piryonesi and El-Diraby (2020) explored the performance of various classification algorithms for the analysis of pavement deterioration using LTPP data by examining the capability of handling limited and low-quality data sets and confirming whether better configurations would help overcome limitations. The algorithms included naïve Bayes classifier, naïve Bayes coupled with kernels, decision trees, logistic regression, random forest, gradient boosted trees, and k-nearest neighbors (k-NN). Suggestions were made to improve the performance of predictive models, and the effect of data segmentation was investigated. It indicated that the data segmentation based on climate region improved the accuracy significantly.

CHAPTER 3 DYNAMIC LOADS OF VEHICLE DUE TO ROUGH PAVEMENT SURFACE

3.1 Estimation of Dynamic Tire Force

3.1.1 Truck Modeling

Dynamic interaction between heavy trucks and pavement surface roughness have been investigated using field experiment or vehicle models (Jarvis and Sweatman, 1982; Sweatman et al., 1997). In this study, pavement profile data was input in the high-fidelity vehicle models available in TruckSim to calculate dynamic loads generated by the vehicle. TruckSim software is capable of vehicle dynamics modeling to calculate vertical, transverse, and longitudinal tire forces (Mechnical Simulation, 2018). Different pavement surface conditions, tire configurations, vehicle suspensions can be considered in the simulation. The vehicle model in TruckSim is composed of car body, aerodynamics, steering system, pneumatics braking system, power transmission system, wheel and suspension system (Sayers and Mousseau, 1990; Gilispie, 1992; Sayers, 2011). TruckSim has been successfully used by several previous researchers to estimate dynamic tire forces (Chatti and Lee, 2002; Steyn et al., 2013).

In order to capture the vehicle-pavement interaction, a comprehensive 14-DOF full vehicle model is efficient to study the dynamic behaviors of vehicles in vertical, longitudinal, and lateral directions (Shim and Ghike, 2007). Figure 3.1 presents a comprehensive 14-DOF full vehicle model which was efficient to study the dynamic behaviors of vehicles in vertical, longitudinal, and lateral directions. The model is consisted of one sprung mass and four unsprung masses. The vehicle body has translational motions

in x, y, and z directions, and angular motions about three axes. Roll, pitch, and yaw motions are the rotation about x, y, and z axes, respectively. The wheels have translational motion in vertical direction and wheel spin about lateral direction (Yang et al., 2013). In this study, a multi-body dynamic tool, TruckSim that was developed by Mechanical Simulation Company, was used in this study to simulate vehicle dynamics (Sayers, 2011).

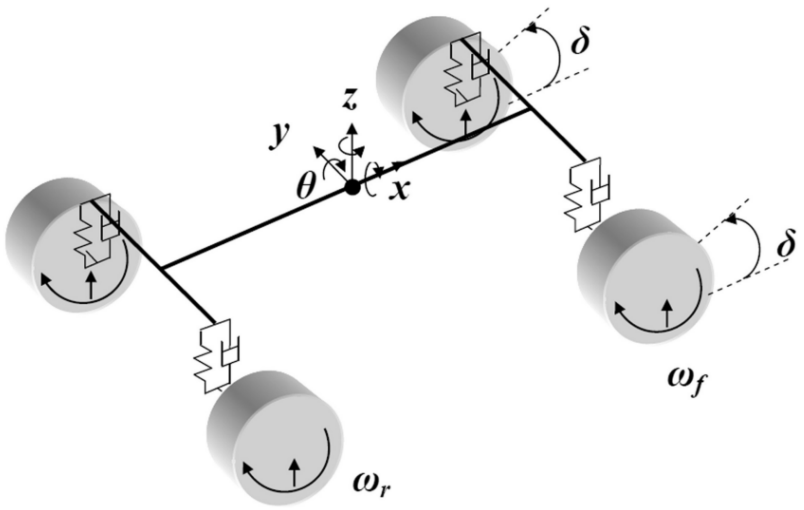

Figure 3.1 14-DOF full vehicle model (Setiawan et al., 2009)

Table 3.1 shows the axle configuration and major parameters of Class-5 single-unit truck used in the analysis. The spacing between Axle 1 and 2 was 5000 mm as shown in Figure 3.2. The sprung weight and applied load were 44 kN and 70 kN, respectively, which were carried by two single axles. For each individual axle, the suspension type was leaf suspension, the tire load rating was 29.4 kN, and the wheel center spacing was 2030 mm. For the steering axle (Axle 1), single tire was used at each side. The effective rolling radius and the unloaded radius of tires were 510 mm and 520 mm, respectively. The tire width was 265 mm with the spring rate of 980 N/mm. For the drive axle (Axle 2), dual-tire assembly was equipped and the spacing of two tires was 122 mm. The effective rolling radius and unloaded radius of tires were 514 mm and 527 mm, respectively. The tire width

was 280 mm with the spring rate of 1290 N/mm. Tire inflation pressure of 724 kPa (105 psi) was used for all tires. These tire parameters were estimated based on tire manufacture data and literature values (Tielking, 1992). Different speeds and pavement surface profiles were used in the simulation to calculate dynamic tire forces of the single-unit Class-5 truck.

Table 3.1 Truck configuration and parameters in TruckSim software

Truck Configurations		**Value**
FHWA Vehicle Classification		Class-5 (single-unit truck)
Single Axle 1 (Steering)	Tire Type	Single
	Effective Rolling Radius	510 mm
	Unloaded Radius	520 mm
	Tire Width	265 mm
	Spring Rate	980 N/mm
Single Axle 2 (Drive)	Tire Type	Dual
	Effective Rolling Radius	514 mm
	Unloaded Radius	527 mm
	Tire Width	280 mm
	Spring Rate	1290 N/mm

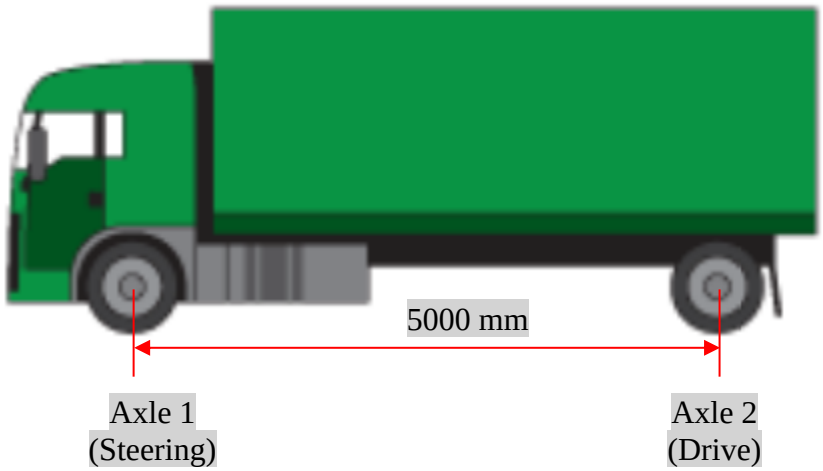

Figure 3.2 Illustration of Class-5 Truck (Texas DOT, 2013)

3.1.2 Pavement Profile Data

The pavement profile data was extracted from LTPP database (Elkins et al., 2016). The ProVAL software was used to estimate the IRI value for each selected pavement segment (The Transtec Group, 2016). The moving average window of profile measurements was 0.30 m (0.98 ft), and the pavement surface elevation data was stored at 0.150 m (0.49 ft) intervals. The total length of each pavement segment was 152.4 m composed of 1017 points. In the study, three pavement profiles data (profile 1, 2, and 3 summarized in Table 3.2) collected in 1996, 1999, and 2003 at the same pavement section located in Nevada (NV) (LTPP Section ID: 320201) were selected. Figure 3.3 presents the comparison of pavement surface profile 1, 2, and 3 at the left and right wheel paths, respectively. It can be seen that the elevations of profile 3 changed more frequently and significantly than those of profile 1. As shown in surface profile 1, the pavement surface profiles at the left and right wheel paths were similar. However, the surface profile at right wheel path deteriorates more than that at left wheel path after seven years, as shown in profile 3.

Table 3.2 IRI of pavement section (320201) in Nevada measured at different years

Profile #	**Year**	**Left IRI (m/km)**	**Right IRI (m/km)**	**Overall IRI (m/km)**
1	1996	0.89	1.13	1.01
2	1999	1.57	2.52	2.05
3	2003	1.63	4.55	3.09

In pavement management system, the IRI values of 1.50 mm/km (95 inch/mile) and 2.68 mm/km (170 inch/mile) were usually used as the thresholds of pavement condition ranging from good, fair/mediocre, to deficient/poor rating (Wang et al., 2015b). The overall

IRI values of profile 1, 2, and 3 used in this study were found to be 1.01 mm/km (64 in/mile), 2.05 mm/km (130 in/mile), and 3.09 mm/km (196 in/mile), which could represent good, fair, and poor pavement surface conditions, respectively.

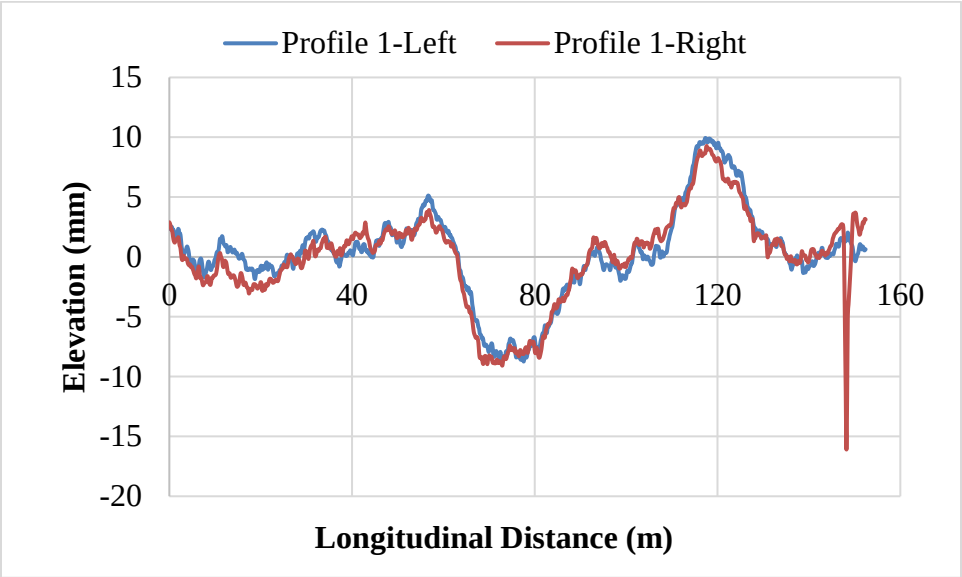

(a)

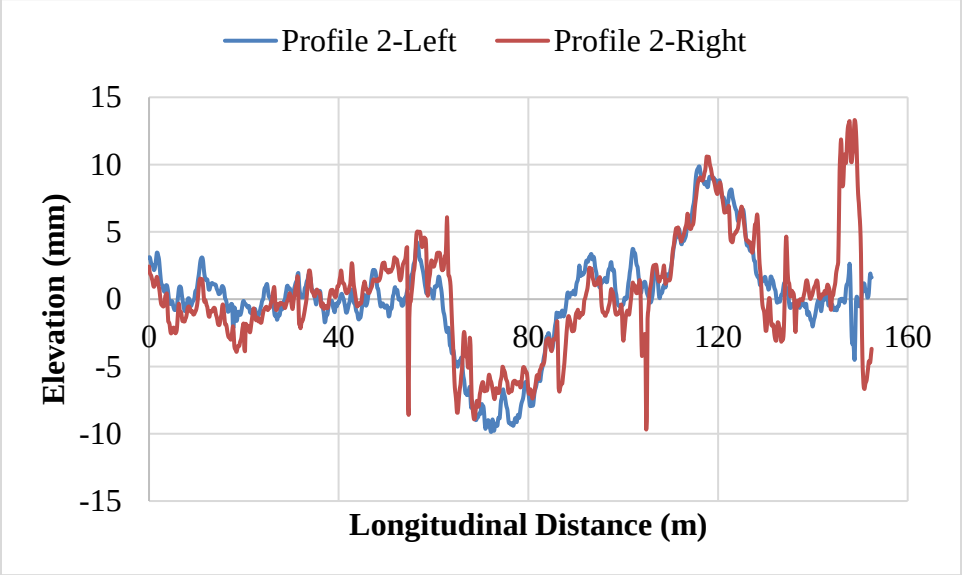

(b)

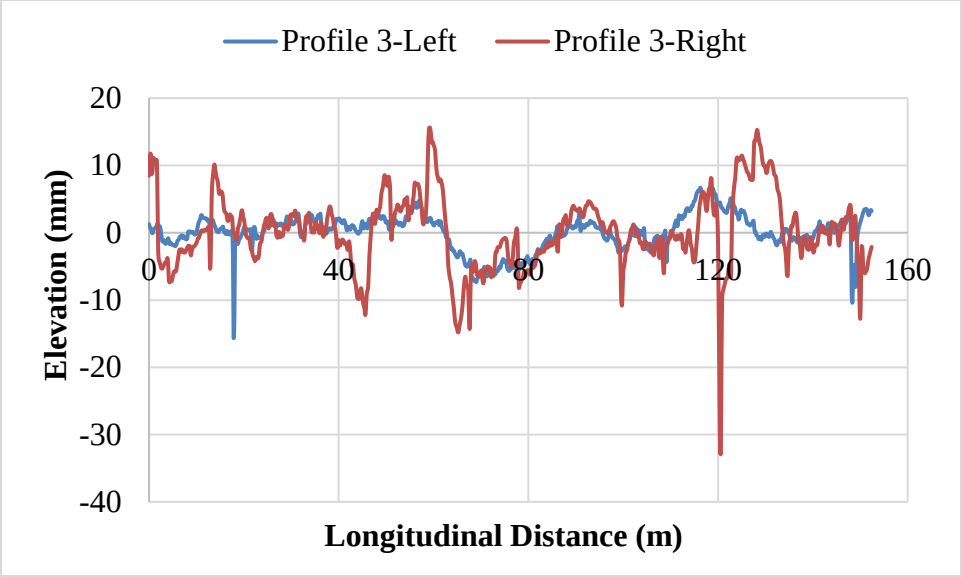

(c)

Figure 3.3 Surface profiles used in the analysis: (a) profile 1; (b) profile 2; and (c) profile 3 at the selected LTPP section

3.1.3 Dynamic Tire Force

The full-vehicle model in TruckSim software was used to simulate vertical tire forces generated by moving truck. Figure 3.4 shows the variation of vertical tire force with time (distance) under the left front tire (Fz_L1), left-rear tire (Fz_L2), right-front tire (Fz_R1), and right-rear tire (Fz_R2) of Class-5 truck, respectively, when the two-axle single unit truck (Class 5) travels at 80 km/h on pavement surface profile 1, 2, and 3, respectively. The vertical tire forces generated by rear tires were found much greater than those generated by front tires due to the effect of payload. The vertical forces under left and right sides of tires were found similar on profile 1; while some differences were observed on surface profile 3. This trend was closely associated with the surface profiles as shown in Figure 3.3.

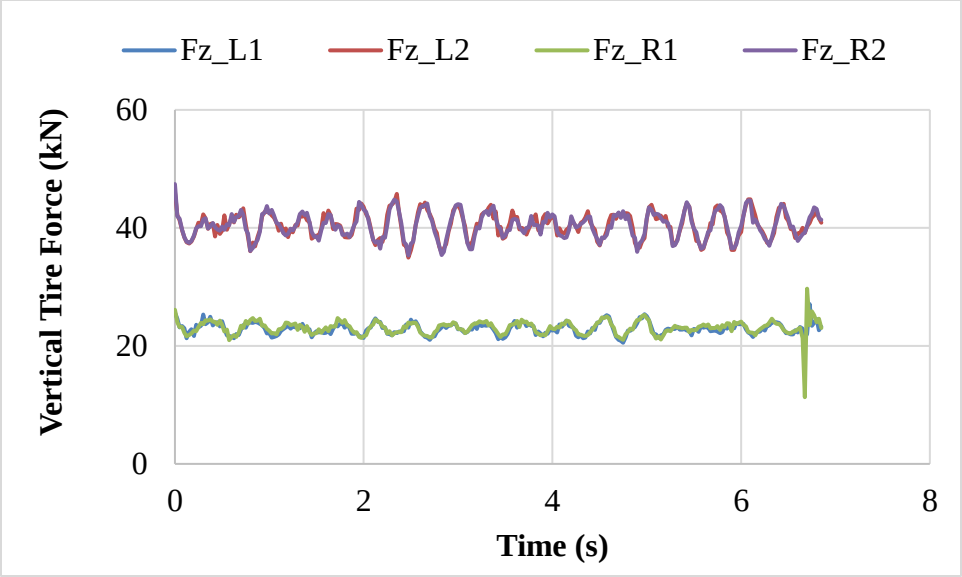
Fz_L1
Fz_L2
Fz_R1
Fz_R2
Vertical Tire Force (kN)
60
40
20
0
0
2
4
6
8
Time (s)

(a)

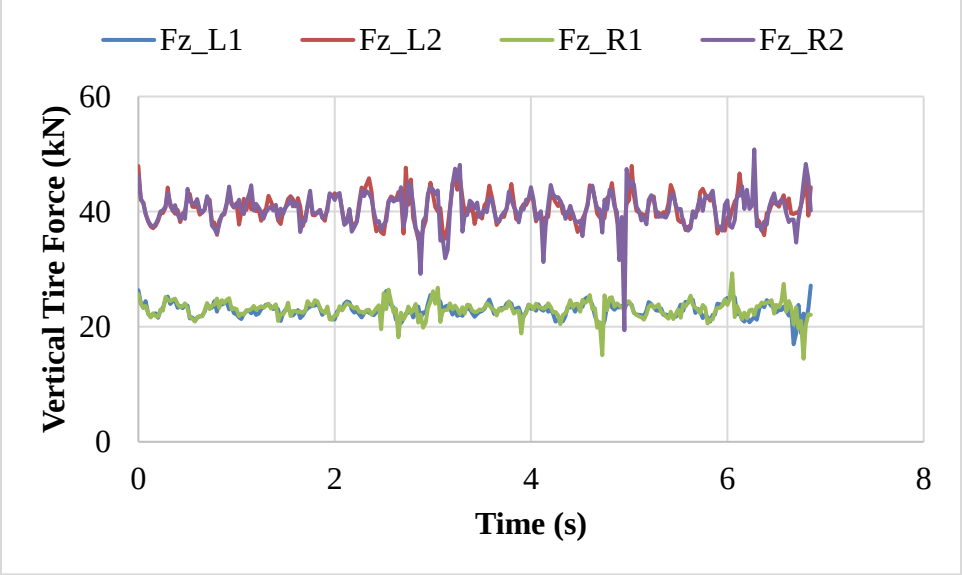
Fz_L1
Fz_L2
Fz_R1
Fz_R2
Vertical Tire Force (kN)
60
40
20
0
0
2
4
6
8
Time (s)

(b)

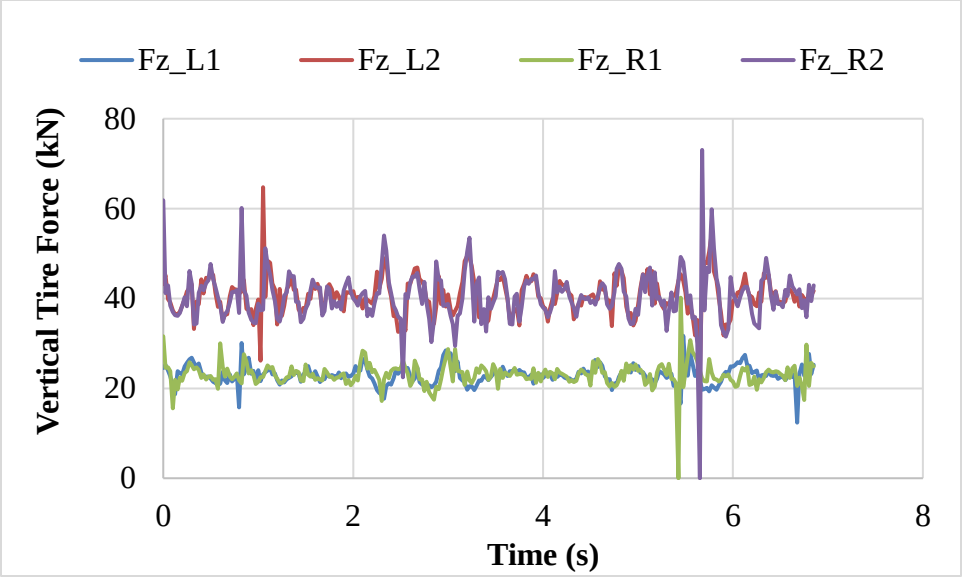

(c)

Figure 3.4 Vertical tire forces under front and rear tires at 80 km/h on (a) profile 1 (IRI= 1.03 mm/km); (b) profile 2 (IRI= 2.05 mm/km); and (c) profile 3 (IRI= 3.09 mm/km)

Figure 3.5 shows the comparison of dynamic loads at the speeds of 32 km/h (20 mph), 80 km/h (50 mph), and 112 km/h (80 mph) under the right rear axle. Due to the fixed length of pavement section, the time histories of dynamic loads at various speeds were different. The up-and-down variations of dynamic loads were found dramatically increased as vehicle speed increased from 32 km/h to 112 km/h. This is reasonable because the axle vibration will increase with speed at the same excitation of surface irregularities.

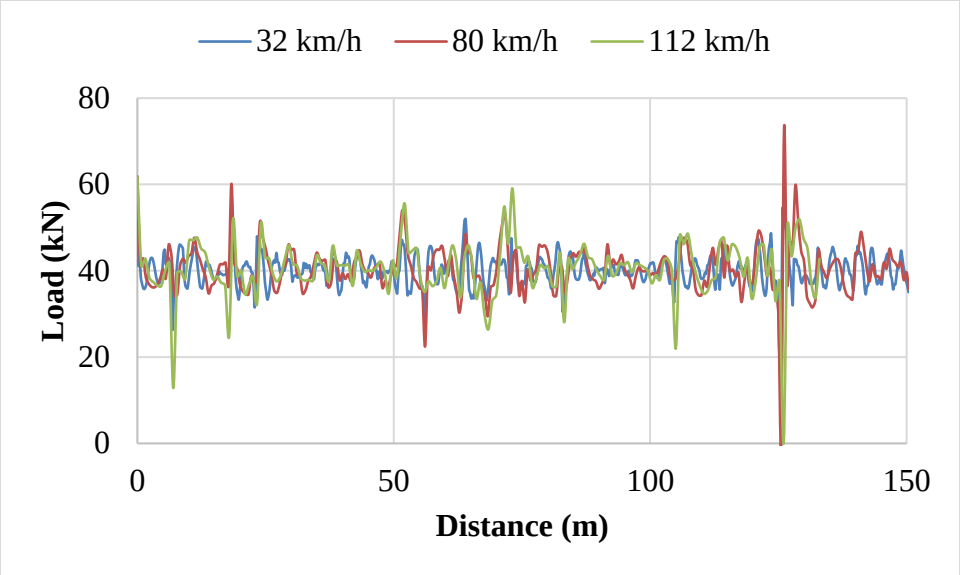

Figure 3.5 Comparison of dynamic loads at different speeds (IRI=3.09m/km)

3.2 Effect of Axle Load on Dynamic Loads

3.2.1 Vehicle Dynamics Simulation

The dominant vehicle class in truck traffic varies depending on the functional classification of road. Previous studies on traffic clustering have found that most of single axles were from vehicle Class-5 (two-axle, single unit) and Class-9 (five-axle, single trailer) vehicle, and most tandem axles were from Class-9 vehicle, while most tridem axles were from Class-7 vehicle (four or more axles, single unit) (Wang et al., 2015c; Jasim et al., 2019). Thus, Class-5, Class-7, and Class-9 vehicles were considered as the typical truck configurations in this study.

The truck configuration of Class-5 two-axle single-unit truck was illustrated in Figure 3.2, and the loads at axle 1 and 2 were 41 kN and 34 kN, respectively. The axle load configuration of Class-7 four-axle single-unit truck and Class-9 five-axle single-unit truck were illustrated in Figure 3.6 (a) and (b), respectively. The tire parameters summarized in Table 3.1 were used for three typical truck configurations in TruckSim simulation.

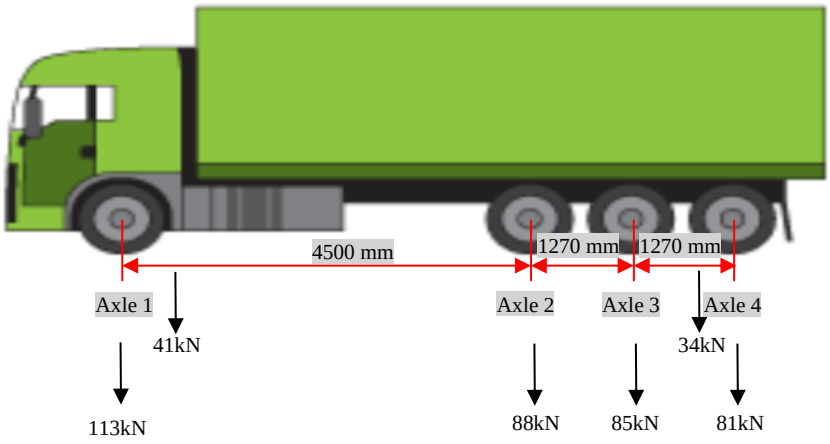

(a)

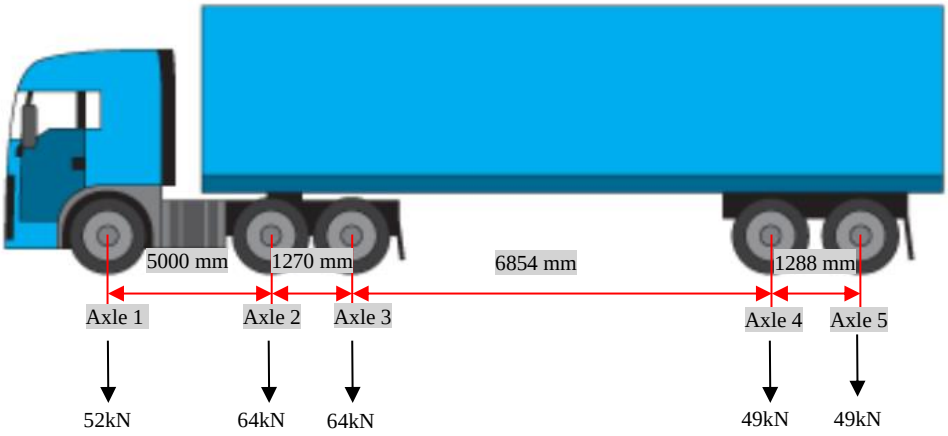

(b)

Figure 3.6 Illustration of axle configurations for (a) Class-7 and (b) Class-9 trucks (after Texas DOT (2013)

3.2.2 Dynamic Loads Due to Pavement Roughness

The dynamic loads induced by different trucks on different pavement roughness conditions were estimated using the corresponding vehicle models in TruckSim. Due to the higher levels of surface roughness, the dynamic loads under the tires at right side were found greater than those under the tire at left side and thus used in the analysis. For tandem

and tridem axles, the load under each axle was found similar, and the axle having the greatest load was selected to calculate pavement responses. Therefore, the second axle of the front tandem axle in Class-9 truck (Fz_R3) and the first axle of the tridem axle in Class-7 truck (Fz_R2) were selected. Figure 3.7 shows the calculated dynamic loads in time domain under the selected axle loads on different pavement surface profiles. As expected, the variation of dynamic loads increased with the change of IRI from 1.01 m/km to 3.09 m/km. On the other hand, it was found that the median values of dynamic loads along the pavement section were very close to the static axle loads.

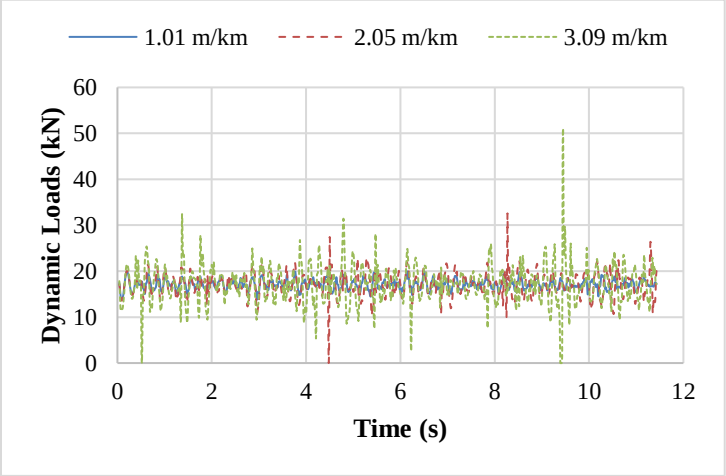

(a)

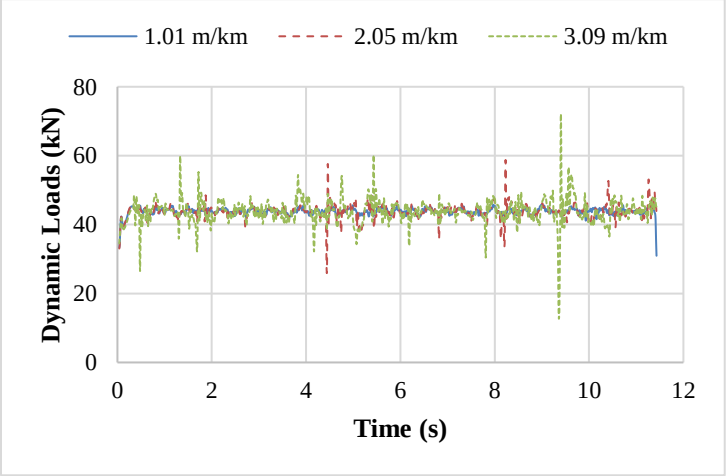

(b)

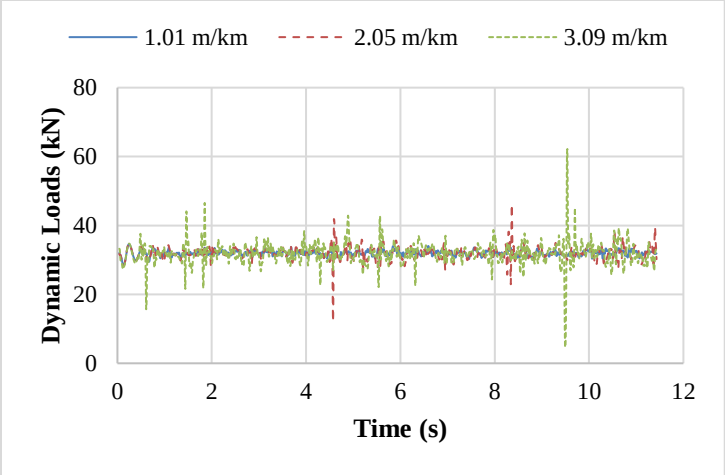

(c)

Figure 3.7 Dynamic tire forces: (a) Class-5 truck (Fz_R2); (b) Class-7 truck (Fz_R2); and (c) Class-9 truck (Fz_R3) at 48 km/h

Figure 3.8 shows the calculated DLCs on three pavement roughness conditions. It was found that DLCs increased as pavement roughness increased but decreased as the applied axle load increased. The finding was consistent with the reported in previous study (Muka, 2017). It was expected that the variation of dynamic loads would impact the pavement responses significantly on rough pavements.

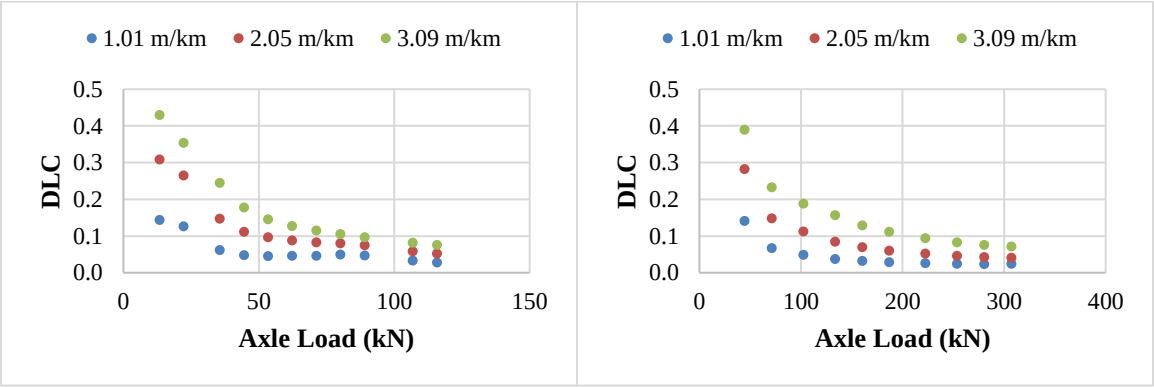

(a) (b)

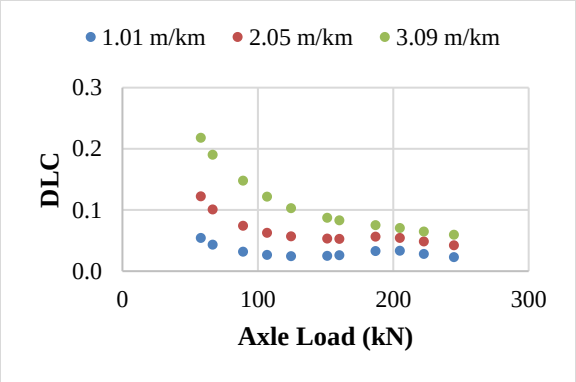

(c)

Figure 3.8 DLCs on different pavement surface conditions: (a) Class-5 truck (Fz_R2); (b) Class-7 truck (Fz_R2); and (c) Class-9 truck (Fz_R3) at 48 km/h

3.3 Effect of Wide-Base Tire on Dynamic Loads

3.3.1 Truck Modeling with Wide-Base Tire

Previous research studies have revealed that wide-base tire would produce less dynamic component of pavement load than dual-tire assembly because of the less load transmissibility of wide-base tire (Tielking, 1994). The wide-base 425/65R22.5 tire generated 10 to 12 % lower dynamic load coefficient (DLC) as compared to 11R22.5 dual-tire assembly (Kulakowski and Kenis, 1995; Streit et al., 1998). Trangsrud et al. (2004) investigated the dynamics of a tractor semi-trailer traveling on a random road profile using dual-tire assembly and wide-base tire. Their initial results indicated that the longitudinal and vertical acceleration of axle was reduced in certain frequency ranges for the truck with wide-base tires.

A Class-5 two-axle single-unit truck and a Class-9 five-axle single-unit truck were used to calculate and compare the dynamic tire forces generated by dual tire assembly and wide-base tire, as shown in Figure 3.2 and Figure 3.6(b), respectively. For the Class-5 truck,

the sprung mass and payload were 44 kN and 70 kN, respectively. For the Class-9 truck, the sprung mass and payload were 120 kN and 162 kN, respectively. All the suspension type is leaf. For Class-5 truck, the static loads of Axle 1 ad Axle 2 were 46 kN and 80 kN. For Class-9 truck, the static loads of Axle 1-5 were 52 kN, 75 kN, 75 kN, 57 kN, and 57 kN, respectively.

Table 3.3 shows the parameters of conventional tires and wide-base tire (445/50R22.5) used in the analysis. The spring rates of tires were calculated based on static load deflection measurements and utilized in the previous work on vehicle dynamics simulation (Law et al., 2002). For the steering axle (Axle 1), the single tire was equipped. The effective rolling radius and unloaded radius were 510 mm and 520 mm, respectively. The tire width was 275 mm, and the spring rate was 932 N/mm. For the drive axles (Axle 2, 3, 4, and 5), dual tire assembly or wide-base tires were equipped. For the conventional tire at drive axle, the effective rolling radius and unloaded radius of tires were 514 mm and 527 mm, respectively. The tire width was 275 mm, and the spring rate was 829 N/mm. For the wide-base tire at drive axle, the effective rolling radius and unloaded radius of tires were 493 mm and 514 mm, respectively. The tire width was 445 mm, and the spring rate was 1197 N/mm.

Table 3.3 Tire configuration and parameters applied in the vehicle simulation

Tire Configuration and Parameters		**Value**
Single Tire (steering axle)	Effective Rolling Radius	510 mm
	Unloaded Radius	520 mm
	Tire Width	275 mm
	Spring Rate	932 N/mm
Dual Tire Assembly (per tire) (drive axle)	Effective Rolling Radius	514 mm
	Unloaded Radius	527 mm
	Tire Width	275 mm
	Spring Rate	829 N/mm
Wide-Base Tire (drive axle)	Effective Rolling Radius	493 mm
	Unloaded Radius	514 mm
	Tire Width	445 mm
	Spring Rate	1197 N/mm

3.3.2 Dynamic Tire Force Comparison

Figure 3.9 shows the dynamic tire forces generated on different pavement roughness conditions under dual-tire assembly and wide-base tire at 48 km/h. The tire force of rear axle on right side (Fz_R2) was shown for Class-5 truck, and the tire force of front tandem axle on right side (Fz_R3) was illustrated for the Class-9 truck. Since the maximum dynamic tire forces generated by the truck corresponded with the irregularities in pavement profiles, the maximum dynamic tire forces generated by different tire configurations were expected to be induced at similar locations. This indicates the spatially repeatability of dynamic loads.

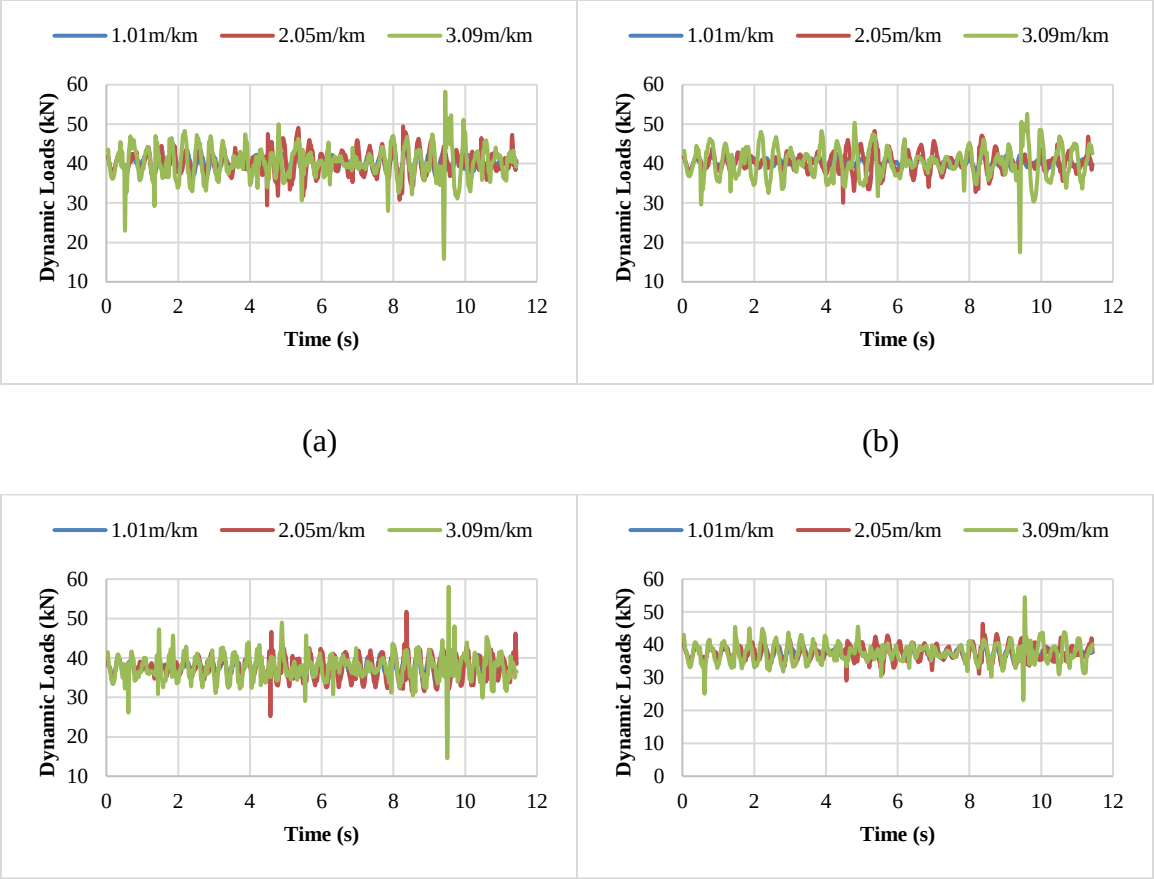

Figure 3.9 Dynamic loads on different pavement surface conditions at 48 km/h: (a) dual-tire assembly (Class-5 truck); (b) wide-base tire (Class-5 truck); (c) dual-tire assembly (Class-9 truck) (d) wide-base tire (Class-9 truck)

Figure 3.10 shows the power spectral density functions of dynamic tire forces on different pavement roughness conditions for Class-9 truck at 48 km/h. The main peak was observed at approximately 2.5 Hz which was determined by the body-bounce mode of vibration (Cebon, 1999). The amplitude differences of dynamic tire forces became less significant on rougher pavement condition, especially at the low frequency range of 0-5 Hz. Although the maximum dynamic tire forces increased as pavement surface roughness

levels increased in time domain, the increase trend in frequency domain was affected by truck configuration, pavement roughness, and speed.

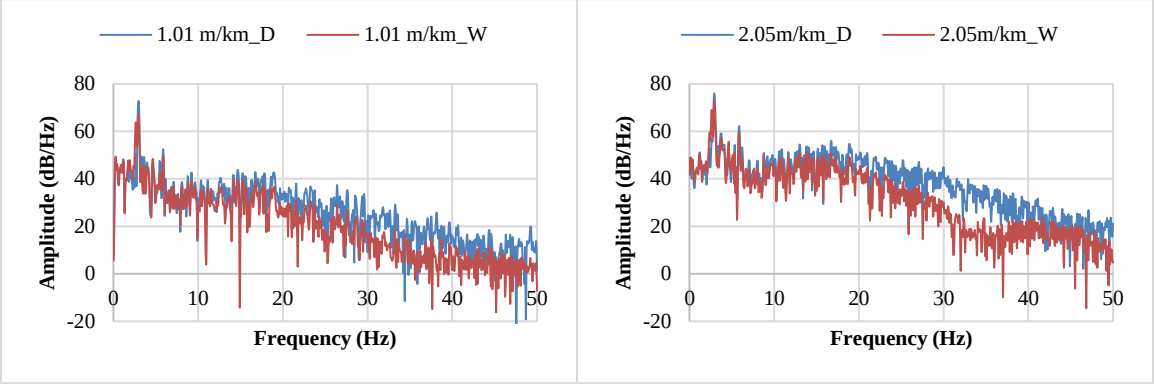

(a) (b)

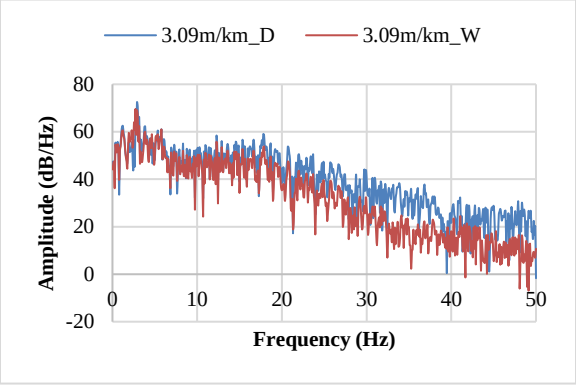

(c)

Figure 3.10 Power spectral density of dynamic tire forces for dual-tire assembly and wide-base tire on different pavement roughness conditions at 48 km/h (Class-9 truck): (a) IRI = 1.01 m/km; (b) IRI = 2.05 m/km; (c) IRI = 3.09 km/h

The dynamic tire forces of dual-tire assembly and wide-base tires were estimated using the full-vehicle model for Class-5 and Class-9 trucks. Figure 3.11 presents the calculated DLCs of dual-tire assembly and wide-base tire at different speeds on three pavement roughness conditions. It was found that the DLCs increased as the pavement roughness condition or vehicle speed increased. For Class-5 truck, the DLCs of dynamic

loads ranged from 0.022 to 0.133 under dual-tire assembly and ranged from 0.024 to 0.125 under wide-base tire. For Class-9 truck, the ranges of DLCs were 0.018-0.153 and 0.015-0.146 for dual-tire assembly and wide-base tire. The DLCs of wide-base tire were found smaller than those of dual-tire assembly and their differences became more significant on rougher pavement roughness.

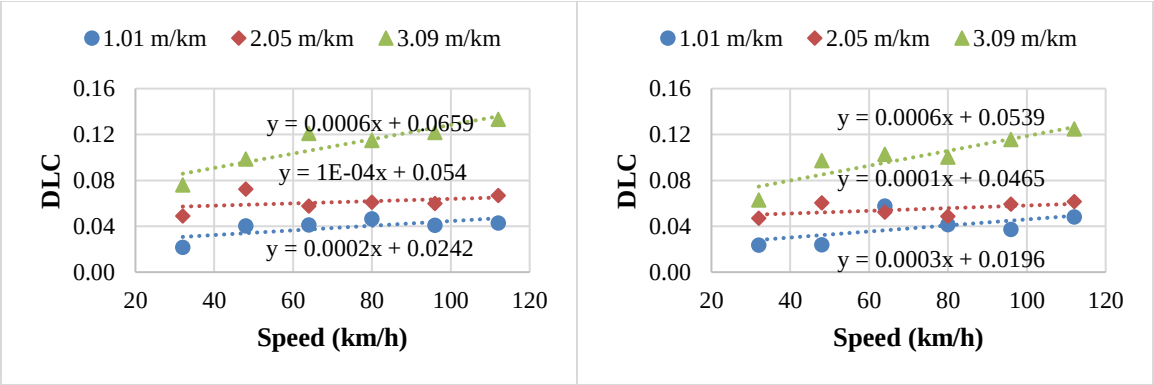

(a) (b)

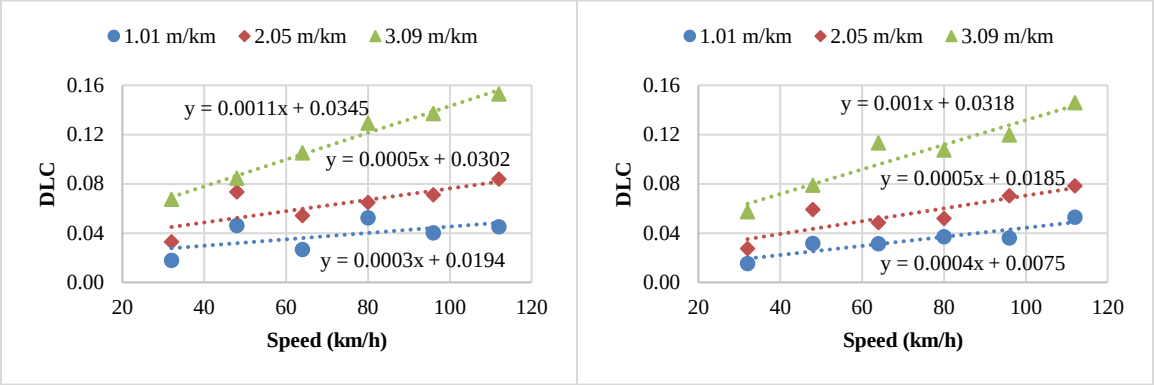

(c) (d)

Figure 3.11 Calculated DLCs of dynamic tire forces: (a) dual-tire assembly (Class-5 truck) (b) wide-base tire (Class-5 truck); (c) dual-tire assembly (Class-9 truck); (d) wide-base tire (Class-9 truck)

3.4 Summary

In this chapter, a full-vehicle model was applied to simulate vehicle dynamics and estimate dynamic tire forces at different vehicle speeds on three pavement surface

conditions. The variation of dynamic loads caused by rough pavement surface conditions was characterized by DLCs. The dynamic loads under the single, tandem, and tridem axles of typical truck configurations were estimated. The impact of axle loads on dynamic loads on three pavement surface conditions was investigated for each truck configuration. The dynamic loads generated by wide-base tire and dual-tire assembly were estimated and compared.

CHAPTER 4 ANALYSIS OF PAVEMENT RESPONSE UNDER DYNAMIC LOADS WITH STOCHASTIC AMPLITUDE

4.1 Principle of Impulse Response Method

4.1.1 Theoretical Background

The process of calculating pavement responses using the impulse response method (Newland (1985) is illustrated in Table 4.1.

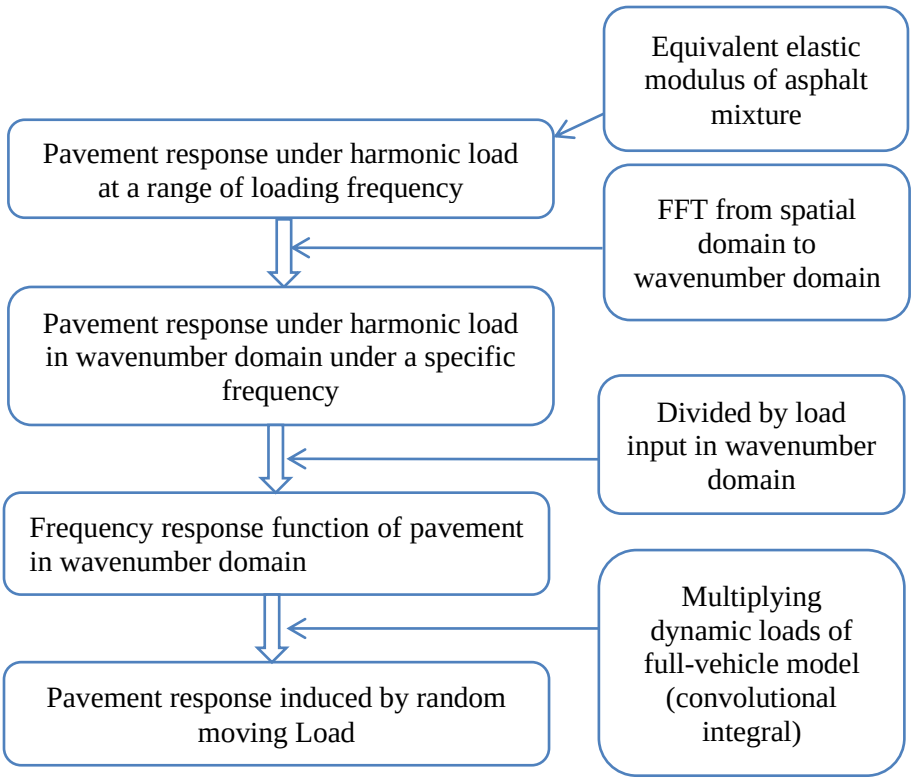

Figure 4.1 Flowchart of the impulse response method

In mathematics, convolution is the mathematical operation of two functions (*f* and *g*); it produces the third function, that is typical viewed as a modified version of the amount that one of the original functions is translated. If *f*(t) and *g*(t) are piecewise continuous functions, then the convolution integral of *f*(t) and *g*(t) is expressed in Eq. 4-1.

$$(f * g)(t) = \int_0^t f(t-\tau)\, g(t)\, d\tau \tag{4-1}$$

The dynamic response of pavement structure, which consisted of multiple elastic or viscoelastic layers, subjected to a force input varying with time can be obtained by the convolution integral, as shown in Eq. 4-2 (Newland, 1985).

$$y(t) = \int_0^t F(\tau)\, h(t-\tau)\, d\tau \tag{4-2}$$

Where, *y(t)* is the pavement response at time t; *F(τ)* is the input of vehicle loads at time τ; and *h(t)* is the pavement response to a unit impulse load.

The convolution integral can be transformed from time domain to frequency domain to convert the convolution integral to the format of simple multiplication, as shown in Eq. 4-3.

$$\tilde{f}(\omega) = \tilde{F}(\omega) \cdot \tilde{h}(\omega) \tag{4-3}$$

Where, $\tilde{f}(\omega)$ is response function in the frequency domain; $\tilde{F}(\omega)$ is input function in the frequency domain; and $\tilde{h}(\omega)$ is the frequency response function (FRF).

For the case where the pavement structure geometry is invariant in the direction y of the moving load, the dynamic responses can be derived using Eq. 4-4:

$$y(x_0, y, z_0, t) = \int_{-\infty}^{t} F(x_0, y, z_0, t)\, h(x_0, y, z_0, t-\tau)\, d\tau \tag{4-4}$$

The similar double forward Fourier transform can be used to efficiently compute dynamic responses by transforming from the time-spatial domain (x, y, z, t) to the frequency-wavenumber domain (x, k_y, z, ω), as shown in Eq. 4-5.

$$\tilde{\tilde{y}}(x_0, k_y, z_0, \omega) = \int\int_{-\infty}^{\infty} F(x_0, k_y, z_0, \omega - k_y v)\, h(x_0, k_y, z_0, \omega)\, e^{-2\pi i t\omega} e^{ik_y y}\, dt dy \tag{4-5}$$

This formula can be further elaborated, yielding the following solution in the frequency-wavenumber domain using Eq. 4-6.

$$\tilde{\tilde{y}}\left(x_0, k_y, z_0, \omega\right) = \tilde{\tilde{h}}\left(x_0, k_y, z_0, \omega\right)\tilde{\tilde{F}}\left(x_0, k_y, z_0, \omega\right) \tag{4-6}$$

To obtain the dynamic responses of the linear system to time-varying loads in time-spatial domain, the double inverse Fourier transform can be applied, as shown in Eqs. (4-7) and (4-8):

$$\tilde{y}\left(x_0, y, z_0, \omega\right) = \int_{-\infty}^{\infty} \tilde{\tilde{f}}\left(x_0, k_y, z_0, \omega\right) e^{-ik_y y} dk_y \tag{4-7}$$

$$y\left(x_0, y, z_0, t\right) = \int_{-\infty}^{\infty} \tilde{f}\left(x_0, y, z_0, \omega\right) e^{2\pi i \omega t} d\omega \tag{4-8}$$

When the response analysis is performed in frequency domain, the pavement response, $\tilde{\tilde{y}}_p\left(x, y, z, \omega\right)$, to the input of vehicle load, $\tilde{\tilde{F}}(x, y, z, \omega)$, is in spatial-frequency domain. The frequency response function or transfer function, including strain, stress, and displacement, is obtained by dividing the response by the input of vehicle loading in the frequency-wavenumber domain using Eq. 4-9. In order to derive frequency response function in term of matrices, harmonic loading is applied on pavement surface.

$$\tilde{\tilde{h}}\left(x_0, k_y, z_0, \omega\right) = \frac{\tilde{\tilde{y}}_p\left(x_0, k_y, z_0, \omega\right)}{\tilde{\tilde{F}}\left(x_0, k_y, z_0, \omega\right)} \tag{4-9}$$

According to the function above, the calculation should be accomplished in frequency domain, and the harmonic loading need to be transformed to frequency domain using the Fourier transform. The Fourier transform of harmonic loading can be easily obtained using MATLAB. Usually, FFT is used to obtain the curve of the Fourier transform of harmonic loading, and hamming window is applied to eliminate spectral leakage of the data.

4.1.2 Non-uniform Tire Contact Stresses

The non-uniform distribution of vertical contact stresses under dynamic loads were calculated based on the tire force (calculated from TruckSim) and tire pressure (724 kPa here). The tire contact stress distribution patterns were described using the peak stress at each tire rib and the non-uniform distribution along the contact length, which were obtained from comprehensive analysis of tire-pavement interaction in previous work (Al-Qadi and Wang, 2011; Wang et al., 2012a). The peak tire contacts stresses in vertical direction at each tire rib were calculated using Eq. (4-10) -(4-12), based on the applied load on tire and tire pressure. An elliptic function was used to describe the variation of vertical contact stresses in the longitudinal direction of contact patch.

$$\text{Center rib:} \quad q_{peak} = 317 + 1.23p + 1.35P \tag{4-10}$$

$$\text{Intermediate rib:} \quad q_{peak} = 100 + 1.20p + 1.27P \tag{4-11}$$

$$\text{Edge rib:} \quad q_{peak} = 12 + 0.48p + 14.84P \tag{4-12}$$

Where, q_{peak} is peak contact stress at each tire rib, in kPa; p is tire pressure, in kPa; and P is total load on tire, in kN.

Figure 4.2 shows the vertical tire contact stresses along longitudinal contact length (32 kN on dual-tire assembly). It is noted that the peak vertical contact stresses at tire center area (center and intermediate ribs) are much greater than tire pressure, while the one at edge rib is much smaller. This certainly proves the non-uniform distribution pattern of tire contact stresses.

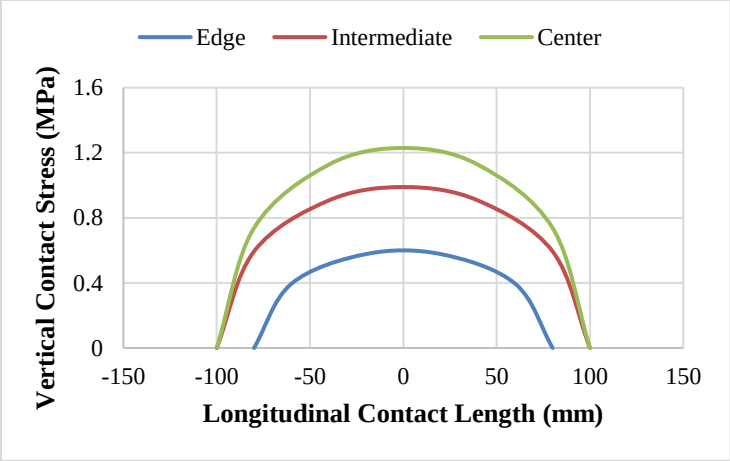

Figure 4.2 Vertical tire contact stresses under each tire rib

4.1.3 Validation of Frequency Response Function

Hardy and Cebon (1989) measured a set of transverse strain responses on an instrumented road and used the Fourier transform to convert these measured impulse responses to harmonic response functions. The measurement was conducted using an instrumented 4-axle articulated vehicle on the Transport Research Laboratory (TRL) test track in the United Kingdom. The instrumented pavement was consisted of a 50-mm wearing course of hot-rolled asphalt, a 150-mm base layer of dense bituminous macadam, a 300-mm subbase layer of crushed granite, and a 100-cm clay layer on a subgrade. The detailed material properties for the layered pavement structure of the instrumented section are summarized in Table 4.1. The damping parameters were used along elastic modulus to consider viscous damping in the pavement.

Table 4.1 Material parameters of the instrumented pavement section at TRL test track (Hardy and Cebon, 1992)

Material	**Elastic modulus (MPa)**	**Damping parameter (sec/rad)**	**Poisson's ratio**	**Density (kg/m^3)**
Hot Rolled Asphalt	3000	$5x10^{-3}$	0.35	1000
Dense Bituminous Macadam	3000	$5x10^{-3}$	0.35	1000
Crushed Rock	140	$5x10^{-3}$	0.40	1500
Clay	140	$1x10^{-4}$	0.45	1000
Hoggin	140	$1x10^{-4}$	0.45	1000

Instead of the layered half-space simulation used by Hardy and Cebon (1992), an advanced 3-D FE model was developed to calculate the frequency response functions of asphalt pavement in this study. The FE model was developed using Abaqus 6.10, commercial FE software. To be consistent with the model developed by Hardy and Cebon (1992), the pavement layers were considered as elastic material with damping parameter which was loss factor of material. The loss factor has positive correlation with damping ratio (Nashif et al., 1985; Graesser and Wong, 1992), which can be used to estimate Rayleigh damping coefficients in FE model (Chopra, 2001).

In order to simulate tire loads more realistically, the non-uniform tire contact stress distribution in the contact area was considered. The tire contact stress patterns were described using the peak stress at each tire rib and the non-uniform distribution along the contact length (Al-Qadi and Wang, 2011; Wang et al., 2012) . In the FE model, the element thicknesses for asphalt layers and base layers were selected at 27.5 mm and 42.3 mm, respectively. The widths of the elements in the loading area were in the range of 10-16 mm,

depending on the tire rib size. The lengths of the elements in loading area were 40 mm in the vehicle moving direction. These element sizes have been used in the implicit dynamic analysis of pavement response (Wang and Al-Qadi, 2013), which satisfied the requirement of maximum element size determined from the minimum wavelength of elastic waves propagation in the pavement (Lysmer and Kuhlemeyer, 1969). The location of infinite boundaries was determined via sensitivity analysis so that the changes of strains in the asphalt layer were less than five percent with the domain sizes increased. The finite dimension size was 4.8×3.2×4.3 m (length × width × depth) with an in-plane loading area of 0.5×2.6 m (length × width), which was selected to balance computation accuracy and time. Figure 4.3 (a) shows the 3D FE model developed for steady-state dynamic analysis. Figure 4.3 (b) presents the non-uniform distribution of loads applied on the 3-D FE model in steady-state dynamic analysis

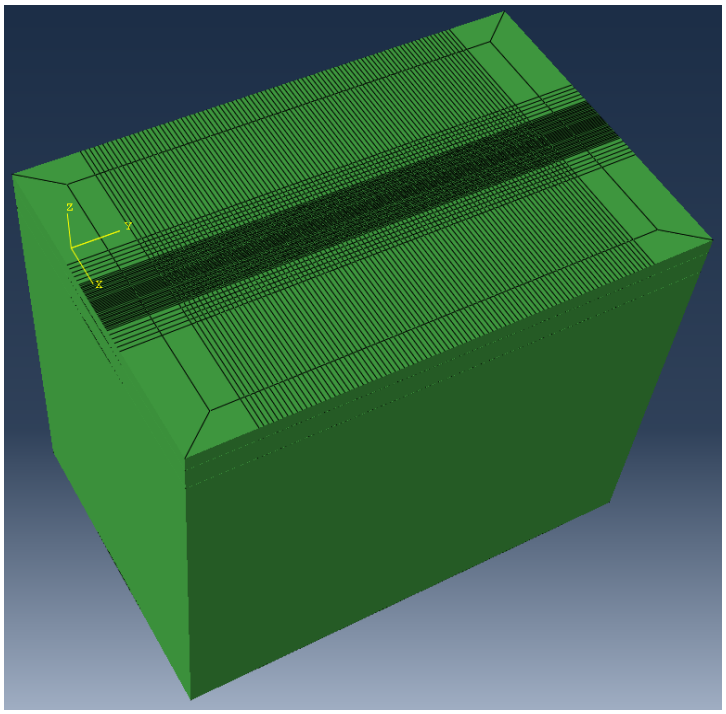

(a)

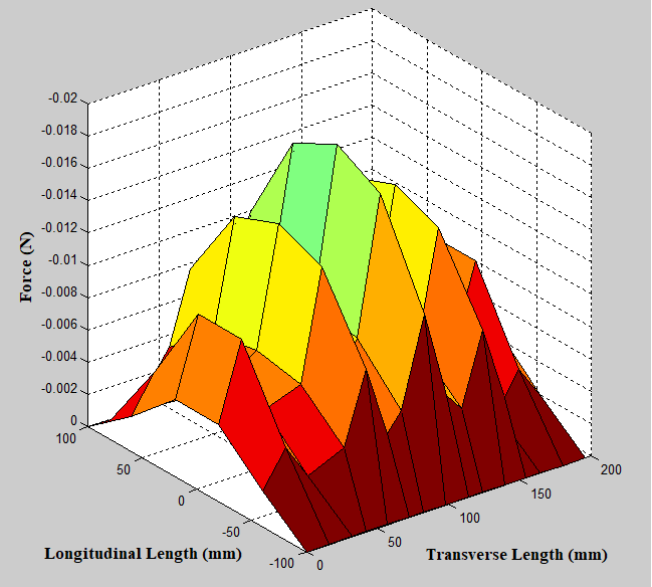

(b)

Figure 4.3 (a) 3D FE model for steady-state dynamic analysis; (b) Non-uniform distribution of loads applied on the 3-D FE model in steady-state dynamic analysis

In the steady-state analysis, the natural frequencies and corresponding mode shapes of the pavement system were first derived in the step of natural frequency extraction. Afterwards, a direct-solution steady-state dynamic (SSD) analysis step was defined in FE model to calculate steady-state dynamic linearized response of a system to harmonic excitations. In steady-state dynamic analysis, the response of pavement structure subjected to dynamic loading is assumed to be a linear combination of the lowest eigenmodes, which is similar to the procedure of modal dynamics, except that the load is harmonic in nature and the steady state response is of interest. The steady-state amplitudes and phases of pavement responses for all the elements and nodal variables in the pavement system due to harmonic excitations at the given frequencies were obtained in SSD analysis.

The predicted frequency response functions of transverse strains at the bottom of asphalt layer using the proposed method were compared to the measured and simulated

results reported by Hardy and Cebon (1992), as shown in Figure 4.4. Since the measured and predicted frequency response functions at the frequency of 0-50 Hz were presented in Hardy and Cebon (1992), the same range of frequency was selected in this study. The comparisons were conducted at the bottom of asphalt layer directly under the load and at 1.8 m away from the load, respectively. The results showed that the transverse strains at the bottom of asphalt layer under the loading area matched the simulated and measured results presented in the previous work. For the transverse strains generated at a distance of 1.8m away from the loading area, the results from the SSD analysis were similar to the simulated results by Hardy and Cebon (1992), although some discrepancies were observed with field measurements as the loading frequency increased. Therefore, the comparisons indicate that the developed 3-D FE model can be used to estimate frequency response functions of asphalt pavement.

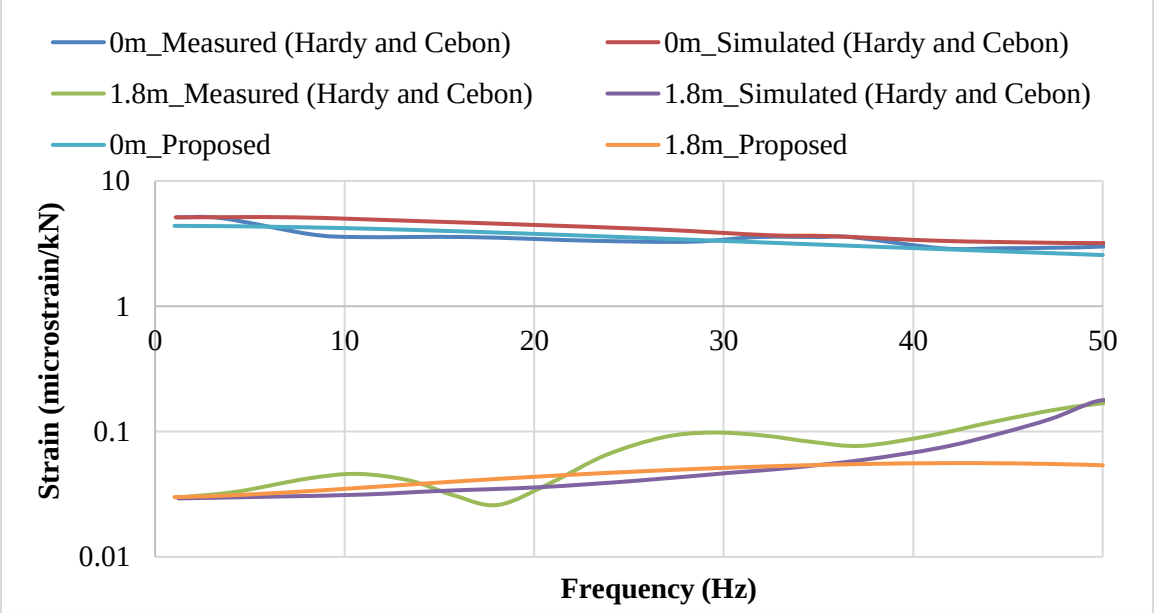

Figure 4.4 Frequency response functions of transverse strains obtained using the proposed FE model and compared to measured and simulated results in Hardy and Cebon (1992)

4.2 Pavement Test Section from LTPP

4.2.1 Field Truck Testing

The LTPP Specific Pavement Studies (SPS) are intensive studies of specific variables on pavement performance including traffic loading, structure design, maintenance treatment, and rehabilitation strategy. The pavement sections in Ohio SPS-1 and SPS-2 were instrumented to investigate dynamic interaction between pavements and truck axle loads, validate dynamic loading models, and establish mechanistic pavement performance prediction models (Agurla and Lin, 2015). The dynamic load response (DLR) data was collected during 1996-1997 from forty pavement test sections located along the 3.5 mile of US-23 in Delaware County north of Columbus, Ohio. All the data were extracted from LTPP InfoPAVE database.

A Class-6 truck consisted of a single steering axle and a tandem axle was utilized in the DLR tests. The tire pressure was 724 kPa, and the tire type was 10R22. The rear tandem axle loading was approximately 146.1 kN (32.8 kips) which was smaller than the maximum weight limit for a short tandem axle as regulated by Ohio Department of Transportation. The test pavement section was equipped with strain gauges (Dynatest®) in transverse and longitudinal directions, linear variable differential transformers, and pressure cell sensors. Strain responses under test truck were recorded with multiple peaks. The first peak value reflected the tensile strain induced by the front axle, and the successive two peak values were corresponding to the tensile strains under the rear tandem axle. It is noted that the quality of measured transverse strain under the AC layer was found not good and thus not used in this study (Ohio Department of Transportation, 2020).

Table 4.2 and Table 4.3 summarize the average and standard deviation values of longitudinal tensile strains measured under front and rear axles of tandem axle at LTPP Ohio SPS-1 section (390108) at 47 km/h and 62 km/h, respectively. Five and six running tests were conducted at 47 km/h and 62 km/h within two hours at 3 pm on August 2, 1996. These strains were measured by three strain gauges (DYN 11, 13, 15) at the bottom of asphalt layer that were located at the interval of 4 ft along the pavement section. The sensors were buried at the right wheel path, which was 30 inches from the right pavement edge. The average tensile strains under the first axle of the rear tandem axle at 47 km/h were found in the range of 102-148 micro; while the average tensile strains under the second axle of the rear tandem axle were found between 103-153 micro between different runs and locations. The average tensile strains under the first axle of the rear tandem axle at 62 km/h were found in the range of 121-136 micro; while the average tensile strains under the second axle of the rear tandem axle were found between 100-164 micro between different runs and locations. The overall average of the rear tandem axle at 47 km/h and 62 km/h were close, and the slight difference may be caused by the increase of dynamic tire force at 62 km/h. The considerable variations of tensile strains between different strain gauges could be caused by two reasons. The first was that the induced dynamic loads varied due to surface profile at different locations; the second was that the strain gauge could not be directly under wheel path. On the other hand, the slight variation of strains between different runs were observed for each strain gauge. This may be caused by the wheel wandering effect and different surface profiles in the wheel path of test truck.

Table 4.2 Measured tensile strains under front and rear axles of tandem axle at LTPP Ohio SPS-1 section (390108) at 47 km/h (unit: micro)

Statistical variable	DYN11 strain		DYN13 strain		DYN15 strain		Overall	
	Front	Rear	Front	Rear	Front	Rear	Front	Rear
Average	102	118	137	103	148	153	129	125
Standard deviation	7.5	4.0	4.8	11.4	10.5	10.5	22	23

Table 4.3 Measured tensile strains under front and rear axles of tandem axle at LTPP Ohio SPS-1 section (390108) at 62 km/h (unit: micro)

Statistical variable	DYN11 strain		DYN13 strain		DYN15 strain		Overall	
	Front	Rear	Front	Rear	Front	Rear	Front	Rear
Average	136	100	129	123	121	164	129	129
Standard deviation	5.8	5.1	8.4	8.1	10.4	4.6	10	28

4.2.2 Pavement Structure and Material Properties

The selected LTPP pavement section (390108) was consisted of an asphalt mixture layer of 165.1 mm, an asphalt-treated base layer of 101.6 mm, and an unbounded aggregate base layer of 203.2 mm laid on the subgrade. The asphalt mixture layer could be divided into 43-mm wearing course and 122.1-mm binder course. Asphalt concrete was considered as linear viscoelastic material. The relaxation moduli were converted based on the creep compliance data in lab test from LTPP database using the approximate method, in which both the relaxation modulus *E(t)* and creep compliance *D(t)* were formulated as a power-law based analytical form, as shown in Eq. 4-13 to 4-15 (Park and Kim, 1999).

$$E(t) = E_1 t^{-n} \tag{4-13}$$

$$D(t) = D_1 t^{n} \tag{4-14}$$

$$E(t)D(t) = \frac{sinn\pi}{n\pi} \quad (4\text{-}15)$$

Where E_1, D_1, and n are positive constants.

Based on the assumption of constant Poisson's ratio, shear and bulk moduli of asphalt concrete were calculated and fitted into Prony series of the generalized Maxwell solid model, as expressed by Eq. 4-16 and 4-17 (Ferry, 1980). The temperature dependency of relaxation modulus was characterized using time-temperature superposition principle. Williams-Landell-Ferry (WLF) function was applied to compute the time-temperature shift factor, as expressed by Eq. 4-18 (Dassault Systèmes, 2014). Table 4.4 shows the Prony series parameters for asphalt mixture at the reference temperature of 5°C, which can be converted to the analysis temperature of 21°C.

$$G(t) = G_0\left[1 - \sum_{i=1}^{N} G_i(1 - e^{-t/\tau_i})\right] \quad (4\text{-}16)$$

$$K(t) = K_0\left[1 - \sum_{i=1}^{N} K_i(1 - e^{-t/\tau_i})\right] \quad (4\text{-}17)$$

Where, G is shear modulus; K is bulk modulus; t is reduced relaxation time; G_0 and K_0 are instantaneous shear and volumetric elastic moduli; G_i, K_i, and $\boldsymbol{\tau}_i$ are Prony series parameters; N is the number of terms in the equation; and e is base of natural logarithm.

$$log(a_T) = -\frac{C_1(T - T_0)}{C_2 + (T - T_0)} \quad (4\text{-}18)$$

Where, T_0 is reference temperature; T is actual temperature corresponding to the shift factor; and C_1, C_2 are regression parameters.

Table 4.4 Prony series parameters for the asphalt mixtures at AC layer at reference temperature of 5°C

	i	Wearing Course		Binder Course	
		E_i	τi	Ei	τi
Prony Series Parameters	**1**	0.644	0.02	0.474	0.013
	2	0.104	1.05	0.211	0.164
	3	0.104	1.06	0.158	2.090
	4	0.100	19.47	0.114	37.695
	5	0.043	545.72	0.038	495.339
WLF function parameters	**C1**	51.2		51.2	
	C2	389.7		389.7	

Figure 4.5 shows the creep compliance of the asphalt mixture measured at the temperatures of -10°C, 5°C, and 25°C from LTPP database. Figure 4.6 illustrates the measured converted relaxation modulus and the fitted relaxation modulus using Prony's series of the asphalt mixtures at the reference temperature of 5°C.

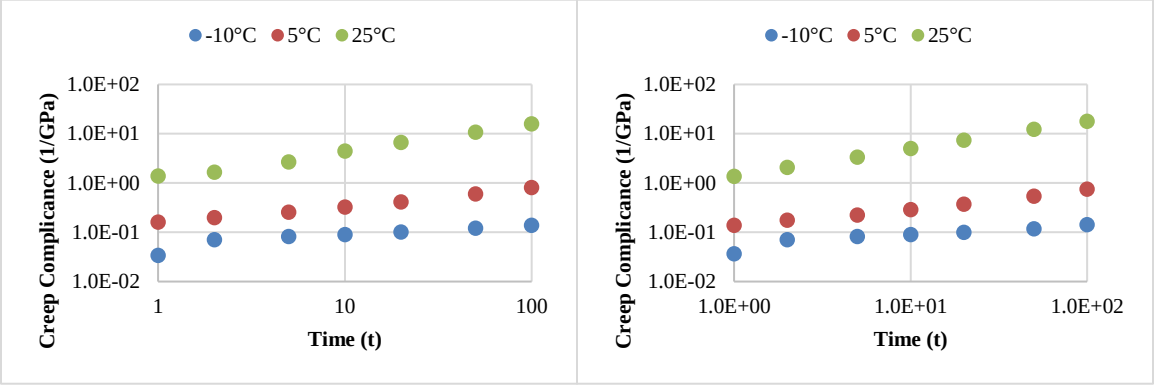

(a) (b)

Figure 4.5 Creep compliance of the asphalt mixture at (a) wearing course; and (b) binder course

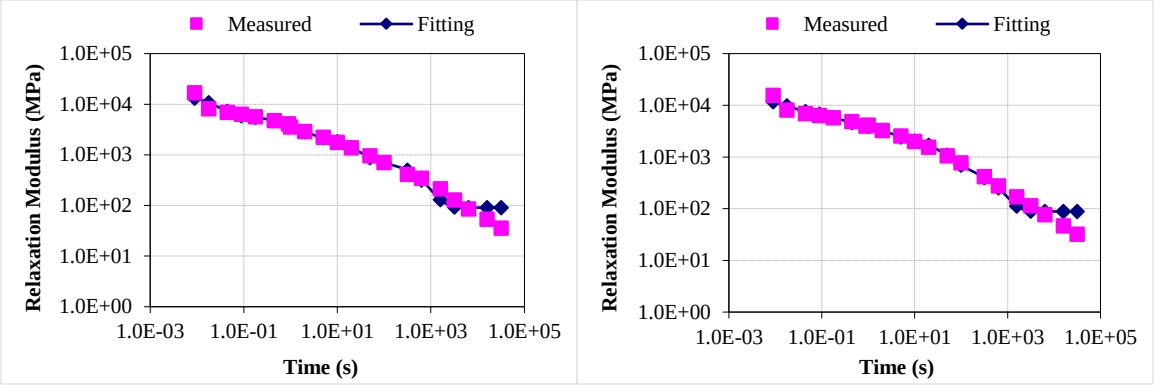

(a) (b)

Figure 4.6 The converted relaxation modulus of the asphalt mixture at (a) wearing course; and (b) binder course (temperature = 5°C)

The base layer of the selected section was asphalt-treated (open-graded, hot-laid, central plant mix AC). The Young's modulus of asphalt-treated base for flexible pavement sections in LTPP was 1882 MPa (Zhang, 2014). The resilient modulus of aggregate base layer (untreated) and subgrade were 178.5 MPa and 84.5 MPa, respectively, as recorded in the LTPP database.

4.3 Analysis of Dynamic Pavement Responses

4.3.1 Road Surface Profile and Dynamic Load

The pavement surface profiles on LTPP Ohio SPS-1 section (390108) were used for model validation. These pavement surface profiles were corresponded to the pavement section where pavement responses under dynamic loading were measured. The moving average of the profile measurements was 0.30 m, and the pavement surface elevation data was stored at 0.15-m intervals (Elkins et al., 2016). The total length of selected test section was 152.4 m and thus it was composed of 1,017 points. Figure 4.7 presents the pavement surface profiles measured on August 14, 1996. The IRI of the left and right wheel path

were 52 m/km (0.83 in./mile) and 60 m/km (0.95 in./mile), respectively. The overall IRI was 56 m/km, which indicated the test section was in good condition based on the recommended IRI thresholds for categorizing different pavement conditions (U.S. Department of Transportation, 2016).

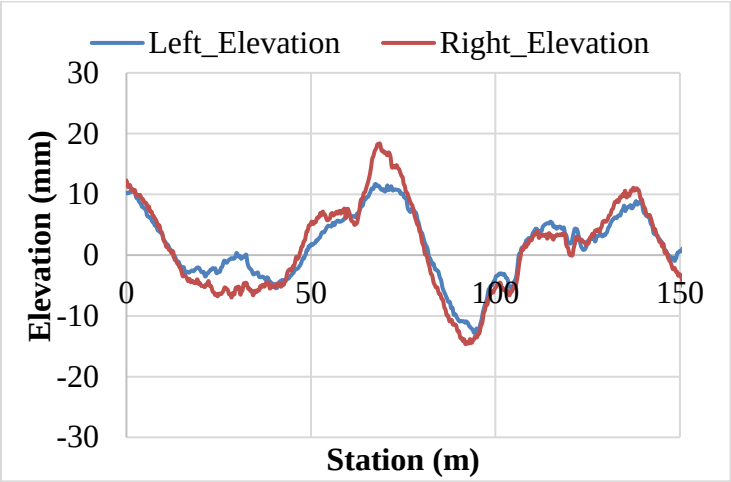

Figure 4.7 Pavement surface profiles on LTPP Ohio SPS-1 section (390108)

TruckSim was used to compute dynamic tire loads generated by the moving truck. TruckSim is commercial software that can be used to simulate full truck behavior and estimate tire forces in vertical, longitudinal, and transverse directions considering different road surface conditions and truck configurations. It has been used by the previous researchers to determine the lower and higher bound values of distress index (Chatti and Lee, 2002) and investigate the impacts of roughness index and vehicle suspension types on pavement damage (Kanai et al., 2010; Park, 2010).

A Class-6 single-unit 3-axle truck was simulated in TruckSim, which was the same type of truck used in the LTPP field test. The vehicle parameters were estimated based on the configuration of typical single-unit 3-axle truck. The sprung mass (empty truck without payload) was 43.66 kN, and the applied payload was 160.52 kN that was adjusted to match

the applied load on the tandem axle of test truck. The suspension type was leaf suspension and dual tires (11R22.5) was applied for the tandem axle (Tielking, 1992). The truck speed was 47 km/h (30 mph) which equaled to the measured vehicle speed in the field test. The sampling interval of tire force was taken at the interval of 0.01 second.

Figure 4.8 (a) shows the time-varying vertical forces under the left side of the front axle of tandem axle (Fz_L2), the left side of the rear axle of tandem axle (Fz_L3), the right side of the front axle of tandem axle (Fz_R2), and the right side of the rear axle of tandem axle (Fz_R3) as the test truck moving over the pavement section at 47 km/h (30 mph). The vertical tire forces under the first axle of tandem axle were observed slightly greater than those under the second axle, which was closely associated with the truck configuration and total truck weight. Vibration signals in time domain can be related to signals in frequency domain using PSD theorem, which is a function describing the power distribution of a signal over a frequency range, also called energy density (National Semiconductor, 1980). Figure 4.8 (b) illustrates the spectral analysis of dynamic loads transformed from time domain to frequency domain (PSD). The energy density induced by the front axle of tandem axle was greater than that of the rear axle, which was consistent with the trend in time domain.

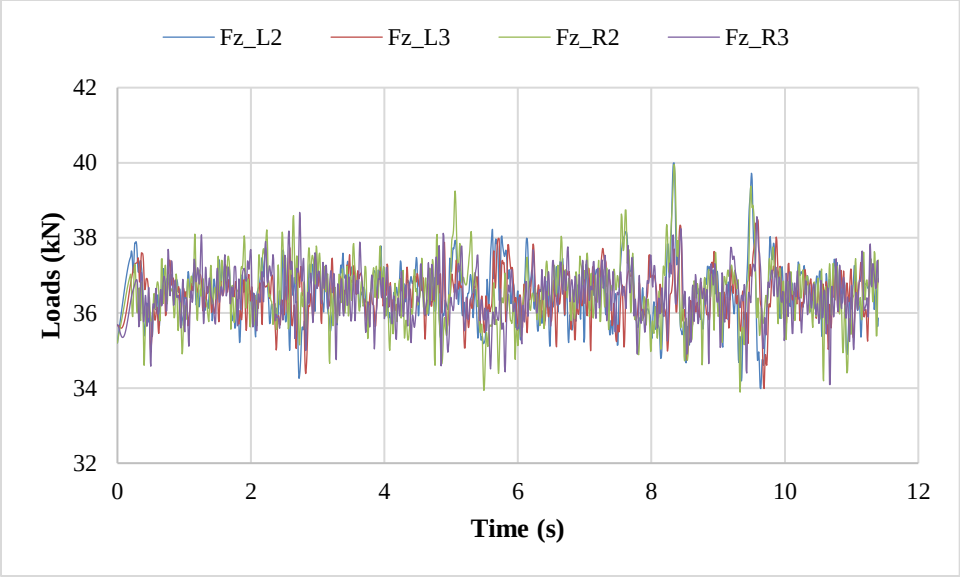

(a)

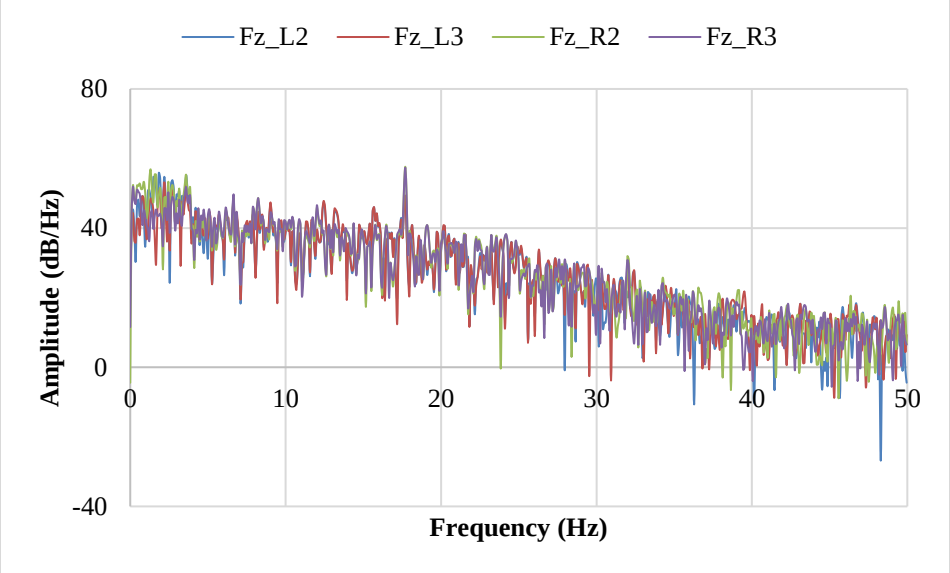

(b)

Figure 4.8 Dynamic loads under tandem axle in (a) time domain; and (b) frequency domain (PSD)

4.3.2 Determination of Equivalent Elastic Modulus of Asphalt Layer

In the impulse response method, steady state response analysis requires elastic material properties. Considering the viscoelastic nature of asphalt concrete, the equivalent elastic modulus of asphalt concrete was determined based on the equivalent loading frequency that is defined as the reverse of loading time at the mid-depth of asphalt layer. The loading time was calculated from the pulse time of compressive stress under moving load (Al-Qadi et al., 2008a). Figure 4.9 (a) presents the calculated vertical stress at the bottom of AC layer, and Figure 4.9 (b) shows the loading time calculation based on the results of the approaching-leaving model at the temperature of 21°C. The calculated loading time was 0.158 s, and the loading frequency was 6.37 Hz for the speed of 48 km/h. The equivalent modulus of asphalt mixture at wearing and binder courses were found to be 1828 MPa and 2143 MPa, respectively.

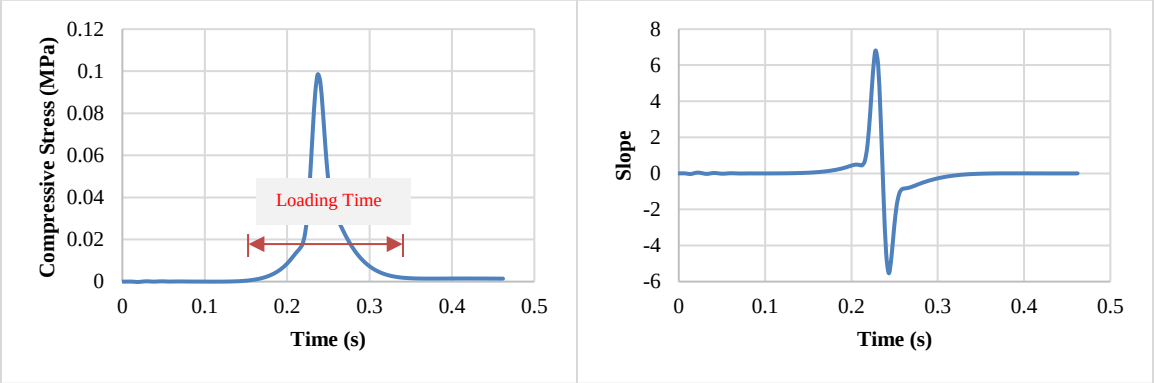

(a) (b)

Figure 4.9 (a) Calculated vertical stress at the bottom of AC layer; (b) loading time calculation based on the results of the approaching-leaving model

4.3.3 Results of Calculated Pavement Responses

The same FE mesh and model dimension used in the validate case were used in the analysis. A direct-solution SSD analysis step was defined in FE model to calculate the steady-state dynamic responses of pavement subject to harmonic excitation. The steady-state dynamic response for linear viscoelastic material can be simulated and computed directly.

The tensile strains at the bottom of asphalt layer were analyzed in this study, which were responsible for fatigue cracking commonly observed in the field. Pavement responses under harmonic loading were predicted by the 3-D FE model defined above. Figure 4.10 plots the calculated frequency response functions of transverse strains (E11) and longitudinal strains (E22) at the bottom of asphalt layer at the selected loading frequency range of 0-50 Hz, respectively. It should be noted that the transverse strains (E11) increased in the frequency range of 0-28 Hz and then decreased with the increase of frequency from 28 Hz to 50 Hz. The longitudinal strains (E22) were relatively stable at the selected frequency range. The comparison between the transverse strains in Figure 4.4 and Figure 4.10 indicates that pavement structures and material properties impacted on the trends of frequency response functions.

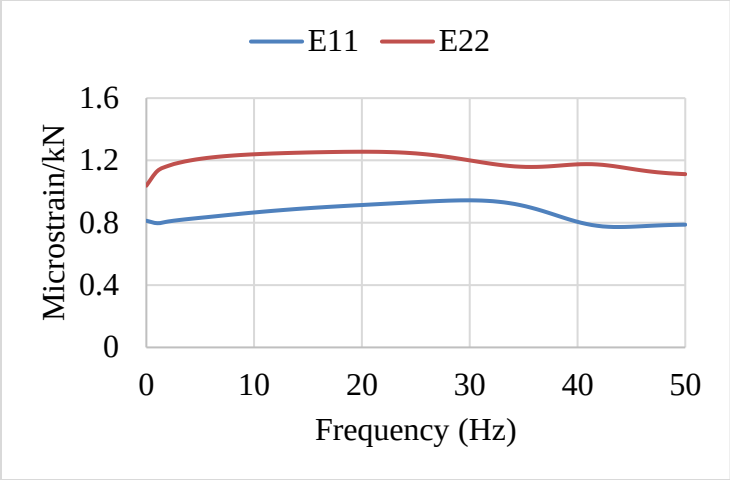

Figure 4.10 Frequency response functions of transverse strains (E11) and longitudinal strains (E22) at the bottom of asphalt layer due to harmonic excitations

The predicted tensile strains at the bottom of asphalt layer in longitudinal direction were then transformed from spatial domain to wavenumber domain by the Fast Fourier Transform. The frequency response functions in wavenumber domain were obtained through dividing pavement responses in the longitudinal direction by the non-uniform loads applied on pavement surface. The frequency response functions of longitudinal tensile trains in wavenumber domain under three selected frequencies are shown in Figure 4.11. It was found that several peaks were observed in the frequency response function in wavenumber (spatial frequency) domain. The specific pattern of frequency response function is dependent on load, pavement structure, material properties, and the selected pavement response. The pavement responses under dynamic loads were then derived by calculating the convolutional integral of response frequency function and the dynamic loads induced by surface roughness in wavenumber domain.

Three natural frequencies of pavement system, 3.06, 9.18 and 15.3 Hz, were selected for comparison based on steady state pavement response analysis. Previous

researches have used the similar range of frequency for dynamic pavement response analysis and found that pavement responses could increase or decrease with the increase of loading frequency (Hardy and Cebon, 1992; 1994; Khavassefat et al., 2014).

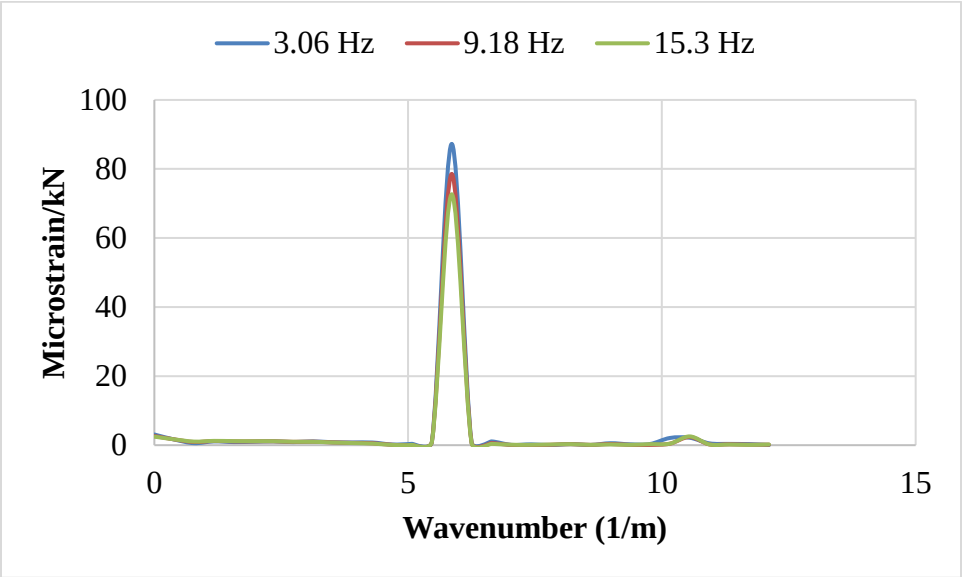

Figure 4.11 Frequency response functions of longitudinal strains (E22) at the bottom of asphalt layer in the wavenumber domain

Figure 4.12 shows the calculated longitudinal strains in the spatial domain (after the inverse Fourier transform from wavenumber domain) under the right side of the front axle of tandem axle (Fz_R2) in the test truck. It was found that the calculated longitudinal tensile strains were about 85-120 microstrain at the selected loading frequencies (3.06 Hz, 9.18 Hz, and 15.31 Hz). As compared to the measured strains shown in Table 4.2, the calculated longitudinal strains were found in agreement in general. The discrepancies could be caused by the exact test truck configuration parameters and pavement temperature were not known although they were estimated with reasonable assumptions.

On the other hand, the longitudinal tensile strains were found similar at the three selected frequencies, although a slight increasing trend was observed. This was consistent

with the finding reported by Hardy and Cebon (1994). The frequency response function at the frequency of 3.06 Hz was selected to further analyze dynamic pavement responses considering different levels of pavement roughness and vehicle speeds. The similar trends would be expected if other frequencies were selected, although the specific pavement responses may be different. It is noted that the loading frequency of dynamic loads is different from the loading frequency resulted from the duration of moving load in the traditional viscoelastic analysis of pavement responses.

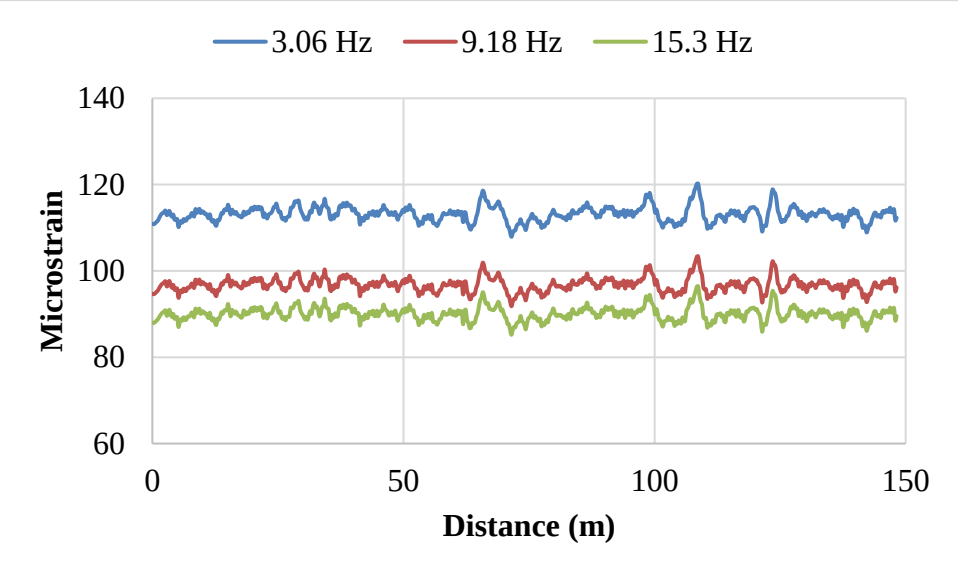

Figure 4.12 Longitudinal strains at the bottom of asphalt layer at the selected loading frequencies in spatial domain (after the inverse Fourier transform)

4.4 Analysis of Asphalt Pavement Fatigue Cracking under Dynamic Loads

4.4.1 Pavement Response Calculation under Dynamic Loads

The tensile strain at the bottom of asphalt surface layer was selected for analysis since it is responsible for the load-induced fatigue cracking. Figure 4.13 presents the

calculated longitudinal tensile strains at different locations of pavement section under the single axle of Class-5 truck and the axle having the greatest load in tandem axle of Class-9 truck and tridem axle of Class-7 truck, respectively. As expected, the heavier axle loads caused the greater tensile strains. Because of the larger axle weight, the tensile strains under single and tridem axles were apparent. On the other hand, the tensile strain induced by axle load varied along the distance due to dynamic loads. The greater tensile strains were induced at the location where the pavement surface was rougher.

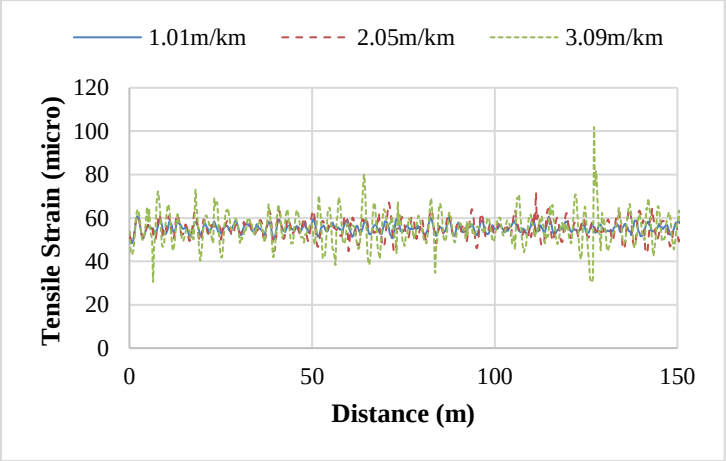

(a)

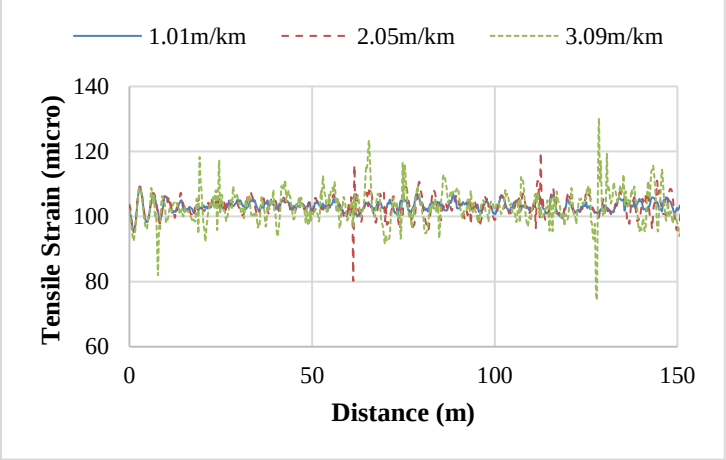

(b)

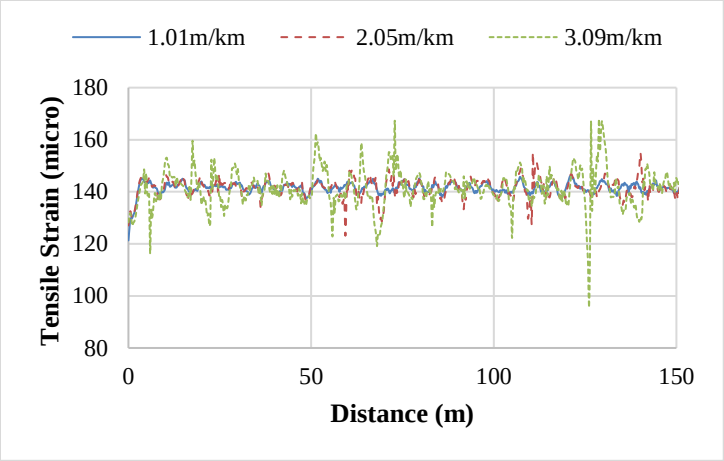

(c)

Figure 4.13 Horizontal strains at the bottom of asphalt concrete layer: (a) single axle, (b) tandem axle, and (c) tridem axle in Class-5, Class-7, and Class-9 trucks

Table 4.5 summarizes the range of calculated tensile strains under the selected axle of single, tandem, and tridem axle loads at three pavement roughness conditions. Due to the variation of tensile strains along the distance, the statistical parameters were given, including maximum, minimum, median, 25th percentile, and 75th percentile. As compared to the median values, the maximum tensile strains due to dynamic loads were about 10-82% greater for single axle, 5-27% greater for tandem axle, and 3-19% greater for tridem axle, respectively. The median value of strains caused by dynamic loads was believed to be similar to the strain caused by static loads since the median value of dynamic load magnitudes was very close to the static load magnitude. The more significant increase of strain responses was resulted on the rougher pavement condition. Therefore, it is expected that the fatigue cracking potential will increase significantly when dynamic loads on rough pavement surface are considered.

Table 4.5 Tensile strains caused by different axle types and loads (micro)

Axle	**Single (Class 5)**			**Tandem (Class 9)**			**Tridem (Class 7)**		
IRI (m/km)	**1.01**	**2.05**	**3.09**	**1.01**	**2.05**	**3.09**	**1.01**	**2.05**	**3.09**
Maximum	61	72	101	109	120	130	146	157	168
75th percentile	57	58	60	104	105	106	143	144	145
Median	55			103			142		
25th percentile	54	52	51	102	101	100	140	140	138
Minimum	48	44	30	96	80	75	121	123	96

4.4.2 Effects of Temperature and Vehicle Speed

Due to the viscoelastic properties of asphalt concrete, it is expected that pavement responses will be impacted by pavement temperature and vehicle speed. To quantify the effect of temperature and vehicle speed, the tensile strains at the bottom of asphalt surface layer were calculated at two pavement temperatures (5°C and 21°C) and two vehicle speeds (48 km/h and 80 km/h). The tensile strains caused by axle loads of Class-9 truck on three pavement surface conditions (IRI = 1.01, 2.05, and 3.09 m/km) were calculated and analyzed.

Table 4.6 summarizes the range of calculated tensile strains under the selected axle loads at different vehicle speeds and temperatures on three pavement roughness conditions. It was found that the tensile strains decreased as pavement temperature decreased due to the viscoelastic properties of asphalt concrete. The median value of tensile strains was found decrease as vehicle speed increased, but the maximum tensile strains caused by dynamic loads increased as vehicle speed increased. This finding corresponds to the greater dynamic loads at higher vehicle speeds when pavement roughness was taken into consideration.

Table 4.6 Tensile strains caused by dynamic axle loads at different vehicle speeds and temperatures (micro)

Speed (km/h)	Temperature (°C)	Axle Loads (kN)	107			125			160		
		IRI (m/km)	1.01	2.05	3.09	1.01	2.05	3.09	1.01	2.05	3.09
48	21	Maximum	93	102	114	109	120	130	135	150	151
		75th percentile	88	89	89	104	105	106	131	132	132
		Median	87			103			129		
		25th percentile	86	86	84	102	101	100	128	126	125
		Minimum	79	64	59	96	80	75	121	110	100
	5	Maximum	37	44	55	44	52	61	55	64	69
		75th percentile	36	36	37	43	43	44	54	54	54
		Median	36			42			53		
		25th percentile	35	35	34	42	41	41	52	51	51
		Minimum	34	30	15	40	37	21	50	48	32
80	21	Maximum	83	103	121	96	113	139	122	132	161
		75th percentile	78	80	80	91	93	94	114	115	118
		Median	76			90			112		
		25th percentile	73	71	70	88	86	83	110	109	104
		Minimum	67	58	48	81	70	56	103	91	74
	5	Maximum	36	49	63	42	53	72	53	61	82
		75th percentile	34	35	35	39	40	41	49	50	51
		Median	33			39			48		
		25th percentile	32	31	30	38	37	36	47	47	45
		Minimum	29	22	11	35	27	13	44	36	20

To evaluate variation of tensile strains caused by dynamic loads on rough pavement surface condition, amplification ratio of tensile strains was defined as ratio of maximum tensile strains to medium values generated by dynamic loads along pavement profile. Table 4.7 summarizes the calculated amplification ratio of tensile strains due to dynamic loads at different vehicle speeds and temperatures on three pavement surface conditions. It indicated that amplification ratios increased as pavement temperature decreased while increased as vehicle speed increased. Besides, the influence of pavement temperature became more significant on rougher pavement surface conditions (IRI = 2.05 and 3.09

m/km). The amplification ratio was found decrease as axle load increased which was consistent with the findings related to the impact of axle loads on DLCs.

Table 4.7 Calculated amplification ratio of tensile strains at different vehicle speeds and temperatures

Speed (km/h)	**Temperature (°C)**	**Axle Loads (kN)**								
		107			125			160		
		1.01 m/km	2.05 m/km	3.09 m/km	1.01 m/km	2.05 m/km	3.09 m/km	1.01 m/km	2.05 m/km	3.09 m/km
48	21	1.06	1.17	1.31	1.05	1.16	1.26	1.04	1.16	1.17
	5	1.05	1.24	1.55	1.05	1.22	1.45	1.05	1.21	1.31
80	21	1.10	1.37	1.61	1.07	1.26	1.55	1.09	1.18	1.44
	5	1.11	1.49	1.94	1.09	1.37	1.86	1.10	1.26	1.70

4.4.3 Fatigue Life Analysis Considering Dynamic Loads

The fatigue life of asphalt pavement with smooth surface condition under traffic loading can be estimated following the approach in MEDPG. The fatigue life of asphalt concrete is determined by the maximum tensile strains at the bottom of asphalt layer induced by axle loads. The number of allowable axle load applications for fatigue cracking was estimated based on the Eq. 4-19, as suggested by MEPDG (ARA Inc., 2019).

$$N = 0.00432 \times k_1' \times C \times \left(\frac{1}{\varepsilon_t}\right)^{3.9492} \left(\frac{1}{E}\right)^{1.281} \quad (4\text{-}19)$$

Where,

N = the number of allowed load applications for fatigue cracking;

ε_t = tensile strain at the bottom of asphalt layer;

E = resilient modulus of asphalt pavement, psi;

k_1' = the parameter related to asphalt concrete thickness; and

C = the parameter related to asphalt mixture volumetric properties.

Since the current framework of MEPDG does not consider dynamic loads caused by rough pavement surface in prediction of flexible pavement life, an approach was proposed here to consider the impact of dynamic loads on fatigue life analysis. The concept of relative ratio of fatigue life was calculated using the maximum tensile strain under dynamic loads and the strain under static loads, as shown in Eq. 4-20. It is worth mentioning that small change of tensile strain may cause greater change of fatigue life due to the power law coefficient of 3.9492 in fatigue model.

$$r = \frac{N_d}{N_s} = \left(\frac{\varepsilon_{t,s}}{\varepsilon_{t,d}}\right)^{3.9492} \quad (4\text{-}20)$$

Where,

r = relative ratio of fatigue life;

N_d, N_s = the number of allowed loading applications for dynamic loads and static loads, respectively; and

$\varepsilon_{t,d}, \varepsilon_{t,s}$ = tensile strain at the bottom of asphalt layer induced by dynamic loads and static loads, respectively.

The relative ratio of fatigue life due to dynamic loads on three pavement roughness conditions (IRI = 1.01, 2.05 or 3.09 m/km) were calculated for different axle types and load magnitudes, as illustrated in Figure 4.14. As expected, the effect of dynamic load causes the greater reduction of fatigue life as the pavement is rougher. It was also found that the influence of dynamic loads on pavement deterioration became more significant under lighter axle loads which was consistent with the findings related to the impact of axle loads on DLCs.

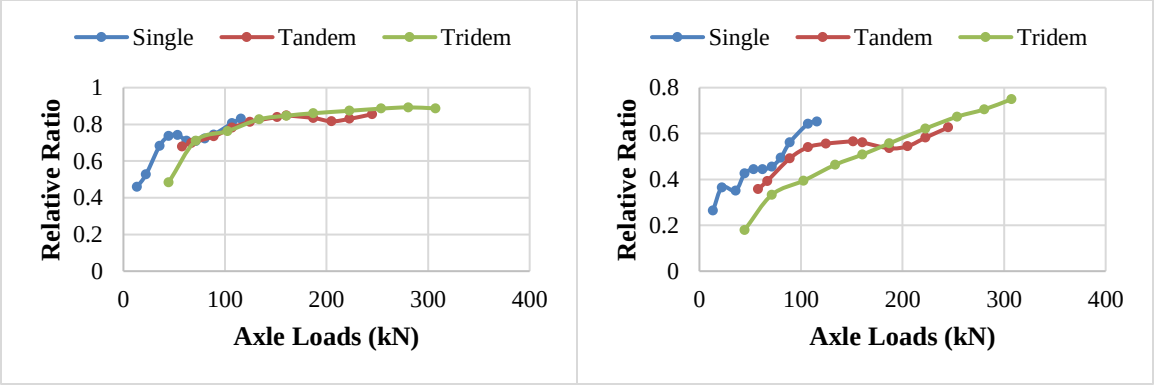

(a) (b)

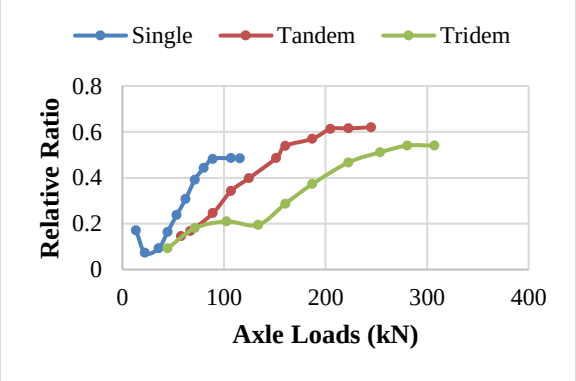

(c)

Figure 4.14 Relative ratio of fatigue life due to dynamic loads of single, tandem, and tridem axles on rough pavement with IRI of (a) 1.01 m/km; (b) 2.05 m/km; and (c) 3.09 m/km

In order to quantify the effect of dynamic loads on fatigue life in an efficient way, a nonlinear regression model was used to fit the relative ratio of fatigue life as the function of axle type, load, and IRI, as shown in Eq. 4-21. The R-square of fitted model was 0.91 which was acceptable. The fitting model can be used to calculate the relative ratio of fatigue life for a wide range of axle load magnitudes and IRI values.

$$r = 0.207 * ln(L) - 0.195 * IRI + SF \quad (4\text{-}21)$$

Where,

IRI = International Roughness Index, m/km;

L = axle load, kN; and

SF = the shift factor for each axle type (0.537 for single; 0.442 for tandem axle; and 0.387 for tridem axle).

4.4.4 Consideration of Dynamic Loads in M-E Pavement Design and Analysis

In the M-E pavement design and analysis, fatigue cracking prediction is based on the cumulative damage concept given by Miner's rule. The accumulated incremental damage was used to consider traffic loading applied at different time periods over the service life of pavement, as expressed by Eq. 4-22. It is noted that the axle factor of 1, 2, and 3 are used for single, tandem, and tridem axle to consider the multiple axle effect during one pass of each axle configuration, since the tensile strain is calculated using the single axle of Class-5 and the axle having the greatest load in tandem axle of Class-9 and tridem axle of Class-7 trucks.

$$D = \sum_{k=1}^{T} \sum_{j=L_{min}}^{L_{max}} \sum_{i=1}^{3} \left(\frac{a_i \times n_{i,j,k}}{N_{i,j,k}} \right) = \sum_{k=1}^{T} \sum_{j=L_{min}}^{L_{max}} \sum_{i=1}^{3} \left(\frac{a_i \times p_{i,j,k} \times n}{N_{i,j,k}} \right) \qquad (4\text{-}22)$$

Where,

D = fatigue damage factor;

T = total number of periods;

i = axle type (1 for single axle, 2 for tandem axle, and 3 for tridem axle);

j = axle load, kN;

k = time period;

L_{min}, L_{max} = the minimum and maximum axle loads in spectra, kN;

a_i = axle factor (1 for single axle, 2 for tandem axle, 3 for tridem axle);

$n_{i,j,k}$ = the number of *i* axles at load *j* for period *k*; and

$p_{i,j,k}$ = the percentage of *i* axles at load *j* in total traffic in period *k*;

n = the number of total axles; and

$N_{i,j,k}$ = the number of allowable loading repetitions of *i* axle at load *j* in period *k*.

The fatigue damage ratios between dynamic loads on rough pavement (IRI =1.01, 2.05 or 3.09 m/km) and static load can be calculated using axle load spectra at the specific time period, as shown by Eq. 4-23. The fatigue damage ratios are determined to be dependent on the percentage of single, tandem, tridem axles at each load interval, the tensile strain at static loads, and the relative ratio of fatigue life due to dynamic loads.

$$R_L = \frac{D_d}{D_s} = \frac{\sum_{k=1}^{T}\sum_{j=L_{min}}^{L_{max}}\sum_{i=1}^{3}\left(\frac{a_i \times p_{i,j,k}}{r_{i,j,k}N_{i,j,k}}\right)}{\sum_{k=1}^{T}\sum_{j=L_{min}}^{L_{max}}\sum_{i=1}^{3}\left(\frac{a_i \times p_{i,j,k}}{N_{i,j,k}}\right)} = \frac{\sum_{k=1}^{T}\sum_{j=L_{min}}^{L_{max}}\sum_{i=1}^{3}\left(\frac{a_i \times p_{i,j,k}}{r_{i,j,k}\left(\varepsilon_{i,j,k}\right)^{-3.9492}}\right)}{\sum_{k=1}^{T}\sum_{j=L_{min}}^{L_{max}}\sum_{i=1}^{3}\left(\frac{a_i \times p_{i,j,k}}{\varepsilon_{i,j,k}{}^{-3.9492}}\right)} \quad (4\text{-}23)$$

Where,

R_L = fatigue damage ratio due to dynamic loads (the relative ratio of accumulative fatigue damage between dynamic loads and static loads);

D_s = fatigue damage caused by static loads;

D_d = fatigue damage caused by dynamic loads;

ai = axle factor (1 for single axle, 2 for tandem axle, 3 for tridem axle);

$p_{i,j,k}$ = the percentage of *i* axles at load *j* in total traffic in period *k*;

$r_{i,j,k}$ = relative ratio of fatigue life of *i* axle at load *j* for the corresponding IRI value in period *k*; and

$\varepsilon_{i,j,k}$= tensile strain at the bottom of asphalt layer induced by *i* axle at load *j* in period *k*.

To illustrate the effect of dynamic loads on fatigue damage factor, an example of analysis was conducted using the strain responses obtained from the above analysis. The axle load spectra at the selected test section was extracted from LTPP database and used

as an example in the analysis. Figure 4.15 shows the percentages of different axle configurations at different load intervals. In this case, single, tandem, and tridem axle were approximately 50%, 49%, and 1% of the total traffic in terms of the number of total axles.

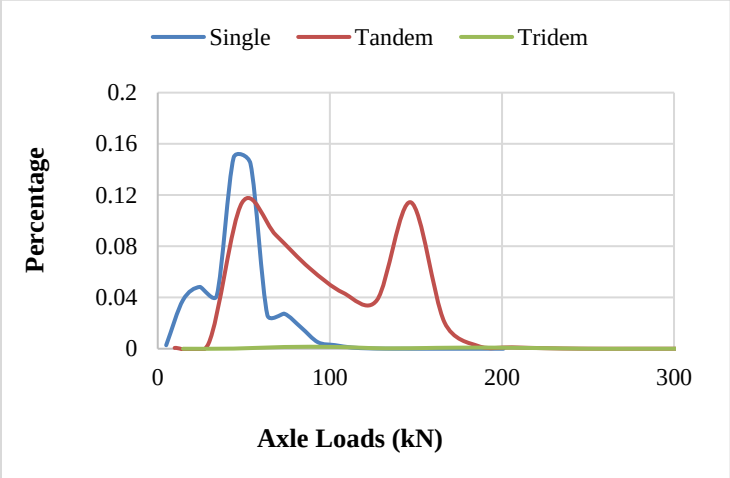

Figure 4.15 Example of axle load distribution used in the analysis

Figure 4.16 shows the calculated fatigue damage ratio (R_L) due to dynamic loads in different roughness conditions using Eq.4-23. It clearly shows that fatigue damage is significantly impacted by roughness levels. The relationship between fatigue damage ratio and IRI can be well fitted with an exponential relationship.

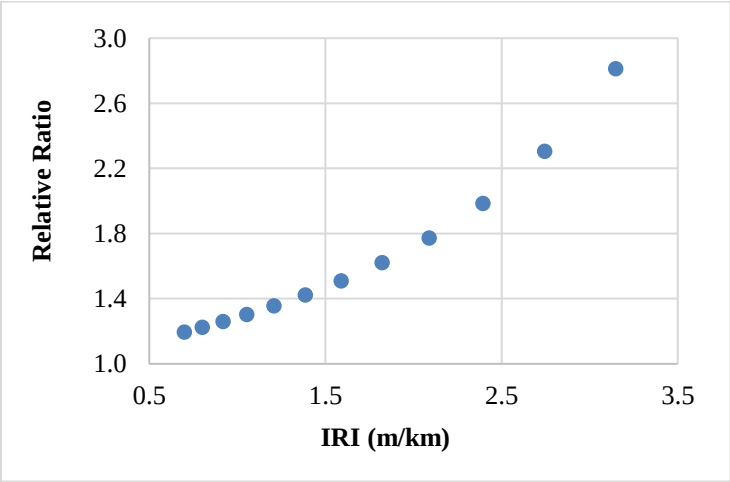

Figure 4.16 Fatigue damage ratios calculated at different IRI values

In M-E pavement design and analysis, the axle load spectra and pavement material properties vary at different time periods, which cause tensile strains and fatigue damage ratios due to dynamic loads changing accordingly. Therefore, a systematic approach is needed to consider dynamic loads in the M-E pavement analysis procedure. Figure 4.17 presents the proposed methodology to consider dynamic load impact in the existing M-E pavement analysis framework. The relative ratio of fatigue life is used to derive the fatigue life under dynamic loading condition, which is further used to calculate the accumulated damage. The initial IRI after construction is used as the input to calculate the relative ratio of fatigue life in the first year. After that, the IRI increase is predicted as the function of pavement distresses based on the existing empirical function in M-E analysis that can be used to determine the relative ratio of fatigue life over the service life of pavement. Finally, the fatigue cracking development over time can be calculated using the transfer functions based on the updated damage accumulation.

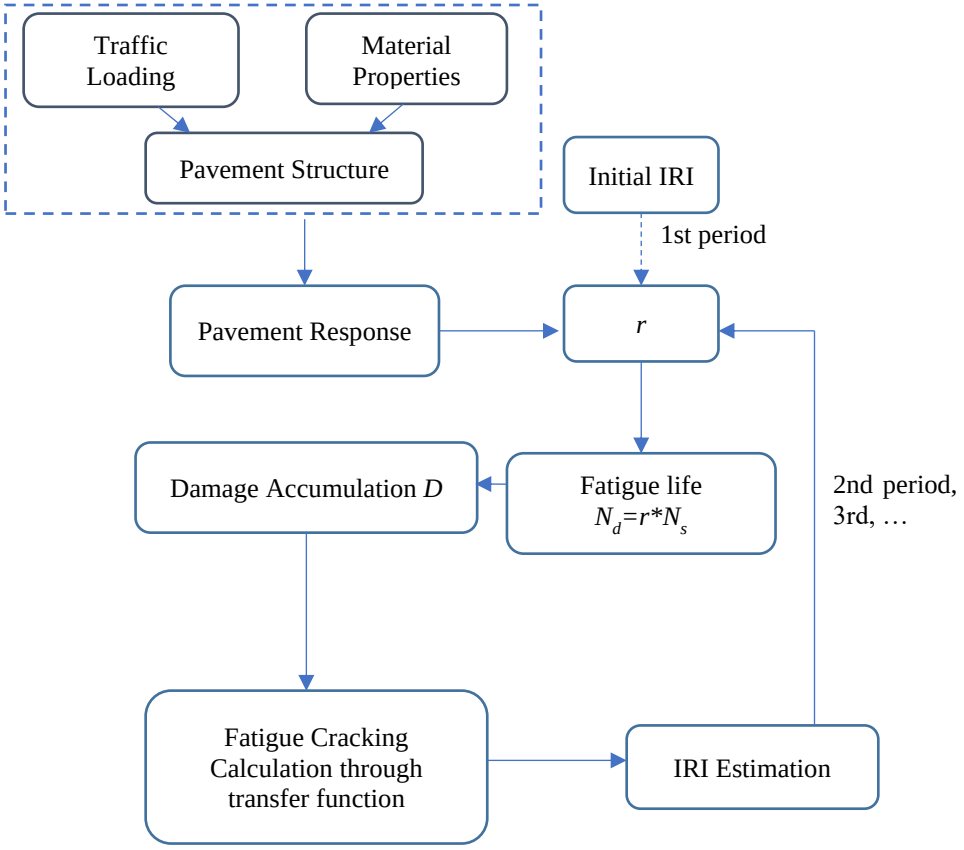

Figure 4.17 Consideration of dynamic loads in M-E pavement analysis

4.5 Impact Analysis of Wide-Base Tire on Pavement Responses

4.5.1 Tire-Pavement Contact Stresses

To simulate tire loads more realistically, the non-uniform distribution of tire-pavement contact stress in the tire-pavement contact area under dual-tire assembly and wide-base tire were considered in the FE model. The peak stress at each tire rib and the non-uniform distribution along the contact length were used to describe the tire contact stress patterns (Wang and Al-Qadi, 2010; Al-Qadi and Wang, 2011). Figure 4.18 shows the contact area and peak contact stresses at each rib for dual-tire assembly and wide-base tire. These detailed value indicates the relative ratio of maximum contact stress applied on

each rib, which was determined according to the measured and simulated contact stresses under different tire configurations (Al-Qadi and Wang, 2011).

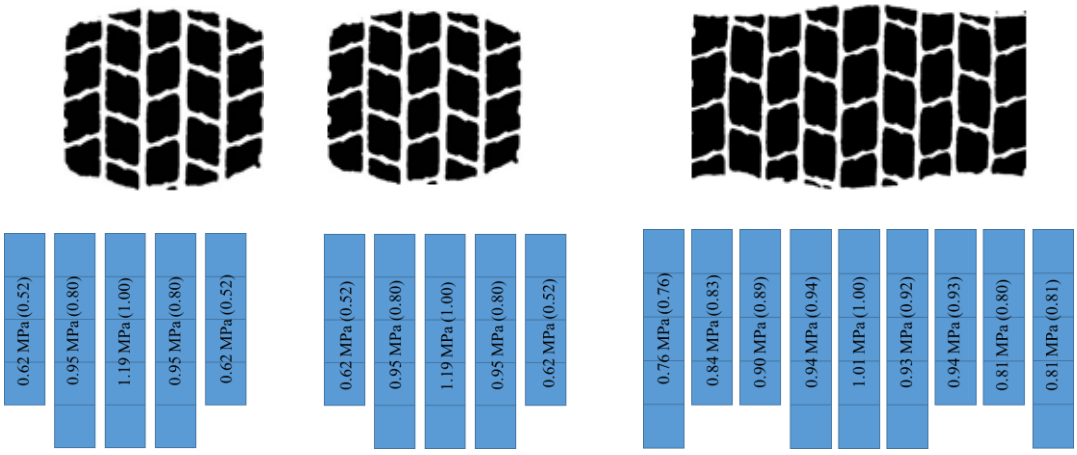

(a) (b)

Figure 4.18 Non-uniform distribution of contact stress (tire inflation pressure: 690 kPa): (a) dual-tire assembly; (b) wide-base tire

4.5.2 Calculation of Pavement Responses

The dynamic tire forces of two truck configurations (Class-5 and Class-9), three pavement roughness conditions (IRI=1.01, 2.05, and 3.09 m/km), and two vehicle speeds (48 and 96 km/h) were considered to analyze the impact of wide-base tire on pavement responses using the proposed method. The steady-state dynamic responses of pavement under harmonic excitations at the specific frequencies were estimated using the FE model. Based on analysis of moving loads at different speeds model, the estimated loading time and frequency were estimated to drive the equivalent elastic modulus of asphalt layers. The pavement temperature considered in the analysis was 21.1°C,

Fatigue cracking and rutting are common pavement distresses occurred at in-service asphalt pavement structure. Fatigue cracking is determined by tensile strain at the

bottom of AC layer, and subgrade rutting is more affected by compressive strain on the top of subgrade. Besides, top-down cracking might be observed for thick asphalt pavement, which is induced by near-surface shear strain (Wang and Al-Qadi, 2009; Al-Qadi and Wang, 2012). Therefore, tensile strain at the bottom of AC layer, compressive strain on the top of subgrade, and near-surface shear strain were considered as critical pavement responses in the analysis. Figure 4.19 shows the comparison of frequency response function at critical locations subjected to unit load of dual-tire assembly and wide-base tire, respectively. The truck configuration was Class-9 truck traveling at 48km/h. Compared to the pavement response generated by dual-tire assembly, the increases of pavement response subjected to wide-base tire were approximately 32% and 13% for the tensile strain at the bottom of asphalt layer and compressive strain on the top of subgrade. The increase was consistent under different frequency. There was only 2% difference between the near-surface shear strains (shear) under the dual-tire assembly and wide-base tires.

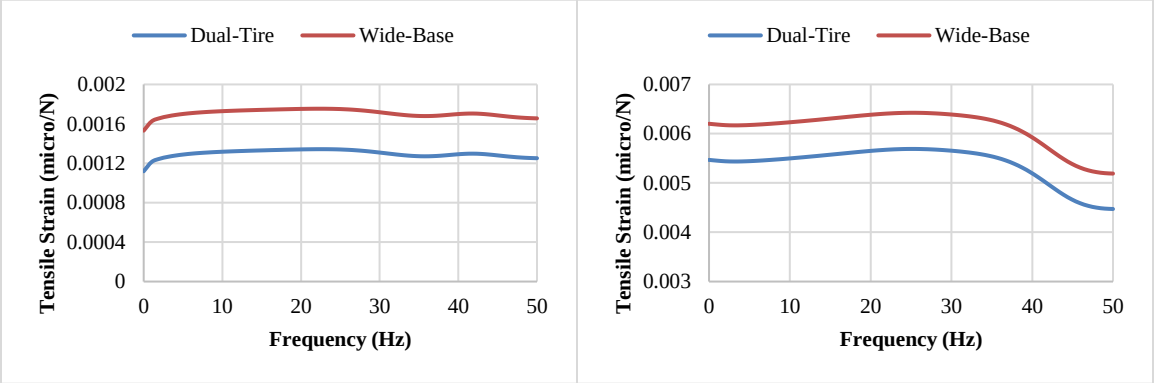

(a) (b)

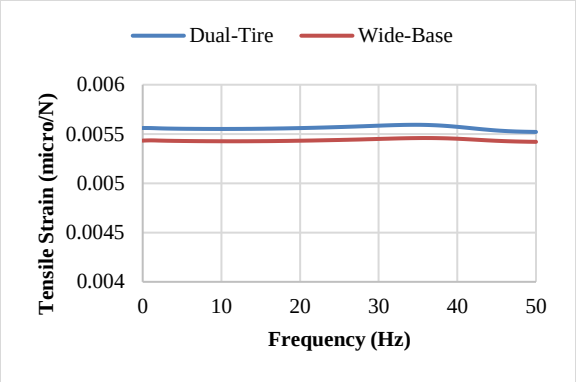

(c)

Figure 4.19 Comparison of pavement responses at critical locations under unit load of dual-tire assembly and wide-base tire (Class-9 truck; 48 km/h): (a) tensile strain; (b) compressive strain; (c) near-surface shear strain

By calculating the convolutional integral of dynamic tire forces and frequency response functions, the pavement responses at critical locations induced by dual-tire assembly and wide-base tire were estimated. Figure 4.20 shows the comparison of pavement responses along the 152-m pavement section induced by dual-tire assembly and wide-base tire. It indicated that the tensile strain at the bottom of asphalt layer was much larger under wide-base tire, while the compressive strain on the top of subgrade and near-surface shear strain under dual-tire assembly and wide-base tire were similar. Since the maximum dynamic loads were spatially repeatable, the maximum pavement responses induced by two tire types on the same pavement section were found at the specific locations on different pavement roughness conditions.

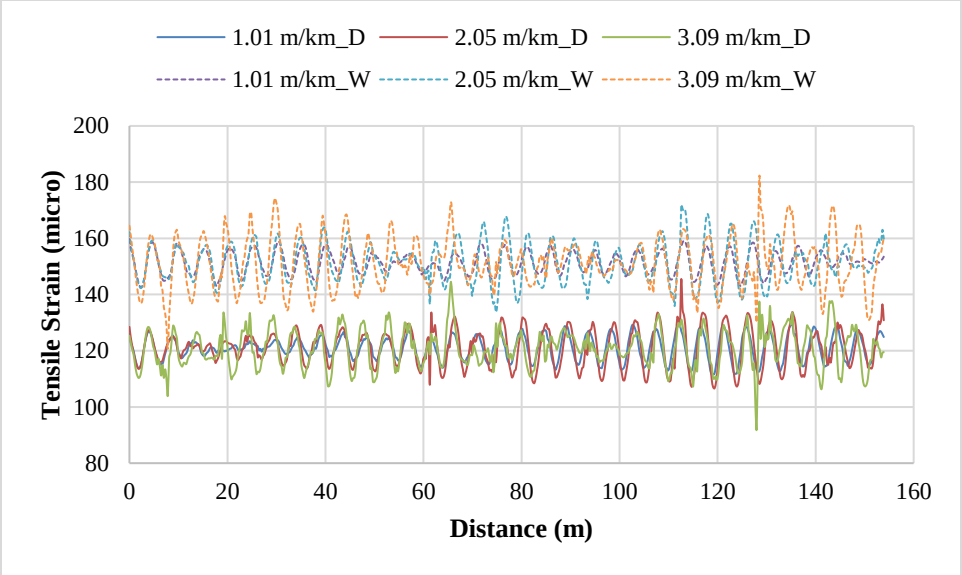
1.01 m/km_D
2.05 m/km_D
3.09 m/km_D
1.01 m/km_W
2.05 m/km_W
3.09 m/km_W
Tensile Strain (micro)
200
180
160
140
120
100
80
0
20
40
60
80
100
120
140
160
Distance (m)

(a)

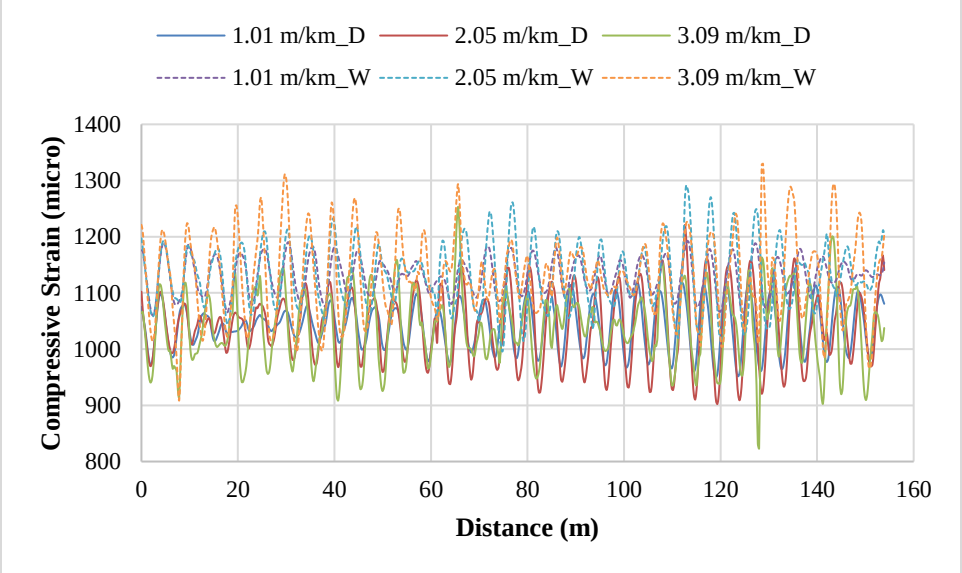
1.01 m/km_D
2.05 m/km_D
3.09 m/km_D
1.01 m/km_W
2.05 m/km_W
3.09 m/km_W
Compressive Strain (micro)
1400
1300
1200
1100
1000
900
800
0
20
40
60
80
100
120
140
160
Distance (m)

(b)

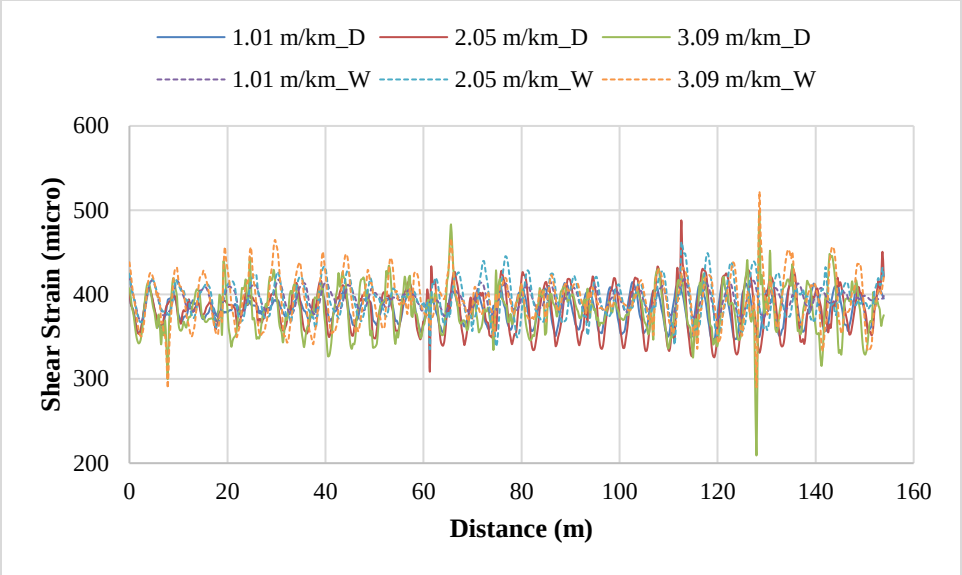

(c)

Figure 4.20 Pavement responses at critical locations along road profile between the dual-tire assembly and wide-base tire (Class-9 truck at 48 km/h): (a) tensile strain; (b) compressive strain; (c) near-surface shear strain

4.5.3 Pavement Response Ratios between Different Tire Configurations

To quantify the impact of wide-base tire, the ratio of pavement response between two tire types was defined by dividing the pavement responses under wide-base tire by those generated under dual-tire assembly.

Table 4.8 and Table 4.9 summarize the ratio of maximum pavement responses, including tensile strain at the bottom of asphalt layer, compressive strain on the top of subgrade, and near-surface shear, on different pavement roughness conditions. As compared to the response ratio under harmonic excitations of unit load as shown in Figure 4.19 (1.32 for tensile strains and 1.13 for compressive strains), the response differences between two tire configurations became smaller. It indicated that the dynamic tire forces under wide-base tire had positive impact on the tensile strains at the bottom of asphalt layer

and compressive strains on the top of subgrade. However, the influence of dynamic tire forces on near-surface shear strains found was not significant.

Table 4.8 Response ratio of maximum pavement response (Class-5 truck)

Speed (km/h)	IRI (m/km)	Pavement response ratio		
		Tensile strain at bottom of asphalt layer	Compressive strain on the top of subgrade	Near-surface shear strain
48	1.01	1.23	1.06	1.00
	2.05	1.24	1.07	1.02
	3.09	1.24	1.08	0.99
96	1.01	1.23	1.05	1.01
	2.05	1.24	1.06	1.00
	3.09	1.25	1.05	1.03

Table 4.9 Response ratio of maximum pavement responses (Class-9 truck)

Speed (km/h)	IRI (m/km)	Pavement response ratio		
		Tensile strain at bottom of asphalt layer	Compressive strain on the top of subgrade	Near-surface shear strain
48	1.01	1.23	1.06	1.02
	2.05	1.18	1.06	0.95
	3.09	1.26	1.06	1.04
96	1.01	1.27	1.08	1.05
	2.05	1.23	1.07	0.99
	3.09	1.30	1.07	0.95

Table 4.10 summarizes the range and average value of response ratio at critical location along pavement section. It was found that the variation of response ratio increased as pavement roughness levels increase, which was consistent with the trends of dynamic

tire forces. In general, wide-base tire caused greater tensile strain but similar compressive strain and near-surface shear strain as compared to dual tire assembly. This trend is consistent with previous research findings from theoretical analysis and field testing (Al-Qadi and Wang, 2012). However, the pavement response ratios caused by two tire configurations show certain variations as truck configuration, speed, or pavement surface roughness changes. The increase of pavement surface roughness may increase or decrease the pavement response ratio, depending on the specific road surface profile and the resulted dynamic tire forces. This emphasizes the importance of considering dynamic tire forces in the accurate calculation of pavement responses considering vehicle-tire-pavement interaction.

Table 4.10 The range of pavement response ratio along pavement section

Truck	**Speed (km/h)**	**IRI (m/km)**	**Pavement response ratio**		
			Tensile strain at bottom of asphalt layer	**Compressive strain on top of subgrade**	**Near-surface shear strain**
Class-5	48	1.01	1.18-1.33	1.01-1.16	0.96-1.11
		2.05	1.12-1.4	0.96-1.23	0.9-1.19
		3.09	1.09-1.42	0.94-1.24	0.88-1.21
	96	1.01	1.17-1.35	1-1.16	0.96-1.12
		2.05	1.17-1.36	1-1.17	0.96-1.16
		3.09	1.11-1.39	0.95-1.2	0.85-1.39
Class-9	48	1.01	1.15-1.37	0.99-1.19	0.93-1.14
		2.05	1.1-1.43	0.94-1.26	0.88-1.22
		3.09	1.11-1.41	0.96-1.24	0.89-1.36
	96	1.01	1.17-1.34	1-1.15	0.96-1.12
		2.05	1.11-1.42	0.94-1.23	0.89-1.2
		3.09	1.07-1.58	0.91-1.38	0.86-1.37

4.6 Summary

In this chapter, the impulse response method was used to calculate flexible pavement responses subjected to moving dynamic loads. The frequency response function was validated using field measurements and calculations reported in the literature. The predicted tensile strains under dynamic loads were found in agreement with field measurements at the selected test section in LTPP. The impulse response method was used to estimate pavement response caused by dynamic loads due to rough pavement surface condition considering vehicle-tire-pavement interaction. The relative ratio of fatigue life was defined to estimate fatigue damage induced by dynamic axle loads on different pavement roughness conditions. A methodology was proposed to incorporate the impact of dynamic loads on fatigue cracking development in the framework of M-E pavement design and analysis. The dynamic pavement responses under wide-base tire and dual tire assembly were estimated considering vehicle-tire-pavement interaction. The impulse response method was used to calculate the flexible pavement responses under random moving loads.

CHAPTER 5 COMPARISON ANALYSIS OF TRAFFIC LOADING IMPACT USING NONLINEAR REGRESSION AND SUPPORT VECTOR REGRESSION MODELS

5.1 Data Collection and Processing

5.1.1 Truck Traffic Data from WIM

Weigh-in-motion devices can continuously capture and record GVW, axle load, and axle spacing with supplementary data including date, time, speed, lane of travel, and vehicle type. Axle load spectra and GVW from WIM database are critical inputs for mechanistic-based pavement design and pavement performance analysis. NJDOT have 95 WIM sites in the highway network. The axle load spectra recorded at 87 WIM sites for both directions were extracted from Vehicle Travel Information System (VTRIS) operated by Federal Highway Administration (FHWA) (Federal Highway Administration, 2017).

The numbers of daily ESALs for flexible and rigid/composite pavement structures were calculated from WIM data based on load equivalency factors derived from AASHO road test (Huang, 1993). Considering that WIM data was not recorded for every segment successively from 2000 to 2014, the daily ESALs were averaged for every five years. Figure 5.1 shows the frequency distribution of average annual daily ESALs for Interstate highways, US highways, and state highways, respectively. Interstate highways are part of the network of controlled-access highways for long-distance travel and freight transport. US highways are mainly consisted of major roads having the designation and numbering coordinated among the states over US. State highways are designed according to various standards or capacity and operated by state governments.

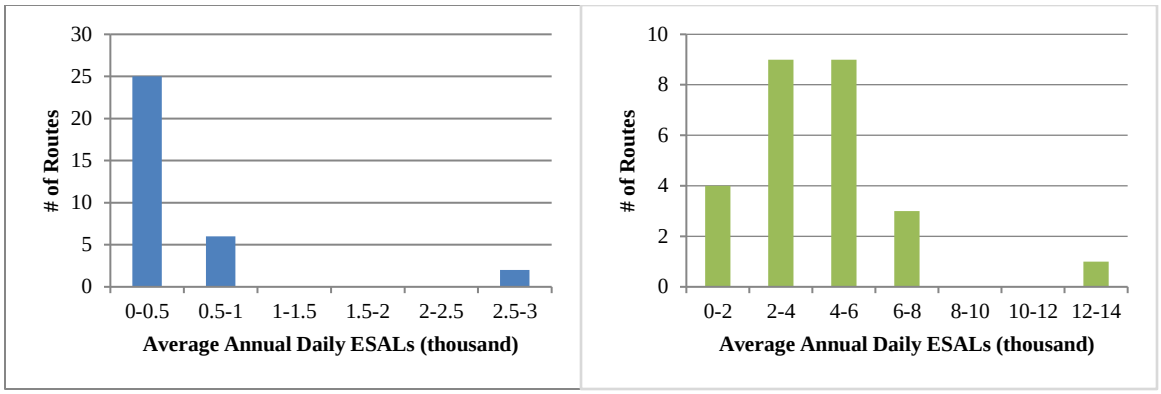

(a) (b)

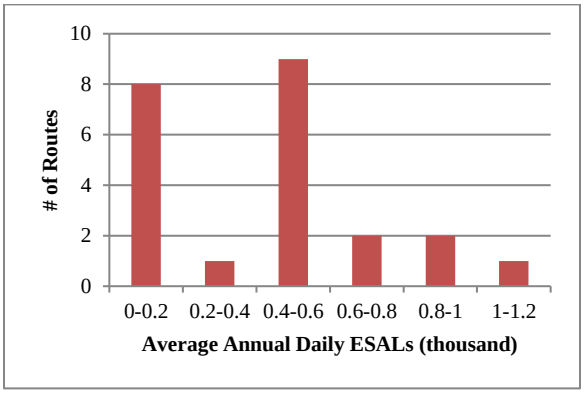

(c)

Figure 5.1 Frequency distribution of average annual daily ESALs on (a) state highways, (b) Interstate highways and (c) US highways in NJ

The number of single, tandem, tridem axle loads and axle load spectra were provided in the Vehicle Travel Information System. Figure 5.2 shows single, tandem, and tridem axle load spectra of all trucks on Interstate highway Route 80 in the year of 2000. It indicated that single axles had the most axle loads around 5 kips, and the axle loads of tandem axles concentrated at 5 kips and 11 kips. Most of tridem axles have loads between 18 and 20 kips. In previous works, Gaussian distribution was applied to fit the observed single and tridem axle load spectra, and the tridem axle load was usually not considered (Haider and Harichandran, 2009; Haider et al., 2009). In this study, the axle load spectra

were fitted using Gaussian distribution, and the amplitude, centroid, and peak width of Gaussian distribution were used to characterize the pattern of traffic loads. The Gaussian distribution fits peaks of axle load spectra and is given by Eq.5-1 (MATLAB, 2010).

$$y = \sum_{i=1}^{n} a_i e^{\left[-\left(\frac{x-b_i}{c_i}\right)^2\right]} \quad (5\text{-}1)$$

Where,

a_i = the amplitude;

b_i = the centroid or location;

c_i = the parameter related to the peak width; and

n = the number of peaks to fit (n =1 for single and tridem axles; n = 2 for tandem axle).

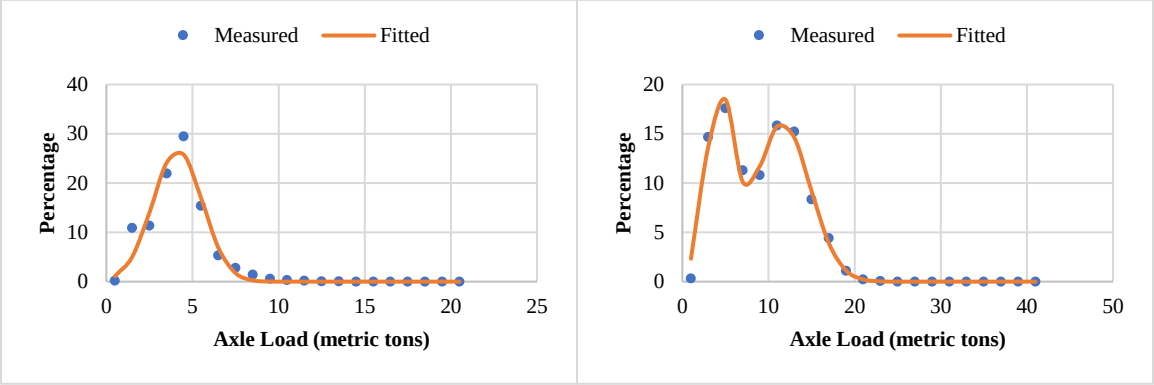

(a) (b)

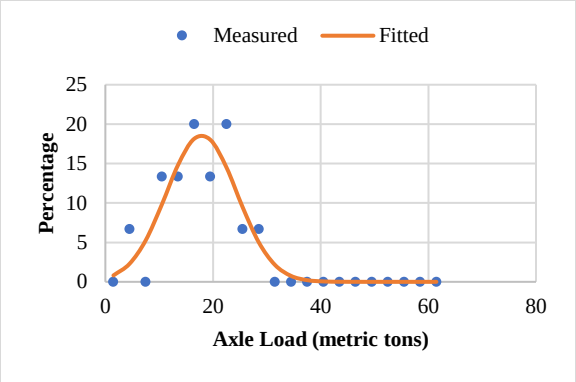

(c)

Figure 5.2 Gaussian distribution of axle load spectra of (a) single, (b) tandem, and (c) tridem axle on I-80 in 2000

5.1.2 Pavement Structure and Field Performance

The pavement structure and field performance data for the two-mile pavement segments nearby the WIM sites were collected from pavement management system of NJDOT. In general, 50% of highways in NJ are composite pavements, 40% are flexible pavements, and the remaining 10% are rigid pavements. Figure 5.3 shows the frequency distribution of thicknesses of flexible and composite/rigid pavements. For the majority of flexible pavements, the thickness of state highways, US highways, and Interstate highways are in the ranges of 2-4 inches, 4-6 inches, and 8-12 inches, respectively. For most of the composite and rigid pavements, the thickness of surface layer of state highways, US highways, and Interstate highways are in the ranges of 6-8 inches, 10-12 inches, and 12-14 inches, respectively.

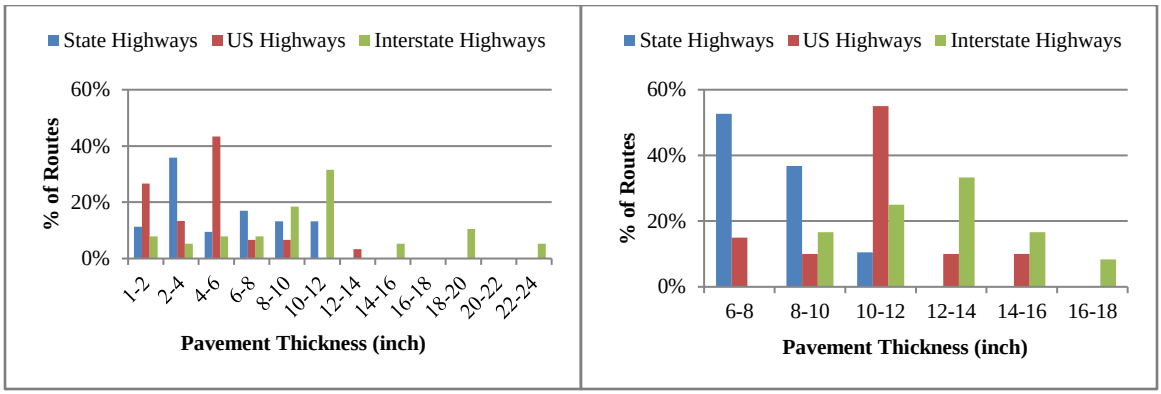

(a) (b)

Figure 5.3 Frequency distribution of (a) surface layer thickness of flexible pavement and (b) surface layer thickness of composite/rigid Pavement

Pavement performance data in terms of Surface Distress Index (SDI) over years were used to estimate pavement service life after major rehabilitation treatments. The SDI has a scale of 0-5 and incorporates both non-load related distresses outside wheel paths (NDI) and load related distress index (LDI) in wheel path (Wang and Wang, 2019). Figure 5.4 shows an example of pavement deterioration showing SDI over years. It can be observed from that the SDI declines slowly during the first several years. Afterward, SDI starts to drop rapidly and finally decreases gradually to a small value. NJDOT defines the pavement condition as poor when SDI < 2.4 or IRI > 2.7m/km and as good when SDI > 3.5 and IRI < 1.5m/km. In real practice, the terminal IRI values are much smaller than 2.7m/km when pavement life is reached based on the SDI threshold (Wang et al., 2020a). Therefore, the pavement service life in the study is determined as the time period before the SDI drops to 2.4.

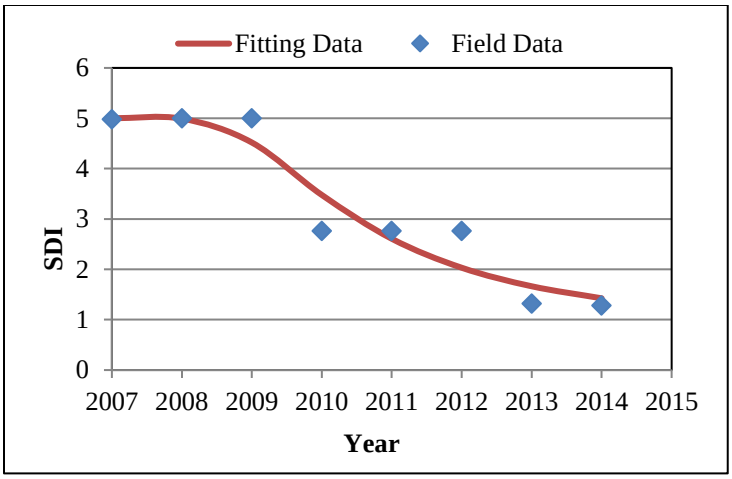

Figure 5.4 Example of deterioration trend of pavement performance (I-80B)

5.1.3 Climate Condition

The office of New Jersey State Climatologist provides average monthly air temperature data. The 21 counties in New Jersey were grouped into three districts: Northern New Jersey (11 counties), Southern New Jersey (10 counties), and Costal New Jersey. The freezing index (FI) is defined by the negative of the sum of all average daily temperatures below 32 °F within the given period, as shown Eq. 5-2 (Ong et al., 2010). The FI was found being 9.3 degree-days in Southern New Jersey, and 175.7 degree-days in Northern New Jersey. As the consequence of using average monthly air temperature instead of daily air temperature, the estimated FI is correspondingly smaller.

$$FI = \sum \left[\frac{1}{2}\left(T_{Max} - T_{Min}\right) - 32 \right] \times n_i \qquad (5\text{-}2)$$

Where,

FI = accumulative FI, degrees Fahrenheit (°F) degree-days;

T_{max} = the maximum monthly temperature in month i, °F;

T_{min} = the minimum monthly temperature in month i, °F; and

n_i = days in month i when average monthly temperature is below freezing (32°F)

5.2 Traditional Nonlinear Regression Model

Traditional nonlinear regression models were first used to investigate traffic loading impact on pavement performance. The average daily ESALs and axle load spectra were considered as traffic variables in the nonlinear regression model to analyze and predict pavement performance. Totally 5,481 data points were used to derive the regression models. The number of data points for flexible pavement structure on state highways, Interstate highways, and US highways were 1,310, 1,368, and 653, respectively. The number of data points for composite and rigid pavement structure on state highways, Interstate highways, and US highways were 402, 960, and 788, respectively. The pavement performance models developed by relating SDI to pavement age, average daily ESALs, and freezing index, as shown in Eq. 5-3.

$$SDI_t = \exp\left(a - b \times Log(T) \times l - c \times Log(FI) \times l\right) \quad (5\text{-}3)$$

Where,

SDI_t = surface distress index in the t^{th} year;

l = pavement age;

T = average annual daily ESALs;

FI = freezing index; and

a, b, and c = model coefficients.

Table 5.1 summarizes the coefficients and R square values of the regression models of flexible and composite/rigid pavements for state highways, Interstate highways, and US highways, respectively. The R square value varies from 0.51 to 0.70 depending on the pavement structure and route type.

Table 5.1 Coefficients and R-square values of regression model based on average daily ESALs

Pavement Type	Highway Type	a	b	c	R-square
Flexible Pavement	State Highway	1.717	0.022	0.038	0.51
	Interstate Highway	1.703	0.004	0.057	0.70
	US Highway	1.742	0.049	0.013	0.56
Composite/Rigid Pavement	State Highway	1.753	0.047	0.054	0.57
	Interstate Highway	1.754	0.021	0.031	0.53
	US Highway	1.838	0.079	0.001	0.62

In order to improve the accuracy of prediction, another pavement performance model was developed by correlating SDI to pavement age, freezing index, the number of axles, and the fitted Gaussian distribution of axle load spectrum for each axle type, expressed by Eq.5-4.

$$SDI_t = exp\big(a - \big((bA_1 + cM_1 + dSD_1) \cdot log(N_1) \cdot k + (eA_2 + fM_2 + gSD_2 + e_2A_3 + f_2M_3 + g_2SD_3) \cdot \log(N_2) \cdot m\big) \cdot l \cdot n - p \cdot log(FI) \cdot l\big) \quad (5\text{-}4)$$

Where,

N1, N2, N3 = the number of single, tandem, and tridem axles;

A_1, M_1, SD_1 = amplitude, location, and peak width of single axle load spectrum as shown in Figure 5.2 (a);

$A_2, M_2, SD_2, A_3, M_3, SD_3$ = amplitude, location, and peak width of tandem axle load spectrum for the first peak and second peak as shown in Figure 5.2 (b);

A_4, M_4, SD_4 = amplitude, location, and peak width of tridem axle load spectrum as shown

in Figure 5.2 (c); and

a, b, c, d, e, f, g, e2, f2, g2, h, i, j, k, m, n, and *p* = model coefficients.

Table 5.3 presents the coefficients of pavement performance models for state highways, Interstate highways, and US highways, respectively. The mean absolute error (MAE), root mean square error (RMSE), and coefficient of determination (R-square) were considered as the error metrics to evaluate the accuracy of fitting model, as shown in Table 5.3. The R-square values varied from 0.51 to 0.71 depending on pavement structure and highway type. The comparison between the R-square values of two nonlinear regression models (Eq. 5-3 and 5-4) indicated that the accuracy of pavement performance prediction was improved by considering the number of axles and the fitted Gaussian distribution of axle load spectra in the model. However, the R-square values are still not very high.

Figure 5.5 illustrates the actual observed and predicted SDI using the nonlinear regression models expressed by Eq.5-4, respectively, for different pavement structures and highway types. The results indicate that more accurate predictive models are needed to investigate the impact of traffic loading on the deterioration trend of pavement performance.

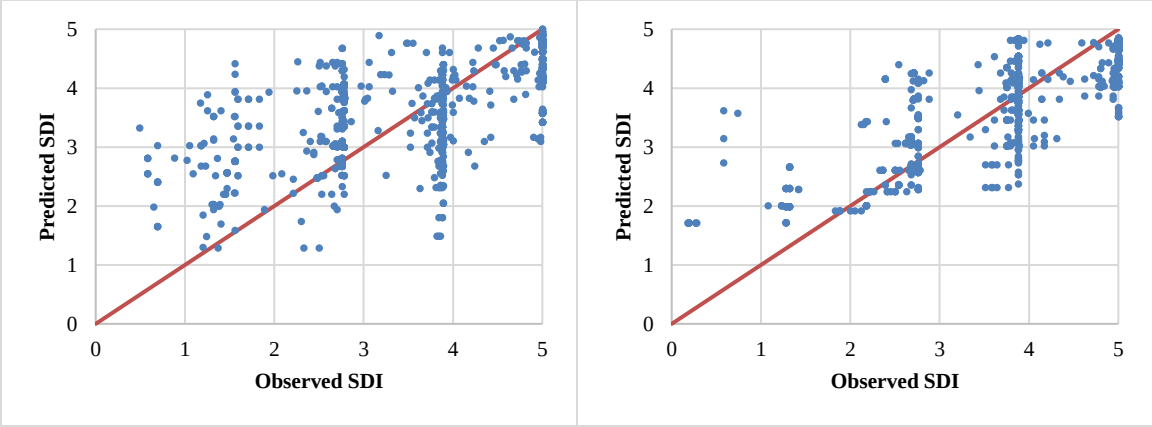

(a) (b)

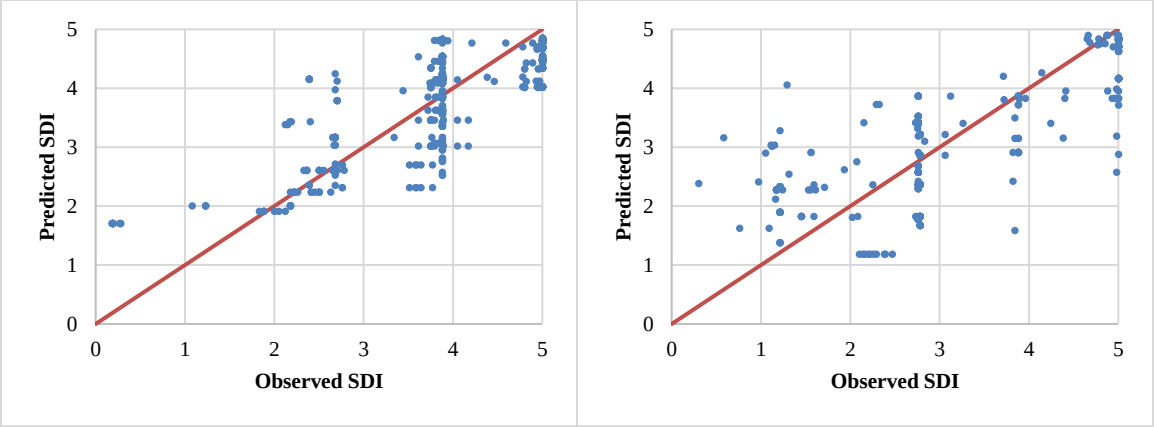

(c) (d)

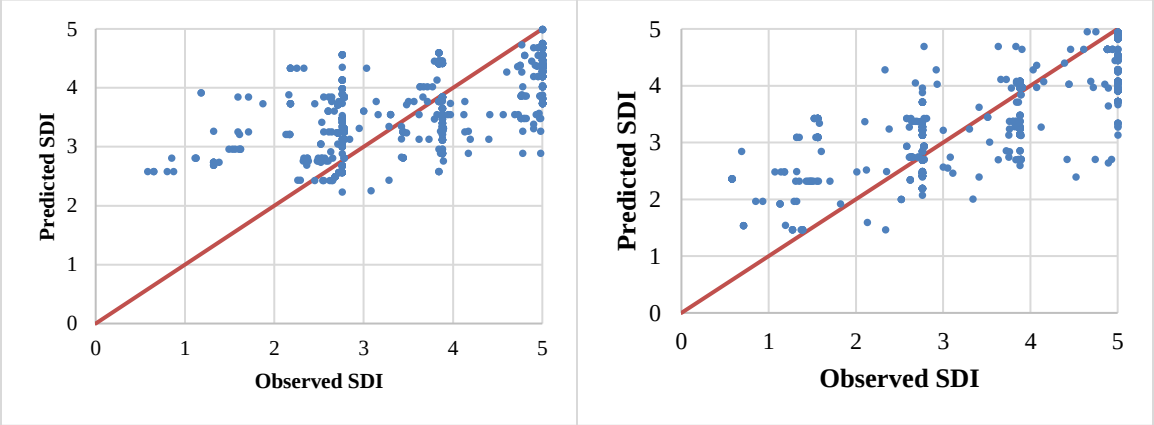

(e) (f)

Figure 5.5 Actual observed and fitted SDI based on multiple nonlinear regression models for flexible pavement structure on (a) state highways; (b) Interstate highways; (c) US highways; and composite/rigid pavement structure on (d) state highways; (e) Interstate highways; (f) US highways

Table 5.2 Coefficients of regression models based on axle load spectra

Pavement Type	Highway Type	a	b	c	d	e	f	g	e2	f2
Flexible Pavement	State	1.716	0.042	0.162	0.001	0.212	0.003	1.456	0.012	0.000
	Interstate	1.708	0.005	0.000	0.001	0.138	0.003	0.001	0.015	0.123
	US	1.736	0.000	0.862	0.001	0.036	0.003	0.000	0.038	0.000
Composite/Rigid Pavement	State	1.804	0.057	0.000	0.001	0.000	0.004	0.000	0.877	0.000
	Interstate	1.767	0.000	0.063	0.001	0.000	0.004	0.021	0.144	0.348
	US	1.844	0.000	1.212	0.000	0.094	0.000	0.000	0.000	0.116
Structure	**Route**	**g2**	**h**	**i**	**j**	**k**	**m**	**n**	**p**	
Flexible Pavement	State	0.000	0.000	0.000	0.000	0.000	0.003	0.041	0.042	
	Interstate	0.183	0.000	0.018	0.364	0.000	0.000	0.004	0.054	
	US	0.113	0.000	0.000	0.000	0.014	0.000	0.005	0.006	
Composite/Rigid Pavement	State	1.692	0.000	0.000	0.024	0.023	0.003	0.000	0.000	
	Interstate	0.000	0.000	0.000	0.000	0.000	0.005	0.003	0.014	
	US	0.000	0.056	0.000	0.000	0.007	0.006	0.030	0.008	

Table 5.3 Error metric of regression model based on axle load spectra

Structure	Route	RMSE	MAE	R-square
Flexible	State	0.82	0.62	0.51
	Interstate	0.57	0.43	0.71
	US	0.75	0.56	0.62
Composite/Rigid	State	0.73	0.55	0.69
	Interstate	0.74	0.58	0.55
	US	0.74	0.55	0.67

5.3 Machine Learning Method

5.3.1 Principle of Support Vector Regression

Support vector method (SVM) is an efficient approach to derive pavement performance model especially when the dataset is small and the correlation is nonlinear (Schlotjes et al., 2015; Ziari et al., 2016). SVM produces nonlinear boundaries by

constructing a linear boundary in a large, transformed version of the feature space. The basic principle behind the linear SVM is to find an optimal separating hyperplane creating the biggest margin between the training data. The closest training points to the hyperplane are called support vectors. SVM can also be used as regression method rather than classification method, this application is also called as SVR (Hastie et al., 2009). SVR uses the same principles as SVM but provides the flexibility to find the appropriate hyperplane in higher dimensions to regress the data and customize controlled errors in an acceptable range.

For the training data consisted of N pairs (x_1, y_1), (x_2, y_2), …, (x_N, y_N), with $x_i \in R^p$ and $y_i \in \{-1,1\}$. Define a hyperplane by Eq. 5-5.

$$\{x : f(x) = x^T\beta + \beta_0 = 0\} \tag{5-5}$$

Where, β is a unit vector $\|\beta\|$=1.

A classification rule induced by *f(x)* is defined by Eq. 5-6.

$$G(x) = \mathrm{sign}\left[x^T\beta + \beta_0\right] \tag{5-6}$$

Where, *f(x)* gives the signed distance from a point x to the hyperplane $f(x) = x^T\beta + \beta_0 = 0$. The classes are separated, so a function $f(x) = x^T\beta + \beta_0$ with $y_i f(x_i) > 0 \ \forall i$. Thus, it is available to find the hyperplane that maximizes the margin between training data for different classes. The optimization problem is defined by Eq. 5-7.

$$\max_{\beta,\beta_0,\|\beta\|=1} M \tag{5-7}$$

$$\text{Subject to } y_i(x_i^T\beta + \beta_0) \geq M, i = 1,\ldots,N \tag{5-8}$$

captures this concept. The band is M units away from the hyperplane on either side, and then 2M units wide, which is called the margin. Therefore, optimization problem can be more conveniently phrased as shown in Eq. 5-9 and 5-10.

$$\min_{\beta,\beta_0} \|\beta\| \tag{5-9}$$

$$\text{Subject to } y_i(x_i^T\beta+\beta_0) \geq 1, i=1,...,N \tag{5-10}$$

Noted that $M = \frac{1}{\|\beta\|}$. Eq. 5-10 is the common approach of expressing the support vector criterion for separable data. When SVM is used for regression to estimate β, the minimization of Eq. 5-11 is considered with Eq. 5-12.

$$H(\beta,\beta_0) = \sum_{i=1}^{N} V\big(y_i - f(x_i)\big) + \frac{\lambda}{2}\|\beta\|^2 \tag{5-11}$$

Where, ϵ - insensitive error function is:

$$V_\epsilon(r) = \begin{cases} 0 & if\ |r| < \epsilon \\ |r| - \epsilon & otherwise \end{cases} \tag{5-12}$$

5.3.2 Results and Discussion

Similar with the nonlinear regression model, the SVR model was developed by relating SDI to pavement age, FI, and truck traffic. The average daily ESALs and fitted Gaussian distribution of axle load spectra were considered as traffic variables, respectively. The data points were categorized into two groups: 80% for model training and 20% for model validation. Parameter values in the SVR models were optimized using grid search (Python Software Foundation). Kernels were used in SVR to solve nonlinear regression problems through decreasing the complexity of calculations by providing an chance to linearly deal with nonlinear functions in high-dimensional spaces (Hastie et al., 2009). Different kernels, including linear, radial basis function, sigmoid, and universal Pearson

VII function, were considered in the model optimization (Üstün et al., 2006). Radial basis function kernel was found work best in the dataset through trial analysis. The radial basis function is expressed by Eq. 5-13.

$$K(x, y) = exp\left(-\frac{\|x-y\|^2}{C}\right) \quad (5\text{-}13)$$

Where, C is constant.

Table 5.4 summarizes the cross-validation results of SVR when different traffic variables were considered in the model. By applying SVR method, the coefficients of determination (R-square values) were found significantly increased as compared to the traditional nonlinear regression models. The mean absolute error (MAE) decreased to 0.17-0.38 and the coefficient of determination (R-square) increased to 0.71-0.93. The predictive models for flexible pavements on Interstate highway and composite/rigid pavements on US highway presented better accuracy than the other highway types. On the other hand, the fitting accuracy was further improved by involving the number of axles and fitted Gaussian distribution of axle load spectra in the SVR model, except for the flexible pavement on US highway. Thus, it was recommended to use the number of axles and the fitted Gaussian distribution of axle load spectra to develop SVR model and predict pavement performance. However, the SVR model based on average daily ESALs provided a simplified way with acceptable accuracy to investigate the influence of traffic loading on pavement deterioration.

Table 5.4 Cross-validation results of SVR with different variables

Model Variables	Pavement Type	Highway Type	RMSE	MAE	R-square
Age, FI, ESALs	Flexible	State	0.46	0.25	0.85
		Interstate	0.41	0.22	0.84
		US	0.54	0.34	0.79
	Composite/Rigid	State	0.58	0.32	0.80
		Interstate	0.58	0.30	0.72
		US	0.45	0.24	0.88
Age, FI, Number of Axles, Fitted Axle Load Spectra	Flexible	State	0.40	0.22	0.89
		Interstate	0.37	0.19	0.88
		US	0.60	0.38	0.74
	Composite/Rigid	State	0.47	0.26	0.87
		Interstate	0.58	0.30	0.71
		US	0.32	0.17	0.93

Figure 5.6 presents the comparison of actual observed and predicted SDI values by using the SVR models based on the fitted Gaussian distribution of axle load spectra and the number of axles. As compared to Figure 5.5, the SVR method shows significant improvement on the accuracy of performance prediction.

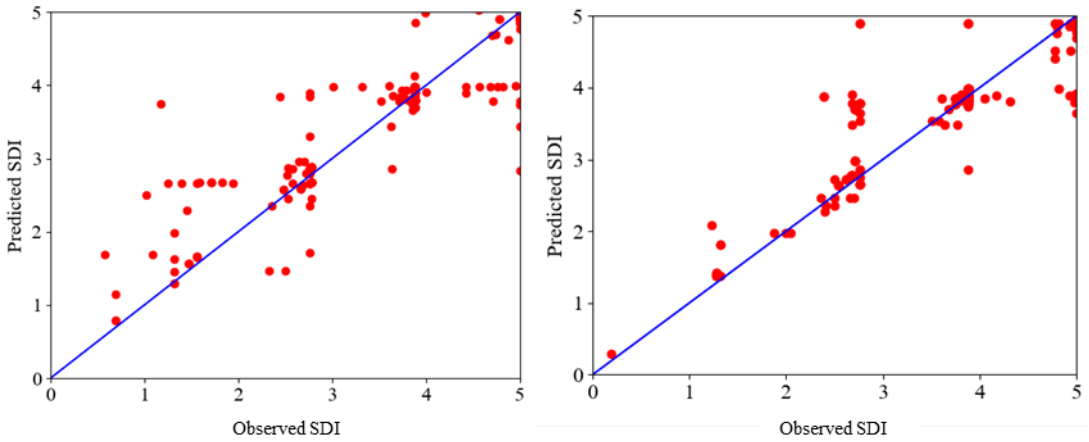

(a) (b)

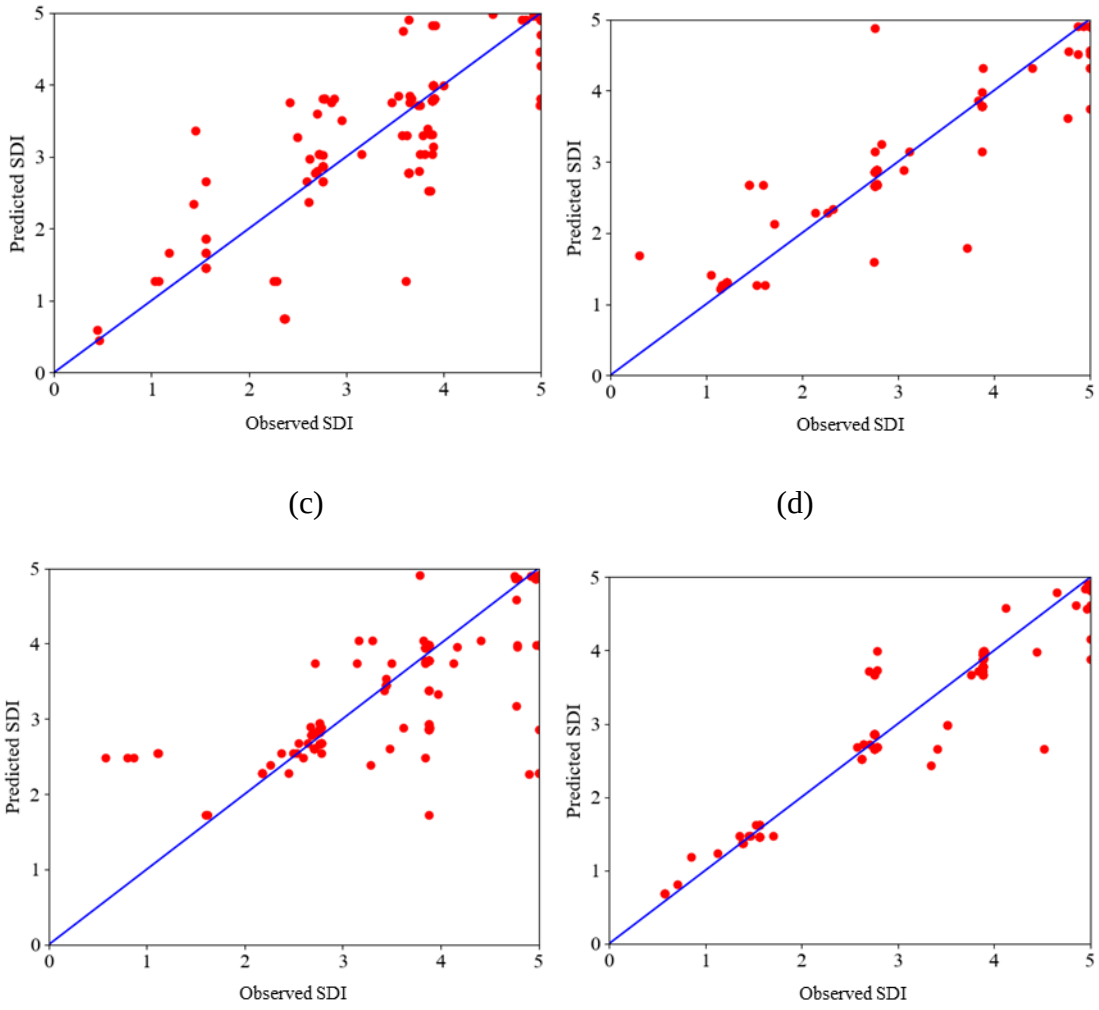

(c) (d)

(e) (f)

Figure 5.6 Actual observed and fitted SDI based on SVR models for flexible pavement structure on (a) state highways; (b) Interstate highways; (c) US highways; and composite/rigid pavement structure on (d) state highways; (e) Interstate highways; (f) US highways

5.4 Impact of Overweight Truck on Pavement Deterioration

It is well accepted that overweight trucks would accelerate pavement deterioration based on mechanistic-empirical (M-E) pavement analysis (Wang et al., 2015c). Wang and Zhao (2016) estimated load equivalency factors of axle load on for fatigue cracking and rutting and quantified the reduction of pavement life caused by overweight traffic on thin and thick asphalt pavements. Rys et al. (2016) investigated asphalt pavement fatigue life caused by mixed traffic based on the axle load distribution and percentage of overweight vehicles. The analysis results indicated that the increase of percentage of overweight vehicles from zero to 20% would cause up to 50% reduction of fatigue life of asphalt pavement. Batioja-Alvarez et al. (2018) predicted rutting and fatigue cracking damage due to overweight vehicle considering the impact of vehicle loading, pavement temperature, and vehicle-miles traveled on pavement performance using mechanistic-empirical approach. It was found that the distribution of load equivalency factor could be incorporated in pavement design to consider the influence of overweight vehicles. Titi et al. (2018) evaluated the impacts of overweight truck traffic on performance of four flexible pavements in Wisconsin and found that the proportion of pavement damage due to overweight trucks increased most of pavement distresses by 0.5% to 4%.

Past studies mainly used field data to quantify pavement damage due to vehicular loading using regression models. Li and Sinha (2000) developed load and non-load factor functions using the relative change in IRI considering cumulative traffic loading, regional and climatic features, subgrade materials, design and construction standards, and pavement ages from Indiana pavement management system. Ong et al. (2010) correlated pavement distresses, such as IRI, rut, and pavement condition rating, with average annual daily truck

traffic and environmental factors on different highways. Gungor et al. (2019) established the relationship between the change of condition rating survey with pavement age, daily traffic, and environmental factors to predict pavement deterioration under various loading conditions. Wu et al. (2019) investigated the influence of overweight traffic on pavement service life considering climatic effects, truck origin and destination, permitted routes, and frequency of the routes.

The developed SVR models were utilized to investigate the impact of overweight truck traffic on pavement damage. Currently, NJDOT legislates 80,000 lbs. as the legal GVW. The legal weight on single axle at Interstate highways and non-Interstate highways are 20,000 lbs. and 22,400 lbs., respectively. The legal weight on tandem axle is 34,000 lbs (Federal Highway Administration, 2015). In order to evaluate the overweight traffic effect on pavement performance, the WIM data was processed and grouped into two traffic groups. The first group included all the trucks within the legal weight limit (non-overweight traffic); while the second group included both the trucks within the legal weight limit and the overweight trucks (total traffic). The considered legal weight limits on single, tandem, and tridem axles were 22,400 lb., 34,000 lb., and 42,000 lb., respectively. Table 5.5 shows the highway type, route number, pavement structure, freezing index (FI), and the number of single, tandem, and tridem axle loads for the total and non-overweight traffic at the selected six sites. One site was selected for each highway type.

Table 5.5 Total and non-overweight (N-O) traffic at the selected routes

Pavement Type	Highway Type	Route #	Traffic	FI (degree-day)	Asphalt concrete (in.)	Cement concrete (in.)	No. of single axle	No. of tandem axle	No. of tridem axle
Flexible	State	NJ-138	Total	-9.3	2	0	412	118	7
		NJ-138	N-O	-9.3	2	0	410	109	1
	Interstate	I-195	Total	-9.3	12	0	3509	3602	201
		I-195	N-O	-9.3	12	0	3505	3562	76
	US	US-30	Total	-9.3	5	0	336	114	10
		US-30	N-O	-9.3	5	0	334	104	1
Composite/ Rigid	State	NJ-33	Total	-9.3	2.5	5.5	664	299	19
		NJ-33	N-O	-9.3	2.5	5.5	659	277	3
	Interstate	I-80	Total	-175.7	3	8	4197	4448	55
		I-80	N-O	-175.7	3	8	4051	3990	30
	US	US-202	Total	-175.7	3.5	7	356	225	25
		US-202	N-O	-175.7	3.5	7	355	211	3

Figure 5.7 shows the axle load spectra at the selected routes, respectively, for single, tandem, and tridem axles. It indicated that most of tridem axles were overweight axles, but it was less than 5% of the total traffic. The majority of overweight axle loads were on tridem and tandem axles, which were expected to have significant influences on pavement deterioration.

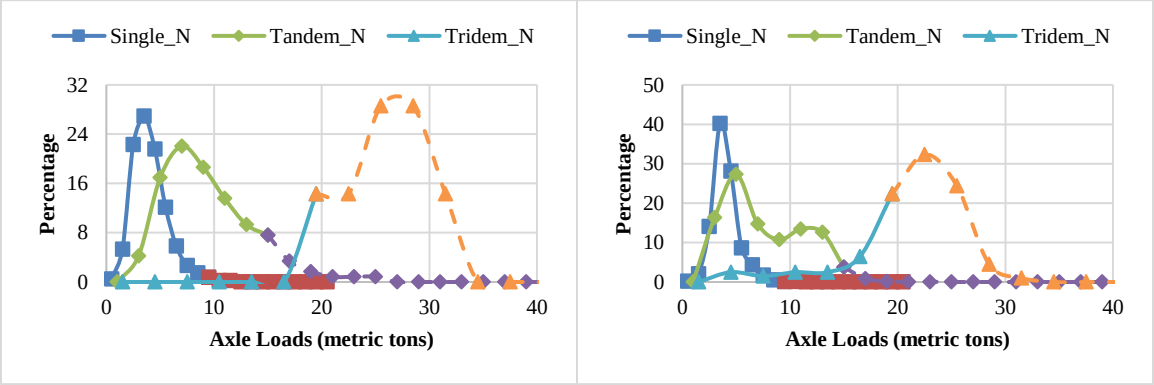

(a) (b)

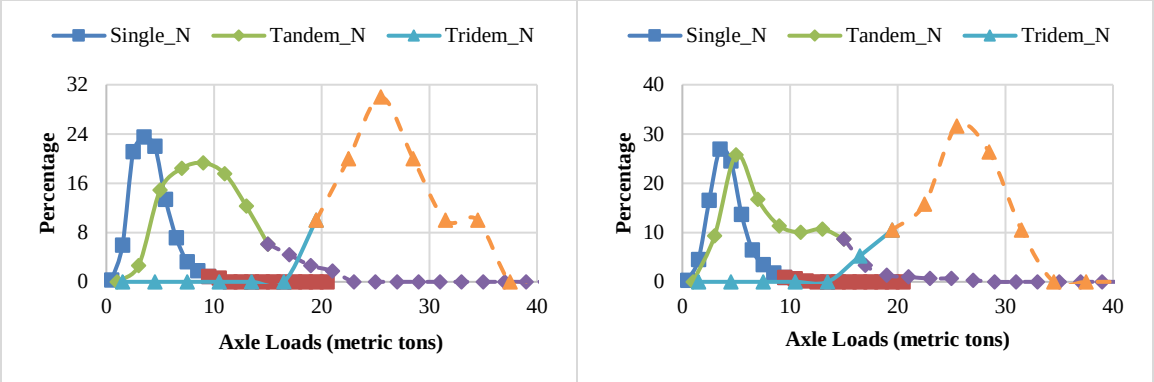

(c)

(d)

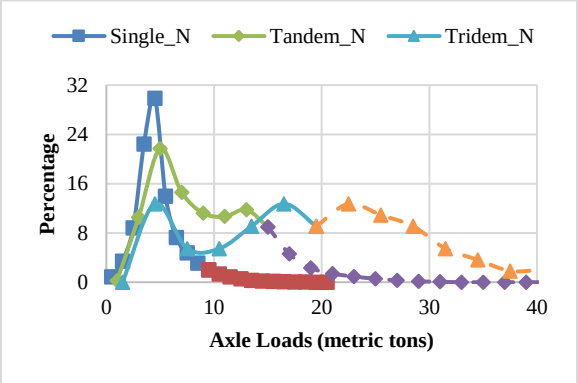

(e)

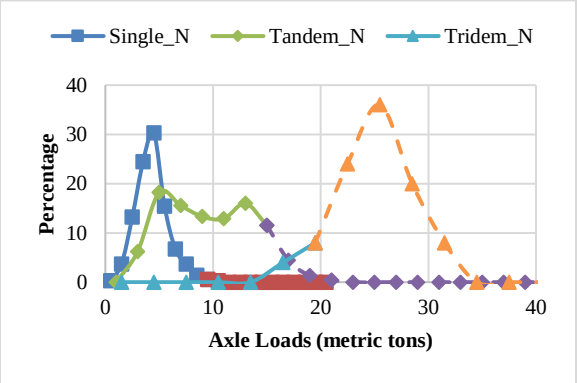

(f)

Figure 5.7 Axle load spectra at the selected sites: (a) NJ-138; (b) I-195; (c) US-30; (d) NJ-33; (e) I-80; (f) US-202 (solid line—: non-overweight; dotte dline---: overweight)

Figure 5.8 illustrates the deterioration trend of flexible and composite pavement under the total and non-overweight truck traffic using the derived SVR models based on the number of axles and the fitted Gaussian distribution of axle load spectra. The deterioration of pavement condition increased with the change of axle load spectra and the increasing number of axles, especially on tridem axle, due to the overweight truck traffic. Since the maintenance or rehabilitation was applied at the pavement sections before the SDI dropped to 2.4, it was difficult to track the pavement sections with the SDI below 2.5. In order to derive the entire curve of SDI deterioration, a sigmoidal model, which has been

proven to provide high accuracy to fit the performance curve, was applied to fit the predicted SDI values, as expressed by Eq. 5-14 (Hajek et al., 1985; Jackson et al., 1996). With the determined model parameters, the pavement life before the SDI decreasing to 2.4 was calculated for total and non-overweight traffic scenarios at each route.

$$SDI = SDI_0 - \exp\left(a - b * c^{\ln\left(\frac{1}{Age}\right)}\right) \quad (5\text{-}14)$$

Where,

SDI = surface distress index;

SDI_0 = surface distress index at year zero;

Age = the year since the construction of rehabilitation; and

a, b, c = model coefficients.

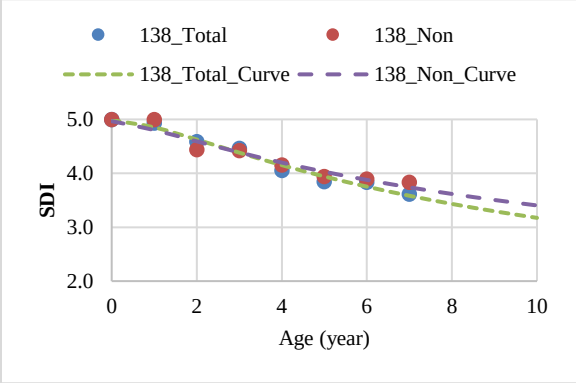

(a)

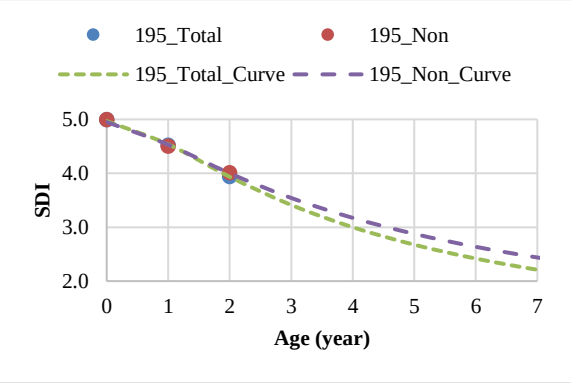

(b)

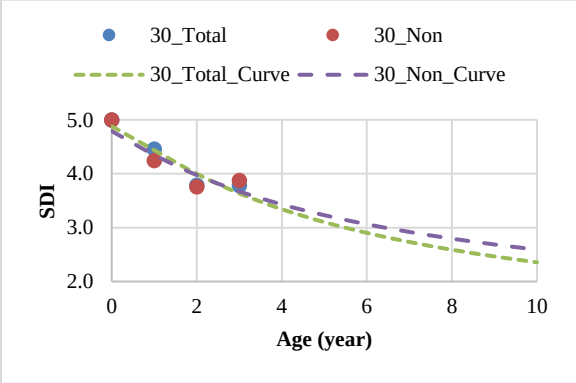

(c)

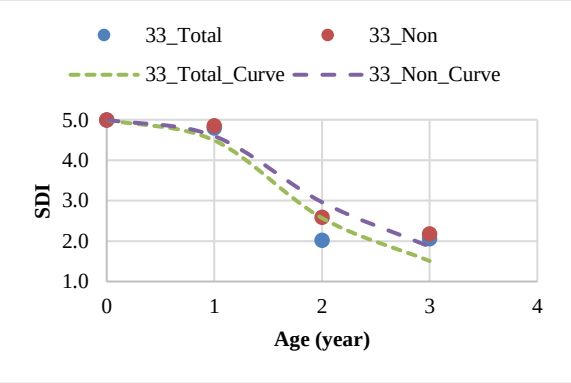

(d)

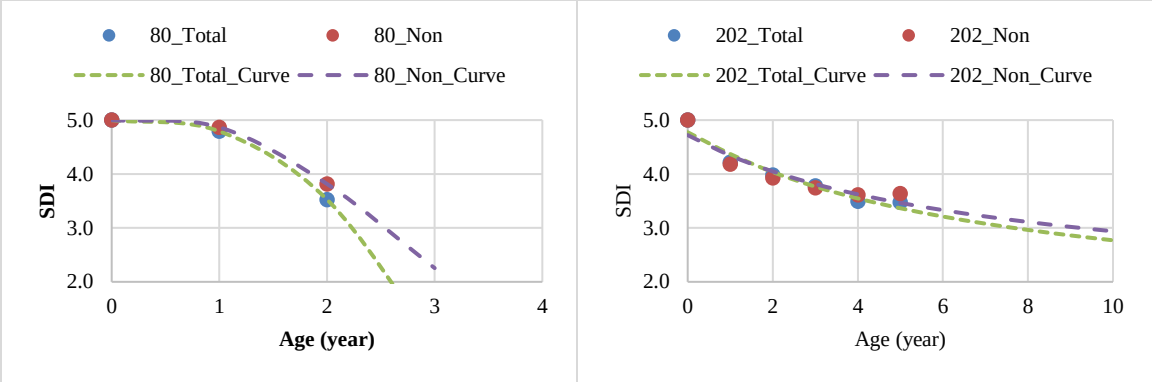

(e) (f)

Figure 5.8 Pavement performance under total and nonverweight truck traffic for flexible pavements (a) state highway; (b) Interstate highway; (c) US highway; and composite pavements (d) state higway; (e) Interstate highway; (f) US highway

To quantify the impact of overweight traffic on pavement damage, the reduction ratio of pavement life was calcualted using Eq. 5-15. Table 5.6 summarizes the overweight percentage on single, tandem, and tridem axles and reduction ratio of pavement life for the selected routes. It indicated that less overweight tridem axles would induce smaller pavement life reduction ratio, like I-195 and I-80. The increase of tandem and tridem axle percentage tended to increase pavement life reduction ratio, for example NJ-138, US-30, and US-202. Since the SVR models were developed for each highway type, the pavement life reduction due to traffic loading varied were acurately captured for different pavement strcutures and highway types.

$$Reduction\ ratio\ of\ pavement\ life = \frac{L_T - L_N}{L_N} \quad (5\text{-}15)$$

Where,

L_T = pavement life caused by total traffic; and

L_N = pavement life caused by the non-overweight traffic.

Table 5.6 Percentage of overweight axles and pavement life ratio for selected routes

Pavement Type	Route	Single	Tandem	Tridem	Pavement Life Reduction (%)
Flexible	NJ-138	0%	8%	86%	29%
	I-195	0%	1%	62%	14%
	US-30	1%	9%	90%	21%
Rigid	NJ-33	1%	7%	84%	9%
	I-80	3%	10%	45%	11%
	US-202	0%	6%	88%	23%

5.5 Summary

In this chapter, traditional nonlinear regression and SVR methods were used to derive pavement performance models under the impact of traffic loading. The model accuracy was further improved by considering the number of axles and fitted Gaussian distribution of axle load spectra in the performance model. The derived SVR models were used to investigate the impact of overweight truck traffic on the deterioration trend of pavement. The proposed pavement performance model can be further used in determining pavement damage caused by overweight trucks for pavement rehabilitation strategy and permit fee analysis.

CHAPTER 6 IMPACT ANALYSIS OF TRAFFIC LOADING ON ASPHALT PAVEMENT LIFE USING RANDOM SURVIVAL FOREST MODEL

6.1 Data Collection and Analysis

6.1.1 Data Collection from LTPP Database

LTPP program was established to collect pavement performance data as one of the major research areas of the Strategic Highway Research Program (SHRP). It provides technical knowledge of pavements currently available and seeks for models that can better explain pavement performance. The LTPP program include the general pavement study (GPS) and the specific pavement study (SPS) with different focuses. The InfoPave is a web interface of LTPP database that is used to deliver data sets of features generated by users.

Totally 128 pavement sections in SPS-5 study located at 12 states were used in this study. The SPS-5 study is conducted to develop improved methodologies and strategies for the rehabilitation of flexible pavements. Each LTPP test section was approximately 3.5-m wide per lane and 152.4-m long (Harold L. Von Quintus et al., 2006). The selected pavement sections were located at four climate regions: dry freeze (Colorado, Montana), dry no freeze (Arizona, California, and New Mexico), wet freeze (Maine), and wet no freeze (Florida, Maryland, Mississippi, New Jersey, Oklahoma, Texas) (Elkins et al., 2016). The climate region of pavement section was considered as environmental factor in the analysis.

The load-related pavement distress data, including alligator cracking, longitudinal cracking at wheel-path, and rut depth of the analyzed pavement sections were identified

and extracted from LTPP database. The pavement age of AC overlay at the time of distress survey was determined by comparing the survey time and construction time of the rehabilitation. It is noted that fatigue cracking and longitudinal cracking were measured at different severity levels (high, medium, and low). Therefore, the overall cracking need be estimated using weight factors. The weight factors for low, medium, and high severity cracking were determined to be 0.2, 0.3, and 0.5, respectively, which were approximated based on the deduct value curves in calculating pavement condition index (PCI) (ASTM, 2018). The IRI after construction of AC overlay was considered as the variable regarding construction quality in the analysis (Smith and Ram, 2016).

Multiple data buckets for desired variables were downloaded from LTPP InfoPave and then organized to create a relational database. Table 6.1 summarizes the LTPP database variables and the extracted data elements in this study, including pavement age, traffic (number of axles and axle load distribution), pavement layer thickness, climate region, overlay treatment (milling and overlay thickness), construction quality, and pavement distresses (alligator cracking, longitudinal cracking at wheel-path, and rutting).

Table 6.1 LTPP InfoPave database tables and extracted data elements

Variables	Symbol	Range	Unit	Relevant Tables in InfoPave
Pavement Age		0.02~24.9	year	EXPERIMENT_SECTION
Number of single axles	Single	65~4541	N/A	YY_AX
Number of tandem axles	Tandem	1~4701	N/A	YY_AX
Number of tridem axles	Tridem	0~100	N/A	YY_AX
Range of single axle loads	Single	0-39	kips	YY_AX
Range of tandem axle loads	Tandem	0-78	kips	YY_AX
Range of tridem axle loads	Tridem	0-117	kips	YY_AX
Thickness of AC layer	AC	2.8~16	inch	TST_L05B
Thickness of bound base layer	TB	0~15	inch	TST_L05B
Thickness of unbound base layer	GB	0~20.7	inch	TST_L05B
Thickness of bound subbase layer	SS	0~66	inch	TST_L05B
Thickness of unbound base layer	GS	0~234	inch	TST_L05B
Climate region	Climate	1~4	Categorical	EXPERIMENT_SECTION
Improvement type	IMP_TYPE	N/A	Categorical	CONSTRUCTION_EVENTS_EXP
Overlay thickness	IMP_h	0.7~7.8	inch	CONSTRUCTION_EVENTS_EXP
Mill thickness	Mill	0.45~4.0	inch	AC_MILLING_EXP
IRI after AC overlay	IRI	0.44~1.8	mm/m	MON_HSS_PROFILE_SECTION
Alligator cracking		0~808 (L) 0~424 (M) 0~817 (H)	m^2	MON_DIS_AC_REV
Longitudinal cracking		0~271 (L) 0~153 (M) 0~48 (H)	m	MON_DIS_AC_REV
Rut Depth		1~25	mm	MON_T_PROF_INDEX_SECTION

6.1.2 Analysis of Axle Load Spectra

LTPP collected traffic data by axle configurations and weights through weigh-in-motion (WIM) stations (FHWA, 2001). The multi-year traffic data for the selected pavement sections were used in the analysis. The same traffic data was used for successive years for the pavement sections where traffic data was not available for certain years.

Given the apparent bell-shaped plot, the axle load spectra were fitted using Gaussian distribution, as shown in Eq. 6-1 (Devore, 1995). The amplitude, mean, and standard

deviation of the Gaussian distribution were utilized to characterize the pattern of traffic load, which provides a simplified but efficient way to take detailed axle load distribution into consideration (Timm et al., 2005; Haider and Harichandran, 2007). Figure 6.1 shows an example of fitted Gaussian distribution of single and tandem axle load spectra. The plots show the fitting model captures the distinctive patterns of axle load spectra.

$$y = \sum_{i=1}^{n} a_i e^{\left[-\left(\frac{x-b_i}{\sqrt{2}c_i}\right)^2\right]} \quad (6\text{-}1)$$

Where, a_i is the amplitude; b_i is the mean; c_i is the standard deviation; and n is the number of peaks to fit (n =1 for single and tridem axles; n = 2 for tandem axle).

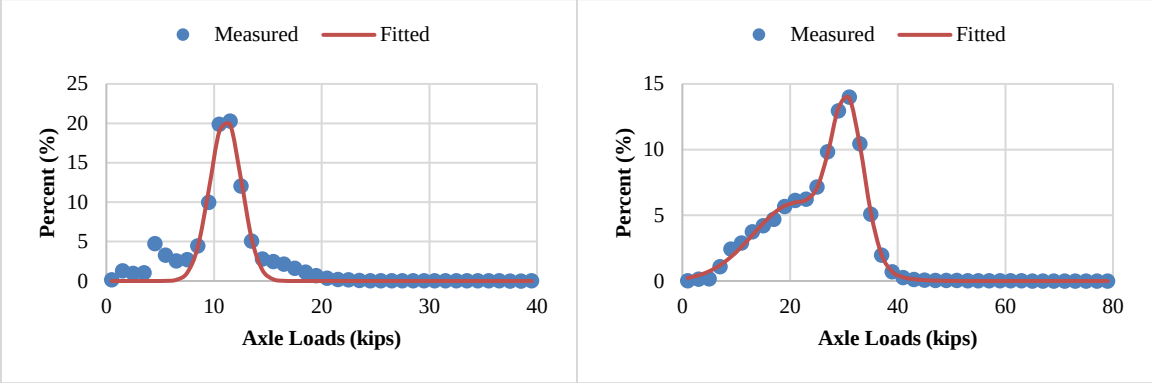

(a) (b)

Figure 6.1Example of fitted Gaussian distribution of axle load spectra: (a) single axle; and (b) tandem axle (SHRP_ID: 040501, 1998)

Table 6.2 presents the summary of variables related to the total number of axles and fitted Gaussian distributions of axle load spectra used in this study. It is noted that the tridem axle load spectra were not included in the analysis due to inconsistent trend of axle load distribution. Since the number of tridem axle was small, this exclusion is believed to not affect analysis results.

Table 6.2 Summary of Gaussian distribution model parameters for axle load spectra

Variable	**Symbol**	**Range of Values**
Amplitude of single axle load spectrum	a	7.94~37.98
Mean of single axle load spectra	b	4.08~11.48
Standard deviation of single axle load spectrum	c	0.68~5.38
Amplitude of tandem axle load spectrum (peak 1)	a1	2.44~15.9
Mean of tandem axle load spectra (peak 1)	b1	8.09~25.23
Standard deviation of tandem axle load spectrum (peak 1)	c1	1.94~9.64
Amplitude of tandem axle load spectrum (peak 2)	a2	3.22~20.15
Mean of tandem axle load spectra (peak 2)	b2	16.76~36.91
Standard deviation of tandem axle load spectrum (peak 2)	c2	1.74~12.55

6.2 Random Survival Forest Model

6.2.1 Algorithm of Random Survival Forest

Survival analysis has been used to analyze pavement service life until distress using parametric (Loizos and Karlaftis, 2005; Dong and Huang, 2015) or semi-parametric cox models (Nakat and Madanat, 2008; Yu et al., 2008) based on condition surveys of in-service pavements. Due to the capability of handling non-linear relationship and enhanced accuracy, machine learning technologies can be employed for survival analysis. Random forest is a modified bagging by building an amount of de-correlated trees and averaging them (Breiman, 2001). By extending random forest method, random survival forest is introduced and used for analysis of right-censored survival data (Ishwaran et al., 2008). The specific details of random survival forest algorithm are as follows:

1) Draw bootstrap samples from the training dataset. Each bootstrap sample excludes approximately one third of the data, called out-of-bag (OOB) data.

2) Grow a survival tree for every bootstrap sample. Randomly select p candidate variables at every node of the survival tree. The candidate variable which maximizes survival difference between daughter nodes is used to split the node.
3) Grow the survival tree to full size under the constraint that a terminal node is supposed to have no less than $d_0>0$ unique deaths.
4) Calculate a cumulative hazard function (CHF) for every survival tree and average to derive the ensemble CHF.
5) Calculate prediction error for the ensemble CHF using out-of-bag data.

6.2.2 Ensemble of Cumulative Hazard Function

The key aspect of random survival forest algorithm is to grow a survival tree and construct the ensemble CHF. Survival trees are consisted of binary trees grown through recursively splitting nodes. A survival tree is grown from the root node, and the root node is split into two daughter nodes according to a predetermined survival criterion. Then, every daughter node is split, and this process is repeated in a recursive order for every subsequent node. The node splitting is optimized by searching over all possible split values and variables and selecting the optimal that maximizes survival differences. Finally, a saturation point is reached when no new daughters can be generated due to the constraint that every node need to contain a minimum of $d_0>0$ unique deaths. The most extreme nodes in a saturated survival tree are named terminal nodes denoted by T.

Let $(T_{1,h}, \delta_{1,h}),\ldots,(T_{n(h),h}, \delta_{n(h),h})$ be the survival times and censoring information for cases in a terminal node $h \in T$. A case i is set to be right-censored at time $T_{i,h}$ if , $\delta_{i,h} = 0$; otherwise, if $\delta_{i,h} = 1$, the case is considered to have died or experienced an event at $T_{i,h}$. Let $t_{1,h} < t_{2,h} < \cdots < t_{N(h),h}$ be the N(h) distinct event times. Define $d_{l,h}$ and $Y_{i,h}$ to be

the number of events and cases at risk at time $t_{l,h}$. The CHF estimate for terminal node h is the Nelson-Aalen estimator, and all individuals in h have the same CHF, as shown in Eq. 6-2.

$$\widehat{H}_h(t) = \sum_{t_{l,h} \le t} \frac{d_{l,h}}{Y_{l,h}} \tag{6-2}$$

Each individual i has a d-dimensional covariate x_i. Let $H(t|x_i)$ be the CHF for i. In order to decide the CHF, drop x_i down the survival tree. Due to the binary characteristic of a tree, x_i will fall into a unique terminal node $h \in T$. The CHF for i is the Nelson-Aalen estimator for the terminal node of x_i. Eq. 6-3 is applied to define the CHF for all cases and estimate CHF for the tree.

$$H(t|x_i) = \widehat{H}_h(t), \text{ if } x_i \in h. \tag{6-3}$$

The CHF is obtained from a single tree, and the CHF are averaged over B survival trees to derive an ensemble CHF. As known, every survival tree in the forest is grown by an independent bootstrap sample. Define $I_{i,b} = 1$ if i is an OOB case for b; otherwise, set $I_{i,b} = 0$. Let $H_b^*(t|x)$ be the CHF for a tree grown using the b_{th} bootstrap sample. The ensemble CHF of OOB data for i is an average over bootstrap samples, as shown in Eq. 6-4.

$$H_e^{**}(t|x_i) = \frac{\sum_{b=1}^{B} I_{i,b} H_b^*(t|x_i)}{\sum_{b=1}^{B} I_{i,b}} \tag{6-4}$$

Drop OOB data down a tree grown from bootstrap data and keep track of the terminal node and CHF of case i. The OOB ensemble CHF is estimated by Eq.6-3. On the contrary, the bootstrap ensemble CHF for i is computed using all survival trees, as shown in Eq. 6-5.

$$H_e^*(t|x_i) = \frac{1}{B} \sum_{b=1}^{B} H_b^*(t|x_i) \tag{6-5}$$

6.2.3 Prediction Error and Cross-Validation

Several measures are available for assessing the probabilistic risk predictions in survival analysis. Brier and logarithmic scoring rules and concordance index which equals the area under the ROC curve for binary responses are commonly selected metrics (Harrell et al., 2005; Gneiting and Raftery, 2007). In this study, the prediction error defined as the time-dependent expected Brier score is discussed and assess the developed model (Mogensen et al., 2012), as shown in Eq. 6-6.

$$BS\left(t,\hat{S}\right) = E\left(Y_i(t) - \hat{S}(t|X_i)\right)^2 \tag{6-6}$$

The expectation is in terms of the data of a case i which is not within the training dataset. $Y_i(t) = I\ (T_i \geq t)$ is the observed status of case i and $\hat{S}(t|X_i)$ is the predicted survival probability at time t for case i with predictor variables x_i. In survival analysis, the Kaplan-Meier estimate of survival is calculated with all training samples.

Several approaches are applied to deal with overfitting issue when only one data set is used to establish the prediction models. The bootstrap cross-validation method splits the data D_N into bootstrap samples D_b and corresponding test samples $D_N \backslash D_b$ (b = 1…, B). Bootstrap samples can either be generated with or without replacement from the original data. Then, models $\hat{S}_b$ are trained using the bootstrap training data D_b, corresponding test samples are predicted, and residuals are calculated. Eventually, the bootstrap cross-validation estimate of prediction error is computed by averaging over the test dataset, as shown in Eq. 6-7.

$$BootCvErr\left(t,\hat{S}\right) = \frac{1}{B}\sum_{b=1}^{B}\frac{1}{M_b}\sum_{i\in\frac{D_N}{D_b}}\widehat{W}_i(t)\left\{\tilde{Y}_i(t) - \hat{S}_b(t|X_i)\right\}^2 \tag{6-7}$$

Where, $\widehat{W}_i$ is the inverse probability of censoring weights. M_b is the size of bootstrap samples for resampling without replacement.

6.3 Random Survival Forest Model Results

Random survival forest approach was applied to investigate asphalt pavement life using the failure threshold of each pavement distress. After combining the pavement distress data and all explanatory variables summarized in Table 6.1 and Table 6.2, the total number of data observations for alligator cracking, longitudinal cracking at wheel-path, and rut depth were 1214, 1214, and 1139, respectively. Based on the current practice of mechanistic-empirical pavement design, the thresholds of alligator cracking, longitudinal cracking at wheel-path, and rut depth were defined be 20% of lane area, 189 m/km (1000 ft/mile), and 12.7 mm (0.5 inch), respectively.

Variable importance measures the change (increase or decrease) of prediction error for the forest ensemble when a variable is randomly "noised-up" (Breiman, 2001). A variable with larger variable importance indicates prediction error is significantly impacted when the variable is "noised-up". Positive variable importance shows variables is potentially predictive variables, and zero or negative variable importance means variables make no contribution to prediction accuracy. Random node assignment is capable of effectively calculating variable importance. In random node assignment, drop cases down a tree and randomly assign to a daughter node when the parent node is split at the target variable.

Figure 6.2 illustrates the variable importance for different pavement distresses. The explanation of each symbol could be found in Table 6.1 and Table 6.2. The results indicated that fatigue cracking was sensitive to climate, the number of tandem axle loads, the number of single axle loads, the thickness of AC overlay, and the thickness of milling. Longitudinal cracking was found more affected by the amplitude of tandem axle load spectrum (first

peak), the number of tandem axles, the standard deviation of tandem axle load spectra (first peak), the number of single axle loads, and the amplitude of tandem axle load spectrum (second peak). On the other hand, the top-five important features for rut depth were the standard deviation of tandem axle load spectrum (second peak), the thickness of AC layer, the amplitude of tandem axle load spectra (second peak), the number of single axle loads, and the thickness of treated base layer. These findings indicated that the explanatory variables regarding axle load spectra would impact pavement distress. Therefore, the derived predictive models were promising to indicate the influence of traffic loading on deterioration trend of each distress.

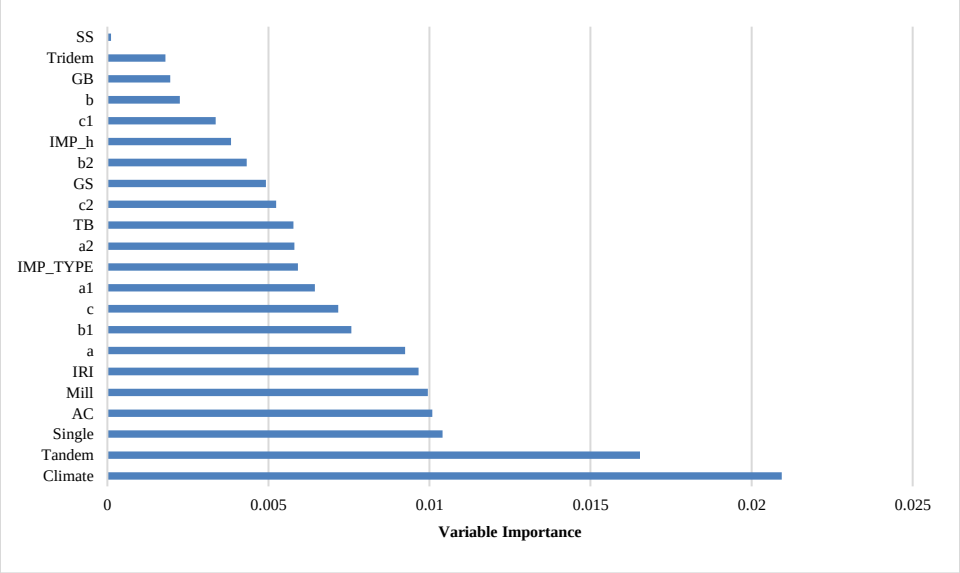

(a)

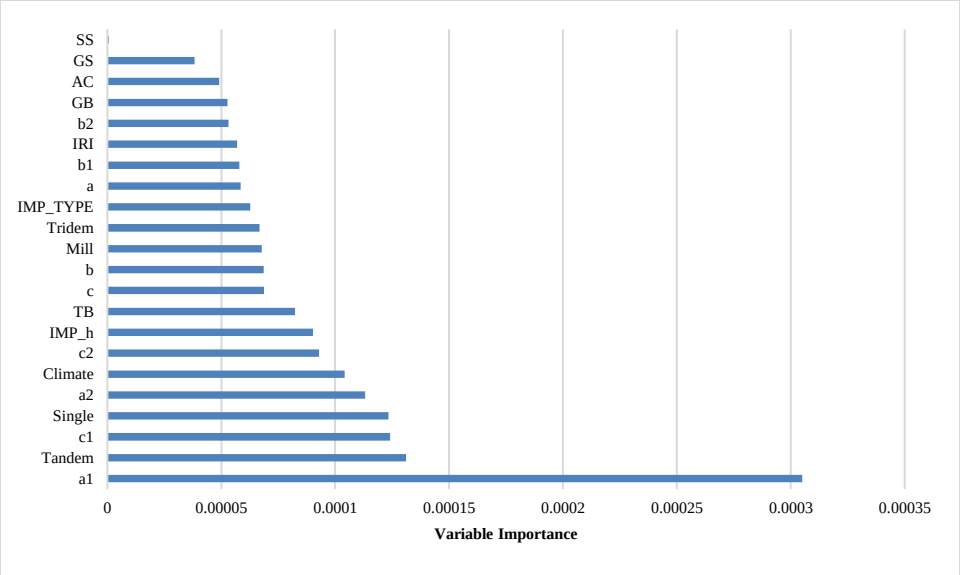

(b)

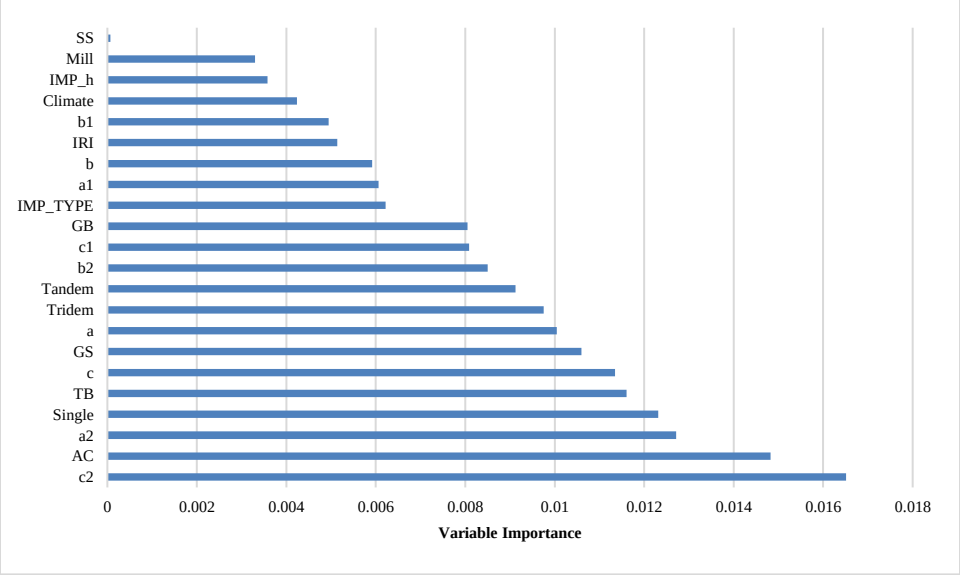

(c)

Figure 6.2 Variable Importance for (a) alligator cracking; (b) longitudinal cracking at wheel-path; and (c) rut depth

The time-dependent Brier score was used to assess the performance of ensembled CHF for each fitted model and select models which better explain pavement performance. The cross-validation bootstrap method was used to compare the time-dependent Brier score

(prediction error) of fitted survival forests. Totally 100 bootstrap samples were considered. Figure 6.3 shows the prediction error curve of random survival forest models (RSF) and the conventional non-parametric survival analysis Kaplan-Meier (K-M) models over 20 years for alligator cracking, longitudinal cracking at wheel-path, and rut depth. For alligator cracking and rutting, random survival forest models outperformed than the conventional survival analysis significantly. As for longitudinal cracking, the prediction error of RSF and K-M models were similar but relatively smaller than other distresses.

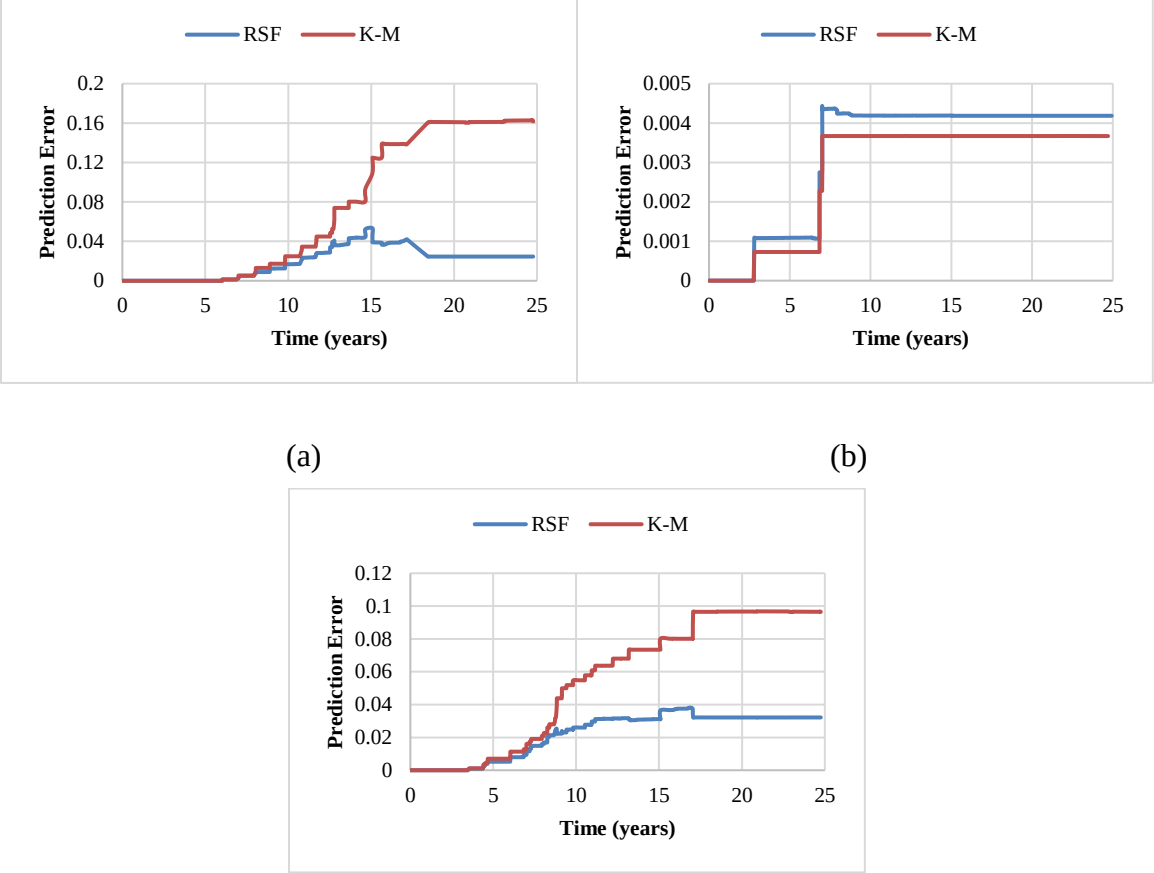

Figure 6.3 Prediction error of survival models: (a) alligator cracking; (b) longitudinal cracking at wheel-path; and (c) rut depth

6.4 Impact of Overweight Traffic on Pavement Life

6.4.1 Effect of Overweight Traffic on Survival Probability

The derived predictive models can be used to analyze the influence of overweight traffic loading on survival probability of AC pavement at the specific pavement section. The selected pavement section (SHRP_ID: 040502) was consisted of 6.5-inch AC layer and 14.7-inch untreated base layer located at dry, no-freeze climate region. The maintenance of milling existing pavement (1.05 inch) and overlaying with AC (2.7 inch) was applied. To evaluate the overweight effect on pavement distress, the WIM data was processed and divided into two traffic categories. The first category only included the trucks within the legal weight limit (non-overweight traffic), and the second category included both the trucks within the legal weight limit and the overweight trucks (total traffic). The legal weight limits on single, tandem, and tridem axles were set as 22,400 lbs., 34,000 lbs., and 42,000 lbs. to distinguish the overweight axles from the total traffic (Federal Highway Administration, 2015). The overweight axles were found approximately 1%, 15%, and 13% of total single, tandem, and tridem axles, respectively. Figure 6.4 shows the axle load spectra of non-overweight and total traffic at the selected section, respectively. The tandem and tridem axle load spectra were significantly influenced by the overweight traffic, especially for amplitude and standard deviation of distribution.

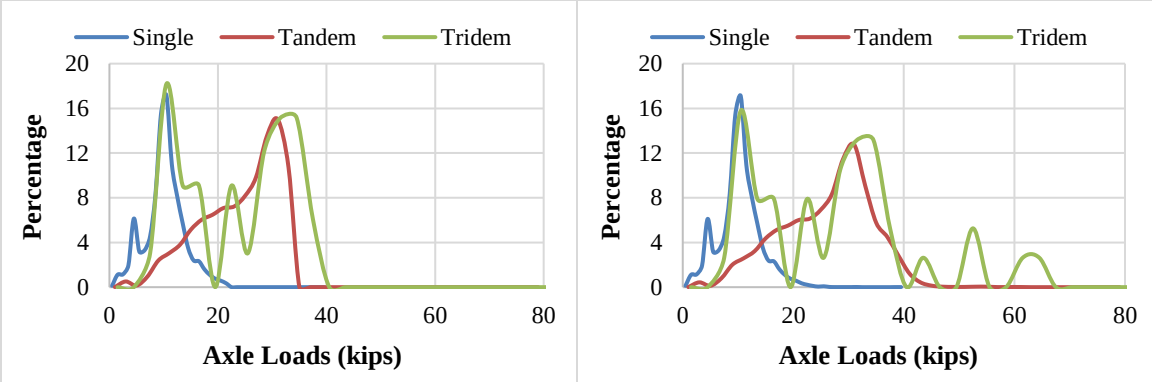

(a) (b)

Figure 6.4 Axle load spectra: (a) non-overweight traffic; (b) total traffic

The deterioration trend of pavement distress under total traffic and non-overweight traffic scenarios were predicted for the selected pavement section. Figure 6.5 presents the survival curves of pavement for alligator cracking, longitudinal cracking at wheel-path, and rut depth, respectively. Survival curves illustrates the probability of pavement life after construction until the pavement distress reached the failure threshold. The decreasing trend of survival curve is expected since pavement sections are likely to fail as service life increases. As expected, overweight truck traffic accelerated pavement deterioration and increased failure risk of pavement. It was found that the pavement life at 50% survival probability were reduced by 1-2 years due to overweight traffic. The reduction of pavement life varied depending on the failure mechanism.

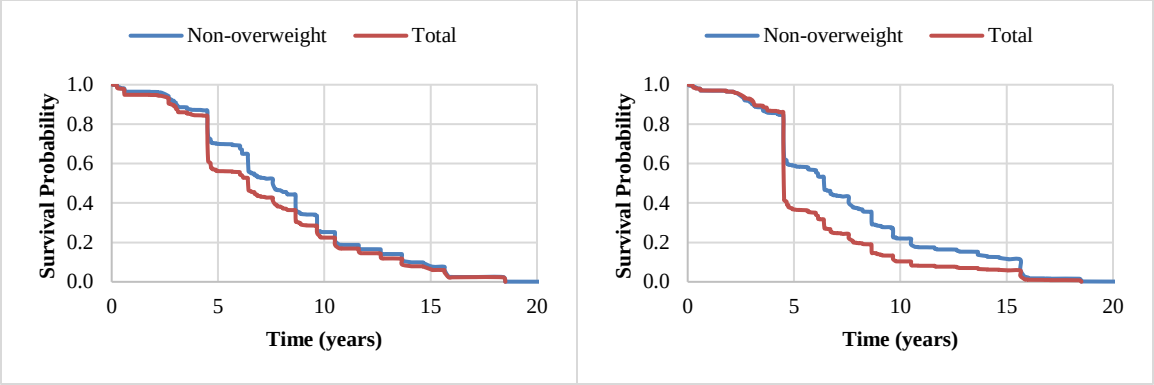

(a) (b)

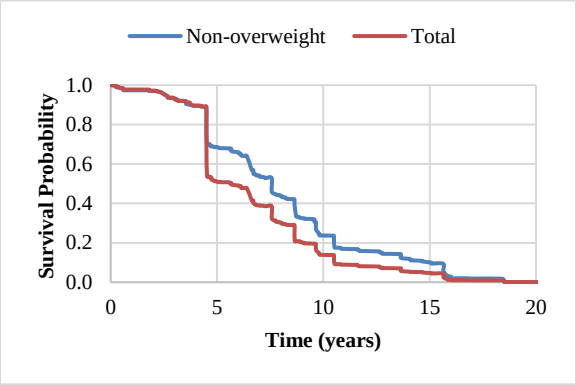

(c)

Figure 6.5 Example of survival curve for total and non-overweight traffic: (a) alligator cracking; (b) longitudinal cracking at wheel-path; (c) rut depth at the selected pavement section

6.4.2 Effect of Overweight Traffic on Pavement Life Reduction

The derived predictive model was further used to evaluate the impact of overweight traffic for all the selected 128 pavement sections. The survival probability of 50% was set as the threshold to estimate the median survival life of pavement section for each load-related pavement distress. Figure 6.6 (a)-(c) illustrate the percentage distributions of pavement service life before failure under total and non-overweight traffic, respectively. It was clear that the overweight traffic caused more pavement sections failing after the shorter

service life. The reduction ratio of pavement life due to overweight traffic was calculated for each pavement section, as shown in Eq. 5-15.

Figure 6.6 (d) shows the life reduction ratio due to overweight traffic in box plots. It should be noted that the negative values are considered as the outliers impacted by the accuracy of predictive models. For most pavement sections, the reduction ratios were found in the range of 16-43% for alligator cracking, 3% to 42% for longitudinal cracking at wheel-path, and 0% to 33% for rut depth. The median values of life reduction ratio were found to be 32%, 24%, and 12% for alligator cracking, longitudinal cracking, and rut depth, respectively. This indicates that alligator cracking is more impacted by overweight traffic loading as compared to longitudinal cracking and rutting.

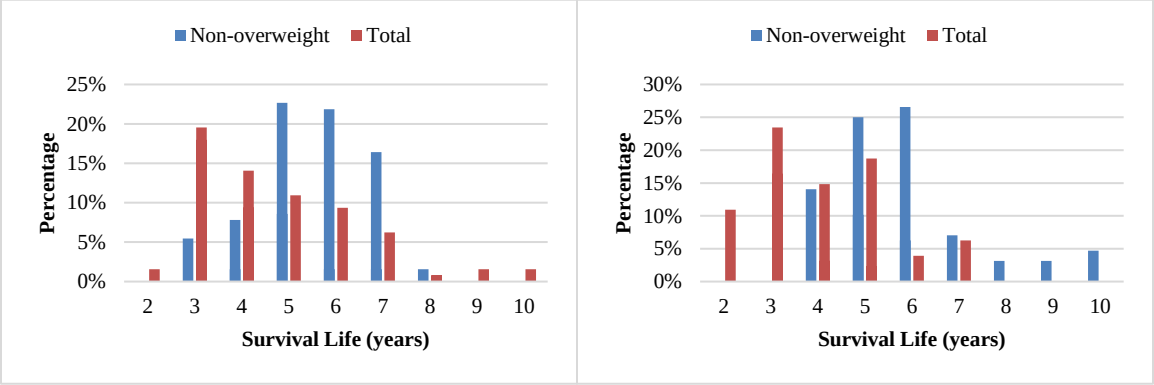

(a) (b)

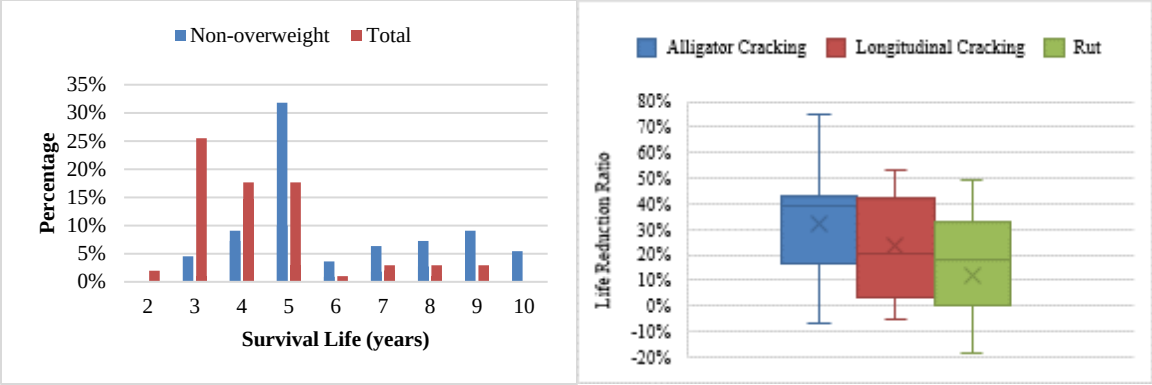

(c) (d)

Figure 6.6 Distribution of survival life: (a) alligator cracking; (b) longitudinal cracking; (c) rut depth; and (d) Boxplots of survival life differences under total traffic and non-overweight traffic

The findings above proved the effectiveness of random survival forest method in analyzing impact of overweight traffic on pavement failure risk for different failure mechanisms when axle load spectra were taken into consideration. Different from regression-based approaches, the pavement service life affected by different traffic scenarios can be obtained with the survival curve directly. Thus, random survival forest method provides an easier and faster manner to investigate the impact of overweight traffic on failure risk of asphalt pavement.

6.5 Summary

In this chapter, random survival forest method was utilized to investigate the impact of overweight traffic on asphalt pavement life using traffic data and field measurements at LTPP database. The traffic data collected from WIM stations in LTPP database were characterized through the number of axles and axle load spectra. Random survival forest was proved to be an efficient risk modeling approach to predict pavement life under

complex interaction of traffic loading, pavement structure, and climate. The proposed random survival forest models were adopted to investigate the impact of overweight traffic on survival curves of pavement life for the specific pavement section. The survival curves were utilized to show the influence of overweight traffic on survival probability of pavement over time for three different failure mechanism.

CHAPTER 7 CONCLUSIONS AND RECOMMENDATIONS

7.1 Findings

This study aims to quantify traffic loading impact on flexible pavement performance using vehicle-tire-pavement interaction modeling and machine learning approaches. The following analysis findings could be summarized:

Dynamic Loads of Vehicle Due to Rough Pavement Surface

1) Pavement surface roughness and vehicle speed significantly affect the variation of dynamic loads. DLCs increased as pavement roughness levels increased but decreased as applied axle load increased.
2) The DLCs of wide-base tire was found smaller than those induced by dual-tire assembly. The differences vary depending on truck configuration, pavement roughness, and speed, and became more significant on rougher pavement roughness.

Analysis of Pavement Response Under Dynamic Loads with Stochastic Amplitude

1) Pavement surface roughness significantly affects the pavement responses at different locations of pavement section. Pavement can fail at the locations where the greater tensile strains are induced due to pavement roughness. As pavement roughness increased, both the maximum strains and the range of strain variations increased.
2) The effect of vehicle speed on pavement responses was complex due to the change of magnitude and frequency of dynamic loads at different speeds. High speed may accelerate pavement deterioration on rough pavement surface. The influence of load frequency on pavement responses under dynamic loads was found not significant. This is different from the finding of traditional viscoelastic analysis of

pavement responses that uses the loading frequency resulted from the duration of moving load.

3) The calculated maximum tensile strain under dynamic loads were found much greater than those under static loads, depending on pavement surface roughness and axle type and load. The relative ratios of fatigue life due to dynamic loads were calculated and fitted as a function of axle type, load magnitude, and IRI, which can be directly used in the current framework of M-E pavement analysis for prediction of fatigue cracking over years. The accumulative fatigue damage ratio between dynamic and static loads was found significantly influenced by IRI values.
4) In general, wide-base tire caused greater tensile strain but similar compressive strain and near-surface shear strain as compared to dual tire assembly. However, the pavement response ratios caused by two tire configurations show certain variations as the truck configuration, speed, or pavement surface roughness changes. This suggests that the prediction of long-term pavement performance under the impact of wide-base tire need consider the evolution of pavement surface condition and different failure mechanisms.

Comparison Analysis of Traffic Loading Impact Using Nonlinear Regression And Support Vector Regression Models

1) Compared to nonlinear regression model, the accuracy of pavement performance prediction was significantly increased by utilizing the SVR method. The model accuracy was further improved by considering the number of axles and fitted Gaussian distribution of axle load spectra in the performance model.

2) The derived SVR models were used to investigate the impact of overweight truck traffic on the deterioration trend of pavement. The analysis indicated that less overweight tridem axles would induce smaller pavement life reduction ratio between non-overweight and total traffic scenarios. The increase of tandem and tridem axle percentage tended to increase pavement life reduction ratio. The proposed pavement performance model can be further used in determining pavement damage caused by overweight trucks for pavement rehabilitation strategy and permit fee analysis.

Impact Analysis of Traffic Loading on Asphalt Pavement Life Using Random Survival Forest Model

1) Random survival forest was proved to be an efficient risk modeling approach to predict pavement life under complex interaction of traffic loading, pavement structure, and climate. The variable importance method was used for selection of explanatory variables in the predictive models. The random survival forest models were developed for three different failure mechanisms (alligator cracking, longitudinal cracking, and rutting).
2) The findings indicated that the explanatory variables regarding axle load spectra of traffic loading explain pavement performance degradation significantly. The random survival forest models showed much greater accuracy for prediction of alligator cracking and rutting, as compared to the conventional survival analysis.
3) The proposed random survival forest models were adopted to investigate the impact of overweight traffic on survival curves of pavement life for the specific pavement section. The survival curves were utilized to show the influence of overweight

traffic on survival probability of pavement over time for three different failure mechanism. The reduction ratio of pavement life due to overweight traffic estimated based on alligator cracking was found greater than longitudinal cracking and rutting for all the pavement sections. It indicated that alligator cracking was more impacted by overweight traffic loading as compared to longitudinal cracking and rutting.

7.2 Conclusions

This study concludes that it is important to consider vehicle-tire-pavement interaction to analyze dynamic pavement responses and fatigue cracking damage in asphalt pavement analysis and design. The magnitude and frequency of dynamic loads generated by axle loads due to rough pavement surface conditions were found impacted by vehicle speeds, truck configurations, pavement profiles, and axle types and loads. The pavement responses and fatigue cracking damage at specific locations along pavement profile were significantly increased by dynamic loads due to pavement roughness. Therefore, dynamic loads should be considered in M-E pavement analysis and design for more accurate pavement performance prediction.

Machine learning approach significantly outperforms traditional statistical regression methods in analyzing pavement performance when complicated explanatory variables are taken into consideration. It is a powerful tool to develop empirical models for pavement performance prediction based on field measurements for pavement management system. Machine learning approach also makes it feasible to consider a variety of explanatory variables in transfer functions in M-E pavement analysis and design according

to realistic pavement performance. The derived models can be utilized to investigate the impact of specific variable such as traffic loading on pavement performance based on different failure mechanisms. It can be further applied to optimally allocating maintenance and rehabilitation costs.

7.3 Limitations of Study

The following limitations of the study should be noted:

1) Limited truck configurations, vehicle speeds, pavement profiles, and axle loads were considered to calculate the dynamic tires forces due to rough pavement surface conditions.
2) Due to the lack of field measurements, limited pavement responses from LTPP database were used to validate the proposed impulse response method to estimate the pavement responses induced by dynamic loads of moving vehicles.
3) The estimated pavement performance using the proposed methodology to consider dynamic loads in M-E analysis and design was not verified using field measurements.
4) The hyperparameters in machine learning models were optimized for model selection, but a comprehensive grid-search for hyperparameter tuning is needed to derive more accurate prediction models of pavement performance.
5) Limited variables related to environmental condition and material properties were taken into account in the random survival forest models of pavement performance.

7.4 Recommendations for Future Work

The following recommendations are suggested for future study:

1) Future researches should be conducted to further validate the accuracy of impulse response method with field measurements other than LTPP data. The combinational effects of load frequency and speed need be studied using dynamic loads induced by a wide range of pavement surface roughness.
2) The study provides an analysis methodology to consider dynamic loads caused by pavement roughness for pavement response calculation and fatigue damage accumulation in M-E pavement analysis. Future study should be conducted to implement the proposed methodology and verify the prediction of pavement performance with field measurements. The propose methodology can be modified for analyzing other failure mechanisms such as rutting in M-E pavement analysis.
3) The findings indicated the proposed random survival forests models are promising to analyze the impact of traffic loading on failure risk of pavement with high accuracy. The proposed models can be further improved by considering more variables related to more detailed climate condition and material properties and used for more accurate pavement performance prediction for pavement management system in the future study.
4) Machine learning approaches can be further used for decision-making to improve pavement performance, for example optimization of maintenance and rehabilitation strategies and determination of overweight permit fee policy based on axle loads.

REFERENCES

Agurla, M., and S. Lin. 2015. "Long-term pavement performance Ohio SPS-1 and SPS-2 dynamic load response data processing." Federal Highway Administration, McLean, VA FHWA-HRT-14-088, 2015.

Al-Qadi, I. L., and M. A. Elseifi. 2007. "New generation of wide-base tires: Impact on trucking operations, environment, and pavements." *Transportation Research Record*(2008), 100-109.

Al-Qadi, I. L., M. A. Elseifi, P. J. Yoo, S. H. Dessouky, N. Gibson, T. Harman, J. D'Angelo, and K. Petros. 2008a. "Accuracy of current complex modulus selection procedure from vehicular load pulse: NCHRP project 1-37a mechanistic-empirical pavement design guide." *Transportation Research Record*(2087), 81-90.

Al-Qadi, I. L., and H. Wang. 2011. "Prediction of tire pavement contact stresses and analysis of asphalt pavement responses: A decoupled approach." *Proc., Asphalt Paving Technology 2011*, Association of Asphalt Paving Technologist, 289-315.

Al-Qadi, I. L., and H. Wang. 2012. "Impact of wide-base tires on pavements: Results from instrumentation measurements and modeling analysis." *Transportation Research Record*, 2304(1), 169-176.

Al-Qadi, I. L., H. Wang, P. J. Yoo, and S. H. Dessouky. 2008b. "Dynamic analysis and in situ validation of perpetual pavement response to vehicular loading." *Transportation Research Record*(2087), 29-39.

Almeida, A. M. M., and L. G. Picado-Santos. 2015. "Methodological framework for truck-factor estimation considering vehicle-pavement interaction." *Journal of Transportation Engineering*, 141(2).

ARA Inc. 2004. "Guide of mechanistic-empirical design of new and rehabilitation pavement structures." Transportation Research Board, National Research Council, Washington, D. C., NCHRP 1-37A.

ARA Inc. 2019. "AASHTOWare Pavement ME Design."

ASTM. 2018. "Standard practice for roads and parking lots pavement condition index surveys." ASTM International.

Barua, L., B. Zou, M. Noruzoliaee, and S. Derrible. 2020. "A gradient boosting approach to understanding airport runway and taxiway pavement deterioration."

Batioja-Alvarez, D., S.-F. Kazemi, E. Y. Hajj, R. V. Siddharthan, and A. J. T. Hand. 2018. "Statistical distributions of pavement damage associated with overweight vehicles: Methodology and case study." *Transportation Research Record*, 2672(9), 229-241.

Beskou, N. D., and D. D. Theodorakopoulos. 2011. "Dynamic effects of moving loads on road pavements: A review." *Soil Dynamics and Earthquake Engineering*, 31(4), 547-567.

Bilodeau, J.-P., L. Gagnon, and G. Dore. 2017. "Assessment of the relationship between the international roughness index and dynamic loading of heavy vehicles." *International Journal of Pavement Engineering*, 18(8), 693-701.

Breiman, L. 2001. "Random forests." *Machine Learning*, 45(1), 5-32.

Cai, Y., Z. Cao, H. Sun, and C. Xu. 2009. "Dynamic response of pavements on poroelastic half-space soil medium to a moving traffic load." *Computers and Geotechnics*, 36(1-2), 52-60.

Cebon, D. 1999. *Handbook of vehicle-road interaction*, Swets & Zeitlinger, Netherlands.

Chatti, K., and D. Lee. 2002. "Effect of surface roughness on truck dynamic loading and pavement damage." *The 7th International Svmposium on Heavy Vehicle Weights & Dimensions*Delft, Netherlands.

Chatti, K., and K. K. Yun. 1996. "SAPSI-M: Computer program for analyzing asphalt concrete pavements under moving arbitrary loads." *Transportation Research Record*(1539), 88-95.

Chen, J., H. Wang, M. Li, and L. Li. 2016. "Evaluation of pavement responses and performance with thermal modified asphalt mixture." *Materials and Design*, 111, 88-97.

Chopra, A. K. 2001. *Dynamics of structures*, Prentice Hall, Upper Saddle River, NJ.

Dassault Systèmes. 2014. "ABAQUS version 6.14."Waltham, MA.

De Barros, F. C. P., and J. E. Luco. 1994. "Response of a layered viscoelastic half-space to a moving point load." *Wave Motion*, 19(2), 189-210.

Devore, J. L. 1995. *Probability and statistics for engineering and the sciences*, Duxbury Press.

Ding, Y. M., and H. Wang. 2020. "Computational investigation of hydroplaning risk of wide-base truck tyres on roadway." *International Journal of Pavement Engineering*, 21(1), 122-133.

Dong, Q., and B. Huang. 2015. "Failure probability of resurfaced preventive maintenance treatments investigation into long-term pavement performance program." *Transportation Research Record*, 2481, 65-74.

Elkins, G. E., T. Thompson, B. Ostrom, A. Simpson, and B. Visintine. 2016. "Long-term pavement performance information management system user guide." Federal Highway Administration, McLean, VA, FHWA-RD-03-088.

Fathi, A., M. Mazari, M. Saghafi, A. Hosseini, and S. Kumar. "Parametric study of pavement deterioration using machine learning algorithms." *Proc., International Airfield and Highway Pavements Conference 2019: Innovation and Sustainability in Highway and Airfield Pavement Technology*, American Society of Civil Engineers (ASCE), 31-41.

Federal Highway Administration. 2015. "Report to congress on compilation of existing state truck size and weight limit laws."

Federal Highway Administration. 2017. "Policy information." <https://www.fhwa.dot.gov/ohim/ohimvtis.cfm>. (April, 27th, 2020).

Ferry, J. D. 1980. *Viscoelastic properties of polymers*, Wiley, Hoboken, NJ.

FHWA. 2001. "Guide to LTPP traffic data collection and processing."

Gilispie, T. D. 1992. *Fundamental of vehicle dynamics*, Society of Automotive Engineering Inc., Warrandale, PA.

Gneiting, T., and A. E. Raftery. 2007. "Strictly proper scoring rules, prediction, and estimation." *Journal of the American Statistical Association*, 102(477), 359-378.

Goenaga, B., L. Fuentes, and O. Mora. 2019. "A practical approach to incorporate roughness-induced dynamic loads in pavement design and performance prediction." *Arabian Journal for Science and Engineering*, 44(5), 4339-4348.

Gong, H., Y. Sun, W. Hu, P. A. Polaczyk, and B. Huang. 2019a. "Investigating impacts of asphalt mixture properties on pavement performance using LTPP data through random forests." *Construction and Building Materials*, 204, 203-212.

Gong, H., Y. Sun, and B. Huang. 2019b. "Gradient boosted models for enhancing fatigue cracking prediction in mechanistic-empirical pavement design guide." *Journal of Transportation Engineering Part B: Pavements*, 145(2).

Gong, H., Y. Sun, X. Shu, and B. Huang. 2018. "Use of random forests regression for predicting IRI of asphalt pavements." *Construction and Building Materials*, 189, 890-897.
Graesser, E. J., and C. R. Wong. "Relationship of traditional damping measures for materials with high damping capacity: A review." *Proc., Symposium on M3D: Mechanics and Mechanisms of Material Damping, March 13, 1991 - March 15, 1991*, Publ by ASTM, 316-343.
Greene, J., U. Toros, S. Kim, T. Byron, and B. Choubane. 2010. "Impact of wide-base single tires on pavement damage." *Transportation Research Record*(2155), 82-90.
Gungor, O. E., A. M. A. Petit, J. Qiu, J. Zhao, H. Meidani, H. Wang, Y. Ouyang, I. L. Al-Qadi, and J. Mann. 2019. "Development of an overweight vehicle permit fee structure for Illinois." *Transport Policy*, 82, 26-35.
Haider, S. W., and R. S. Harichandran. 2007. "Relating axle load spectra to truck gross vehicle weights and volumes." *Journal of Transportation Engineering*, 133(12), 696-705.
Haider, S. W., and R. S. Harichandran. 2009. "Effect of axle load spectrum characteristics on flexible pavement performance." *Transportation Research Record*(2095), 101-114.
Haider, S. W., R. S. Harichandran, and M. B. Dwaikat. 2009. "Closed-form solutions for bimodal axle load spectra and relative pavement damage estimation." *Journal of Transportation Engineering*, 135(12), 974-983.
Hajek, J. J., W. A. Phang, A. Prakash, and G. A. Wrong. 1985. "Performance prediction for pavement management." *North American Pavement Management Conference*Toronto, Canada.
Hardy, M. S. A. 1995. "The generation of waves in infinite structures by moving harmonic loads." *Journal of Sound and Vibration*, 180(4), 637-644.
Hardy, M. S. A., and D. Cebon. "Measurement and analysis of the dynamic of flexible pavements." *Proc., The 2nd International Symposium on Heavy Vehicle Weights and Dimensions*.
Hardy, M. S. A., and D. Cebon. 1992. "Flexible pavement response models for assessing dynamic axle loads." *The third international symposium on heavy vehicle weights and dimensions*, Thomas Telford Ltd.
Hardy, M. S. A., and D. Cebon. 1993. "Response of continuous pavement to moving dynamic loads." *Journal of Engineering Mechanics*, 119(9), 1762-1780.
Hardy, M. S. A., and D. Cebon. 1994. "Importance of speed and frequency in flexible pavement response." *Journal of Engineering Mechanics*, 120(3), 463-492.
Harold L. Von Quintus, Amy L. Simpson, and A. A. Eltahan. 2006. "Rehabilitation of asphalt concrete pavements: Initial evaluation of the SPS-5 experiment—final report." FHWA-RD-01-168.
Harrell, F. E., K. L. Lee, and D. B. Mark. 2005. "Multivariable prognostic models: Issues in developing models, evaluating assumptions and adequacy, and measuring and reducing errors." wiley, 223-249.
Hastie, T., R. Tibshirani, and J. Friedman. 2009. *The element of statistical learning: Data mining, interface, and prediction*.
Hernandez, J. A., A. Gamez, and I. L. Al-Qadi. 2016. "Effect of wide-base tires on nationwide flexible pavement systems: Numerical modeling." *Transportation Research Record*, 2590, 104-112.

Hu, X., S. Zhong, and L. F. Walubita. 2015. "Three-dimensional modelling of multilayered asphalt concrete pavement structures: Strain responses and permanent deformation." *Road Materials and Pavement Design*, 16(3), 727-740.

Huang, Y. H. 1993. *Pavement analysis and design*, Prentice Hall, Englewood Cliffs, New Jersey.

Inkoom, S., J. Sobanjo, A. Barbu, and X. Niu. 2019. "Pavement crack rating using machine learning frameworks: partitioning, bootstrap forest, boosted trees, Naive Bayes, and K - nearest neighbors." *Journal of Transportation Engineering Part B: Pavements*, 145(3).

Ishwaran, H., U. Kogalur, E. Blackstone, and M. Lauer. 2008. "Random survival forests." *The Annals of Applied Statistics*, 2.

Ishwaran, H., and U. B. Kogalur. 2007. "Random survival forests for R." *R News*, 7(2), 25–31.

Jackson, N. C., R. Deighton, and D. L. Huft. 1996. "Development of pavement performance curves for individual distress indexes in South Dakota based on expert opinion." *Transportation Research Record*(1524), 130-136.

Jasim, A. F., H. Wang, and T. Bennert. 2019. "Evaluation of clustered traffic inputs for mechanistic-empirical pavement design: case study in New Jersey." *Transportation Research Record*, 0361198119853557.

Jia, X., M. Woods, H. Gong, W. Hu, B. Huang, and B. Faraj. 2019. "Utilization of state performance indices to correlate national performance measures for asphalt pavements in Tennessee." *Transportation Research Record*, 2673(6), 379-388.

Kanai, T., K. Tomisawa, T. Endoh, and K. Himeno. 2010. "Analysis of damage of asphalt pavement due to dynamic load of heavy vehicles caused by surface roughness." *Proc., The 11th International Conference on Asphalt Pavements–ISAP*, Nagoya, Aichi, Japan.

Karballaeezadeh, N., D. Mohammadzadeh S, S. Shamshirband, P. Hajikhodaverdikhan, A. Mosavi, and K.-w. Chau. 2019. "Prediction of remaining service life of pavement using an optimized support vector machine (case study of Semnan–Firuzkuh road)." *Engineering Applications of Computational Fluid Mechanics*, 13(1), 188-198.

Khavassefat, P., D. Jelagin, and B. Birgisson. 2014. "Dynamic response of flexible pavements at vehicle–road interaction." *Road Materials and Pavement Design*, 16(2), 256-276.

Kim, S. M., and J. M. Roesset. 1998. "Moving loads on a plate on elastic foundation." *Journal of Engineering Mechanics*, 124, 1010-1017.

Kulakowski, B. T., and W. J. Kenis. 1995. "A study of dynamic wheel loads conducted using a four-post road simulator." *Proc., The 4th International Symposium on Heavy Vehicle Weights and Dimensions*, Int Forum Road Transp Technol, Ann Arbor, MI, USA, 301-307.

Law, E. H., I. Janajreh, and N. Frey. "Vehicle ride response to new widebase tires and conventional dual tires." *Proc., International Truck and Bus Meeting and Exhibition, November 18, 2002 - November 20, 2002*, SAE International.

Li, Z., and K. Sinha. 2000. "A methodology to estimate load and non-load shares of highway pavement routine maintenance and rehabilitation expenditures." U.S. Department of Transportation, FHWA/IN/JTRP-2000/4.

Liu, C. 2001. "Pavement response to moving loads." *Road Materials and Pavement Design*, 2(3), 263-282.

Liu, C., R. Herman, and B. F. McCullough. 1998. "Pavement deterioration, rate of dynamic force, and ride quality." *Transportation Research Record*(1643), 14-19.

Loizos, A., and M. G. Karlaftis. 2005. "Prediction of pavement crack initiation from in-service pavements: A duration model approach." *Transportation Research Record*, 1940, 38-42.

Lombaert, G., G. Degrande, and D. Clouteau. 2000. "Numerical modelling of free field traffic-induced vibrations." *Soil Dynamics and Earthquake Engineering*, 19(7), 473-488.

Lombaert, G., G. Degrande, and D. Clouteau. 2004. "The non-stationary freefield response for a moving load with a random amplitude." *Journal of Sound and Vibration*, 278(3), 611-635.

Lu, Z., and H. Yao. 2013. "Effects of the dynamic vehicle-road interaction on the pavement vibration due to road traffic." *Journal of Vibroengineering*, 15(3), 1291-1301.

Lu, Z., H. Yao, J. Liu, and Z. Hu. 2014. "Dynamic response of a pavement-subgrade-soft ground system subjected to moving traffic load." *Journal of Vibroengineering*, 16(1), 195-209.

Lv, P., R. Tian, and X. Liu. 2010. "Dynamic response solution in transient state of viscoelastic road under moving load and its Application." *Journal of Engineering Mechanics*, 136(2), 168-173.

Lysmer, J., and R. L. Kuhlemeyer. 1969. "Finite dynamic model for infinite media." *Journal of Engineering Mechanics*, 95(4), 859-877.

Marcelino, P., M. d. Lurdes Antunes, E. Fortunato, and M. Castilho Gomes. 2019. "Machine learning approach for pavement performance prediction." *International Journal of Pavement Engineering*.

MATLAB. 2010. *version 7.10.0 (R2010a)*, The MathWorks Inc., Natick, Massachusetts.

Mechnical Simulation. 2018. "Trucksim." <https://www.carsim.com/downloads/pdf/trucksim_handout.pdf>. (May 28, 2019).

Mikhail, M. Y., and M. S. Mamlouk. 1997. "Effect of vehicle-pavement interaction on pavement response." *Transportation Research Record*, 1570(1), 78-88.

Mogensen, U. B., H. Ishwaran, and T. A. Gerds. 2012. "Evaluating random forests for survival analysis using prediction error curves." *Journal of Statistical Software*, 1(1), 1253-1257.

Muka, P. 2017. "Road roughness limit values based on measured vehicle vibration." *Journal of Infrastructure Systems*, 23(2).

Nakat, Z. S., and S. M. Madanat. 2008. "Stochastic duration modeling of pavement overlay crack initiation." *Journal of Infrastructure Systems*, 14(3), 185-192.

Nashif, A. D., D. I. G. Jones, and J. P. Henderson. 1985. *Vibration damping*, John Wiley & Sons, New York, NY.

National Semiconductor. 1980. "Power spectra estimation. Application note 255." Texas Instruments Incorporated, Dallas, Texas.

Navarrina, F., L. Ramirez, J. Paris, X. Nogueira, I. Colominas, M. Casteleiro, and J. R. Fernandez-De-Mesa. 2015. "Comprehensive model for fatigue analysis of flexible pavements considering effects of dynamic axle loads." *Transportation Research Record*, 2524, 110-118.

Newland, D. E. 1985. *Random vibrations and spectral analysis*, Longman, U.K.

Ohio Department of Transportation. 2020. "Ohio special hauling permits axle weight guidelines."

<https://www.dot.state.oh.us/Divisions/Operations/Maintenance/Permits/Pages/AXLEWEIGHTGUIDELINES.aspx>. (March 24, 2020).

Ong, G. P., T. Nantung, and K. C. Sinha. 2010. "Indiana pavement preservation program." U.S. Department of Transportation, FHWA/IN/JTRP-2010/14.

Park, D.-W. 2010. "Evaluation of predicted pavement fatigue life based on surface profiles and asphalt mixture types." *KSCE Journal of Civil Engineering*, 14(2), 191-196.

Park, S. W., and Y. R. Kim. 1999. "Interconvesion between relaxation modulus and creep compliance for viscoelastic solids." *Journal of Materials in Civil Engineering*, 11(1), 76-82.

Piryonesi, S. M., and T. E. El-Diraby. 2020. "Role of data analytics in infrastructure asset management: Overcoming data size and quality problems." *Journal of Transportation Engineering Part B: Pavements*, 146(2).

Python Software Foundation. "Python language reference, version 3.5."

Rys, D. 2019. "Consideration of dynamic loads in the determination of axle load spectra for pavement design."

Rys, D., J. Judycki, and P. Jaskula. 2016. "Analysis of effect of overloaded vehicles on fatigue life of flexible pavements based on weigh in motion (WIM) data." *International Journal of Pavement Engineering*, 17(8), 716-726.

Sayers, M. W. 2011. "Road characterization for the simulation of automotive vehicle dynamics." *SAE International Journal of Materials and Manufacturing*, 4(1), 251-262.

Sayers, M. W., and C. W. Mousseau. 1990. "Real-time vehicle dynamic simulation obtained with a symbolic multibody program." *Winter Annual Meeting of the American Society of Mechanical Engineers.*, ASME, Dallas, TX, USA, 51-58.

Schlotjes, M. R., T. F. P. Henning, M. P. N. Burrow, and H. T. Evdorides. 2015. "Using support vector machines to predict the probability of pavement failure." *Proceedings of the Institution of Civil Engineers: Transport*, 168(3), 212-222.

Setiawan, J. D., M. Safarudin, and A. Singh. "Modeling, simulation and validation of 14 DOF full vehicle model." *Proc., International Conference on Instrumentation, Communication, Information Technology, and Biomedical Engineering 2009*, IEEE Computer Society.

Shim, T., and C. Ghike. 2007. "Understanding the limitations of different vehicle models for roll dynamics studies." *User Modeling and User-Adapted Interaction*, 45(3), 191-216.

Smith, K., and P. Ram. 2016. "Measuring and specifying pavement smoothness." FHWA-HIF-16-032.

Steyn, W. J. v., N. Viljoen, L. Popescu, and L. du Plessis. 2013. "Freight-truck-pavement interaction, logistics, & economics: Final phase 1 report." UCPRC-RR-2013-08.

Streit, D. A., B. T. Kulakowski, P. E. Sebaaly, and R. J. Wollyung. 1998. *Road simulator study of heavy-vehicle wheel forces*.

Sun, L. 2001. "Developing, spectrum-based models for international roughness index and present serviceability index." *Journal of Transportation Engineering*, 127(6), 463-470.

Sun, L. 2003. "Simulation of pavement roughness and IRI based on power spectral density." *Mathematics and Computers in Simulation*, 61(2), 77-88.

Sun, L. 2005. "Dynamics of plate generated by moving harmonic loads." *Journal of Applied Mechanics, Transactions ASME*, 72(5), 772-777.

Sun, L. 2006. "Analytical dynamic displacement response of rigid pavements to moving concentrated and line loads." *International Journal of Solids and Structures*, 43(14-15), 4370-4383.

Sun, L. 2013. "An overview of a unified theory of dynamics of vehicle–pavement interaction under moving and stochastic load." *Journal of Modern Transportation*, 21(3), 135-162.

Texas DOT. 2013. "Traffic recorder instruction manual notice 2012-1: Vehicle classification using FHWA 13-category scheme, appendix A." (Nov, 25, 2019).

The Transtec Group. 2016. "ProVAL user's guide version 3.6."

Tielking, J. T. 1992. "Conventional and wide base radial truck tyres." *Proc., The Third International Symposium on Heavy Vehicle Weights and Dimensions*, Thomas Telford Ltd, 182-182.

Tielking, J. T. 1994. "Force transmissibility of heavy truck tires." *Tire Science and Technology*, 22(1), 60-74.

Timm, D. H., S. M. Tisdale, and R. E. Turochy. 2005. "Axle load spectra characterization by mixed distribution modeling." *Journal of Transportation Engineering*, 131(2), 83-88.

Titi, H. H., N. J. Coley, and V. Latifi. 2018. "Evaluation of pavement performance due to overload single-trip permit truck traffic in Wisconsin." *Advances in Civil Engineering*, 2018.

Trangsrud, C., E. H. Law, and I. Janajreh. "Ride dynamics and pavement loading of tractor semi-trailers on randomly rough roads." *Proc., SAE Commercial Vehicle Engineering Congress and Exhibition*, SAE International.

U.S. Department of Transportation. 2016. "2015 status of the nation's highways, bridges, and transit: Condition and performance."Washington, DC.

Ueckermann, A., and M. Oeser. 2015. "Approaches for a 3D assessment of pavement evenness data based on 3D vehicle models." *Journal of Traffic and Transportation Engineering (English Edition)*, 2(2), 68-80.

US Department of Transportation. 2018. "Oversize/overweight load permits." <https://ops.fhwa.dot.gov/freight/sw/permit_report/index.htm>. (June 19, 2020).

Üstün, B., W. J. Melssen, and L. M. C. Buydens. 2006. "Facilitating the application of support vector regression by using a universal Pearson VII function based kernel." *Chemometrics and Intelligent Laboratory Systems*, 81(1), 29-40.

Wang, H., and I. Al-Qadi. 2010. "Near-surface pavement failure under multiaxial stress state in thick asphalt pavement." *Transportation Research Record*(2154), 91-99.

Wang, H., and I. L. Al-Qadi. 2009. "Combined effect of moving wheel loading and three-dimensional contact stresses on perpetual pavement responses." *Transportation Research Record*(2095), 53-61.

Wang, H., and I. L. Al-Qadi. 2011. "Impact quantification of wide-base tire loading on secondary road flexible pavements." *Journal of Transportation Engineering*, 137(9), 630-639.

Wang, H., and I. L. Al-Qadi. 2013. "Importance of nonlinear anisotropic modeling of granular base for predicting maximum viscoelastic pavement responses under moving vehicular loading." *Journal of Engineering Mechanics*, 139(1), 29-38.

Wang, H., I. L. Al-Qadi, and D. L. Huft. 2014. "Pavement-dependent load limits: Case study in South Dakota for different tire configurations." *Transportation Research Record*, 2456, 107-114.

Wang, H., I. L. Al-Qadi, and I. Stanciulescu. 2012. "Simulation of tire–pavement interaction for predicting contact stresses at static and various rolling conditions." *International Journal of Pavement Engineering*, 13(4), 310-321.

Wang, H., and M. Li. 2015. "Evaluation of effects of variations in aggregate base layer properties on flexible pavement performance." *Transportation Research Record*, 2524, 119-129.

Wang, H., M. Li, and N. Garg. 2015a. "Airfield flexible pavement responses under heavy aircraft and high tire pressure loading." *Transportation Research Record: Journal of the Transportation Research Board*, 2501, 31-39.

Wang, H., and Z. Wang. 2019. "Deterministic and probabilistic life-cycle cost analysis of pavement overlays with different pre-overlay conditions." *Road Materials and Pavement Design*, 20(1), 58-73.

Wang, H., Z. Wang, R. J. Blight, and E. C. Sheehy. 2015b. "Derivation of pay adjustment for in-place air void of asphalt pavement from life-cycle cost analysis." *Road Materials and Pavement Design*, 16(3), 505-517.

Wang, H., Z. Wang, J. Zhao, and J. Qian. 2020a. "Life-cycle cost analysis of pay adjustment for initial smoothness of asphalt pavement overlay." *Journal of Testing and Evaluation*, 48(2).

Wang, H., and J. Zhao. 2016. "Development of overweight permit fee using mechanistic-empirical pavement design and life-cycle cost analysis." *Transport*, 31(2), 156-166.

Wang, H., J. Zhao, and Z. Wang. 2015. "Impact of overweight traffic on pavement life using weigh-in-motion data and mechanistic-empirical pavement analysis." *Proc., 9th International Conference on Managing Pavement Assets*.

Wang, X., J. Zhao, Q. Li, N. Fang, P. Wang, L. Ding, and S. Li. 2020b. "A hybrid model for prediction in asphalt pavement performance based on support vector machine and grey relation analysis." *Journal of Advanced Transportation*, 2020.

Wu, D., J. Zhao, H. Liu, and C. Yuan. 2019. "The assessment of damage to Texas highways due to oversize and overweight loads considering climatic factors." *International Journal of Pavement Engineering*, 20(7), 853-865.

Xue, W., and E. Weaver. 2011. "Pavement shear strain response to dual and wide-base tires." *Transportation Research Record*(2225), 155-164.

Yang, S., Y. Lu, and S. Li. 2013. "An overview on vehicle dynamics." *International Journal of Dynamics and Control*, 1(4), 385-395.

Yao, H.-L., Z. Lu, H.-N. Luo, and Y. Yang. 2009. "Dynamic response of rough pavement on Kelvin foundation subjected to traffic loads." *Yantu Lixue/Rock and Soil Mechanics*, 30(4), 890-896.

Yu, J., E. Y. Chou, and J.-T. Yau. 2008. "Estimation of the effects of influential factors on pavement service life with cox proportional hazards method." *Journal of Infrastructure Systems*, 14(4), 275-282.

Zeiada, W., S. Abu Dabous, K. Hamad, R. Al-Ruzouq, and M. Khalil. 2020. "Machine learning for pavement performance modelling in warm climate regions." *Arabian Journal for Science and Engineering*.

Zhang, M., H. Gong, X. Jia, R. Xiao, X. Jiang, Y. Ma, and B. Huang. 2020. "Analysis of critical factors to asphalt overlay performance using gradient boosted models." *Construction and Building Materials*, 262.

Zhang, Y. 2014. "Characterization of high porosity drainage layer materials for M-E pavement design." Ph.D Dissertation, Virginia Polytechnic Institute and State University.

Zhao, Y., S. Y. Oderji, and P. Chen. 2015. "Analysis of transient viscoelastic response of asphalt concrete using frequency domain approach." *Journal of Traffic and Transportation Engineering (English Edition)*, 2(6), 414-421.

Ziari, H., M. Maghrebi, J. Ayoubinejad, and S. T. Waller. 2016. "Prediction of pavement performance: Application of support vector regression with different kernels." *Transportation Research Record*, 2589, 135-145.